

Aspects of Electron Correlations in Two-dimensional Metals

Dissertation
zur Erlangung des Doktorgrades
der Naturwissenschaften

vorgelegt beim Fachbereich Physik der
Goethe-Universität Frankfurt
in Frankfurt am Main

von
Casper Drukier
aus
Hvidovre

Frankfurt (2014)
(D30)

vom Fachbereich Physik der
Goethe Universität Frankfurt
als Dissertation angenommen.

Dekan: Prof. Dr. Joachim Stroth

Gutachter: Prof. Dr. Peter Kopietz
Prof. Dr. Walter Hofstetter

Datum der Disputation: 2/2-2015

Moim rodzicom

Contents

Abstract	7
1 Background	11
1.1 Many-body methods	11
1.1.1 Green's functions and the Dyson equation	11
1.1.2 Feynman diagrams	14
1.1.3 Functional representation	15
1.1.4 Skeleton equations	17
1.2 Functional Renormalization Group	18
1.3 Fermi liquid theory	20
2 The Ising-nematic quantum critical point in two-dimensional metals	27
2.1 Introduction	27
2.1.1 Hertz-Millis theory	28
2.1.2 $1/N$ -expansion	30
2.1.3 The genus expansion and breakdown of large- N counting	34
2.2 Functional Renormalization Group approach to the Ising-nematic quantum-critical point in two-dimensional metals	38
2.2.1 Model	39
2.2.2 FRG flow equations	40
2.2.3 Skeleton equations	45
2.2.4 Obtaining the anomalous dimensions	47
2.2.5 Recovering one loop	50
2.2.6 The symmetrised three-loop	54
2.2.7 The mixed fermion-boson vertex	57
2.2.8 Results for the anomalous dimensions	65
2.3 Implications for experiments	68
2.4 Summary and conclusions	68
3 Non-analytic corrections in Fermi liquid theory	71
3.1 Introduction	71
3.1.1 How to break the Sommerfeld expansion	72
3.1.2 The susceptibility	75
3.1.3 Renormalization group	79

3.2	Non-analytic magnetic field dependence of quasi-particle properties	80
3.2.1	Model	81
3.2.2	Extracting quasi-particle properties	83
3.2.3	The second order self-energy	83
3.2.4	The opposite-spin particle-hole bubble	84
3.2.5	Numerical results	87
3.2.6	Phase-space decomposition	91
3.2.7	Scaling analysis	94
3.2.8	Analytic results	96
3.3	Non-analytic frequency and temperature dependence	103
3.3.1	Non-analytic frequency dependence of the self-energy	103
3.3.2	Non-analytic temperature dependence	106
3.4	Implications for experiments	109
3.4.1	Tunnelling experiments	109
3.4.2	Magnetoconductivity	110
3.5	Summary and conclusions	120
A	Disorder averaging	123
B	Deutsche Zusammenfassung	127
B.1	Ising-nematischer quantenkritischer Punkt in zweidimensionalen Metallen	128
B.2	Nicht-analytische Korrekturen in Fermi-Flüssigkeitstheorie	135
	Bibliography	141

Abstract

Landau's Fermi liquid theory has been the main tool for investigating interactions between fermions at low energies for more than 50 years. It has been successful in describing, amongst other things, the mass enhancement in ^3He and the thermodynamics of a large class of metals. Whilst this in itself is remarkable given the phenomenological nature of the original theory, experiments have found several materials, such as some superconducting and heavy-fermion materials, which cannot be described within the Fermi liquid picture. Because of this, many attempts have been made to understand these "non Fermi liquid" phases from a theoretical perspective. This will be the broad topic of the first part of this thesis and will be investigated in Chapter 2, where we consider a two-dimensional system of electrons interacting close to a Fermi surface through a damped gapless bosonic field. Such systems are known to give rise to non Fermi liquid behaviour. In particular we will consider the Ising-nematic quantum critical point of a two-dimensional metal. At this quantum critical point the Fermi liquid theory breaks down and the fermionic self-energy acquires the non Fermi liquid like $\omega^{2/3}$ frequency dependence at lowest order and within the canonical Hertz-Millis approach to quantum criticality of interacting fermions. Previous studies have however shown that, due to the gapless nature of the electronic single-particle excitations, the exponent of $2/3$ is modified by an anomalous dimension η_ψ which changes, not only the exponent of the frequency dependence, but also the exponent of the momentum dependence of the self-energy. These studies also show that the usual $1/N$ -expansion breaks down for this problem. We therefore develop an alternative approach to calculate the anomalous dimensions based on the functional renormalization group, which will be introduced in the introductory Chapter 1. Doing so we will be able to calculate both the anomalous dimension renormalizing the exponent of the frequency dependence and the exponent renormalizing the momentum dependence of the self-energy. Moreover we will see that an effective interaction between the bosonic fields, mediated by the fermions, is crucial in order to obtain these renormalizations.

In the second part of this thesis, presented in Chapter 3, we return to Fermi liquid theory itself. Indeed, despite its conceptual simplicity of expressing interacting electrons through long-lived quasi-particles which behave in a similar fashion as free particles, albeit with renormalized parameters, it

remains an active area of research. In particular, in order to take into account the full effects of interactions between quasi-particles, it is crucial to consider specific microscopic models. One such effect, which is not captured by the phenomenological theory itself, is the appearance of non-analytic terms in the expansions of various thermodynamic quantities such as heat-capacity and susceptibility with respect to an external magnetic field, temperature, or momentum. Such non-analyticities may have a large impact on the phase diagram of, for example, itinerant electrons near a ferromagnetic quantum phase transition. Inspired by this we consider a system of interacting electrons in a weak external magnetic field within Fermi liquid theory. For this system we calculate various quasi-particle properties such as the quasi-particle residue, momentum-renormalization factor, and a renormalization factor which relates to the self-energy on the Fermi surface. From these renormalization factors we then extract physical quantities such as the renormalized mass and renormalized electron Landé g -factor. By calculating the renormalization factors within second order perturbation theory numerically and analytically, using a phase-space decomposition, we show that all renormalization factors acquire a non-analytic term proportional to the absolute value of the magnetic field. We moreover explicitly calculate the prefactors of these terms and find that they are all universal and determined by low-energy scattering processes which we classify. We also consider the non-analytic contributions to the same renormalization factors at finite temperatures and for finite external frequencies and discuss possible experimental ways of measuring the prefactors. Specifically we find that the tunnelling density of states and the conductivity acquire a non-analytic dependence on magnetic field (and temperature) coming from the momentum-renormalization factor. For the latter we discuss how this relates to previous works which show the existence of non-analyticities in the conductivity at first order in the interaction.

Inhaltsangabe

Die Landau'sche Fermi-Flüssigkeitstheorie ist seit mehr als 50 Jahren das wesentliche Werkzeug zur Untersuchung von wechselwirkenden Fermionen bei niedrigen Energien. Unter anderem konnten damit die Massenzunahme in ^3He und die thermodynamischen Eigenschaften einer breiten Klasse von Metallen erfolgreich beschrieben werden. Während dies für sich genommen bemerkenswert ist, wenn man die phänomenologische Natur der Theorie berücksichtigt, haben Experimente mehrerer Materialien wie Supraleiter und Schwere-Fermionen-Systeme gefunden, welche nicht innerhalb der Fermi-Flüssigkeitstheorie beschrieben werden können. Aufgrund dessen sind viele Versuche unternommen worden, diese Nicht-Fermi-Flüssigkeitstheoretisch zu beschreiben. Dies wird Gegenstand des ersten Teils dieser Doktorarbeit sein und in Kapitel 2 näher untersucht werden, wo wir ein zweidimensionales System von Fermionen betrachten, welche nahe der Fermifläche mittels eines gedämpften, lückenlosen bosonischen Feldes wechselwirken. Diese Systeme sind dafür bekannt, dass sie sich nicht als Fermi-Flüssigkeit beschreiben lassen. Insbesondere werden wir den Ising-nematischen quantenkritischen Punkt eines zweidimensionalen Metalls untersuchen. An diesem quantenkritischen Punkt bricht das Fermi-Flüssigkeitsbild zusammen und die fermionische Selbstenergie entwickelt eine $\omega^{2/3}$ Frequenzabhängigkeit in niedrigster Ordnung Störungstheorie und innerhalb der kanonischen Hertz-Millis Theorie der Quantenkritikalität von wechselwirkenden Fermionen. Laut früheren Studien ist jedoch das Fehlen einer Lücke bei den Fermionen dafür verantwortlich, dass der Exponent von $2/3$ durch eine anomale Dimension η_ψ modifiziert wird, welche nicht nur den Exponent der Frequenzabhängigkeit der Selbstenergie ändert, sondern auch der Impulsabhängigkeit. Diese Studien zeigen ebenfalls, dass die übliche $1/N$ -Entwicklung für dieses Problem zusammenbricht. Wir entwickeln daher einen alternativen Ansatz zur Berechnung der anomalen Dimension, basierend auf der funktionalen Renormierungsgruppe, welche wir in Kapitel 1 einführen werden. Dies ermöglicht uns die Berechnung der beiden anomalen Dimensionen, welche sowohl den Exponent der Frequenzabhängigkeit der Selbstenergie als auch den der Impulsabhängigkeit renormieren. Darüber hinaus finden wir, dass eine durch Fermionen vermittelte effektive Wechselwirkung zwischen den bosonischen Feldern entscheidend ist, um diese Renormierungen zu erhalten.

Im zweiten Teil dieser Doktorarbeit, in Kapitel 3, kehren wir zur Fermi-Flüssigkeitstheorie selbst zurück. Trotz der Tatsache, dass diese in der Be-

schreibung von wechselwirkenden Fermionen durch langlebige Quasiteilchen, welche sich ähnlich wie freie Teilchen, nur mit renormierten Parametern, verhalten, konzeptionell sehr einfach ist, stellt sie nach wie vor einen aktiven Forschungszweig dar. Insbesondere ist es entscheidend, spezifische mikroskopische Modelle zu betrachten, um alle Effekte der Wechselwirkung zwischen Quasiteilchen zu berücksichtigen. Einer dieser Effekte, welche nicht durch die phänomenologische Theorie selbst erfasst wird, ist das Auftreten nicht-analytischer Terme in der Entwicklung verschiedener thermodynamischer Größen wie Wärmekapazität und Suszeptibilität nach der Stärke des externen magnetischen Feldes, der Temperatur oder des Impulses. Solche nicht-analytischen Beiträge können einen großen Einfluss auf das Phasendiagramm haben, beispielsweise für itinerante Elektronen nahe eines ferromagnetischen Quanten-Phasenübergangs. Daran angelehnt betrachten wir ein System von wechselwirkenden Fermionen in einem schwachen externen Magnetfeld innerhalb der Fermi-Flüssigkeitstheorie. Für dieses System berechnen wir verschiedene Quasiteilcheneigenschaften wie beispielsweise das Quasiteilchenresiduum, den Impuls-Renormierungsfaktor und einen Renormierungsfaktor bezüglich der Selbstenergie auf der Fermifläche. Aus diesen Renormierungsfaktoren extrahieren wir anschließend physikalische Größen wie die renormierte Masse und den renormierten Landé-Faktor g der Fermionen. Indem wir die Renormierungsfaktoren numerisch und analytisch, mittels Phasenraum-Zerlegung, in zweiter Ordnung Störungstheorie berechnen, können wir zeigen, dass alle Renormierungsfaktoren einen nicht-analytischen Term proportional zum Betrag des magnetischen Feldes aufweisen. Weiterhin berechnen wir explizit die Vorfaktoren und finden, dass diese universal sind und durch niederenergetische Streuprozesse bestimmt werden, welche wir dann klassifizieren. Außerdem betrachten wir die nicht-analytischen Beiträge zu denselben Renormierungsfaktoren bei endlichen Temperaturen und für endliche externe Frequenzen und diskutieren verschiedene experimentelle Möglichkeiten, diese Vorfaktoren zu messen. Im Speziellen finden wir, dass durch den Impuls-Renormierungsfaktor sowohl für die Zustandsdichte als auch für die Leitfähigkeit eine nicht-analytische Abhängigkeit vom Magnetfeld (und der Temperatur) auftritt. Für letztere diskutieren wir, wie dies im Zusammenhang mit vorherigen Arbeiten steht, welche die Existenz von nicht-analytischen Korrekturen zur Leitfähigkeit in erster Ordnung in der Wechselwirkung vorhersagen.

Chapter 1

Background

This thesis will discuss fermions in two dimensions in the presence of a Fermi surface. In order to investigate these topics, several concepts and mathematical methods will be used. In this chapter these concepts and methods will be reviewed. We start by considering common many-body techniques in Section 1.1 and then, in Section 1.2, turn to a discussion of the functional renormalization group (FRG). We finally conclude the chapter with a discussion of Fermi liquid theory. As most methods can be found in standard textbooks such as [1, 2, 3, 4, 5, 6], we will refer to these for details. Before beginning let us moreover note that, throughout this work, we use units such that $\hbar = k_B = 1$. Thus temperatures and frequencies are measured in units of energy.

1.1 Many-body methods

In this section we discuss the main many-body techniques used in this thesis.

1.1.1 Green's functions and the Dyson equation

In the theory of inhomogeneous linear differential equations, the Green's function is a tool for finding solutions of equations of the form

$$\mathcal{L}y = f, \tag{1.1}$$

where \mathcal{L} is a linear differential operator acting on the function y . The Green's function, $G(x - \zeta)$ is then the solution to the corresponding equation

$$\mathcal{L}G(x, \zeta) = \delta(x - \zeta), \tag{1.2}$$

with \mathcal{L} acting on the first argument of the Green's function. Given the Green's function, $y(x)$ can also be found¹.

¹Mathematically the Green's function is an integral kernel representing \mathcal{L}^{-1} . More details can be found in standard textbooks such as [7].

In many-body physics the n -body real-time Green's function (or propagator) is defined as

$$G(j_1 t_1, \dots, j_n t_n; j'_1 t'_1, \dots, j'_n t'_n) = (-i)^n \left\langle T \left(A_{j_1}(t_1) \dots A_{j_n}(t_n) A_{j'_n}^\dagger(t'_n) \dots A_{j'_1}^\dagger(t'_1) \right) \right\rangle, \quad (1.3)$$

where A_j^\dagger and A_j denote fermionic or bosonic creation and annihilation operators in the Heisenberg picture and the angular brackets stand for thermal averaging. T denotes time-ordering which places operators evaluated at later times to the left such that, for two bosonic operators a and b , it is defined as

$$T(a(t_1)b(t_2)) = \begin{cases} a(t_1)b(t_2) & t_1 > t_2, \\ b(t_2)a(t_1) & t_2 > t_1, \end{cases} \quad (1.4)$$

with its obvious generalisation to arbitrary products of operators. For fermionic operators there is an additional sign coming from the anti-commutation relations for fermions. For $n = 1$ the Green's function has the physical interpretation as the amplitude of propagation of a particle from a state $|j_1 t_1\rangle$ to a state $|j'_1 t'_1\rangle$. From now on, unless explicitly stated, we will use Green's functions as meaning one-body Green's functions.

Consider now for concreteness a system of free fermions described by the Hamiltonian²

$$H = \sum_{\mathbf{k}} \xi_{\mathbf{k}} a_{\mathbf{k}}^\dagger a_{\mathbf{k}}, \quad (1.5)$$

where $\xi_{\mathbf{k}}$ is the dispersion and $a_{\mathbf{k}}^\dagger$ and $a_{\mathbf{k}}$ are now fermionic operators. In this case the free (retarded) Green's function is given by

$$G_0(t_1 - t_2, \mathbf{k}) = -i\theta(t_1 - t_2) e^{i\xi_{\mathbf{k}}(t_1 - t_2)}. \quad (1.6)$$

As this depends only on the difference between the times t_1 and t_2 we may perform a Fourier transform to get

$$G_0(\omega, \mathbf{k}) = \frac{1}{\omega - \xi_{\mathbf{k}} + i\eta}, \quad (1.7)$$

where $\eta > 0$ is an infinitesimal regularization factor which is sent to zero at the end of the calculation and which appears due to the step function in (1.6). The corresponding advanced Green's function is found by replacing $i\eta$ by $-i\eta$.

The above however is only valid for a non-interacting system. To take into account interactions one introduces the self-energy $\Sigma(\omega, \mathbf{k})$. This quantity

²In principle the dispersion and operators could of course also depend on spin but for simplicity we ignore this dependence here.

contains all information about interactions with the system. The full, renormalized Green's function, including interactions, is then given by the Dyson equation

$$G(\omega, \mathbf{k}) = \frac{1}{G_0(\omega, \mathbf{k})^{-1} - \Sigma(\omega, \mathbf{k})}. \quad (1.8)$$

Hence, once the self-energy is computed, one has access to the full Green's function from which many physical quantities can be generated (for example the density of states is proportional to the imaginary part of the advanced Green's function[8]). To evaluate the self-energy, however, it is often necessary to employ different approximations. We shall discuss a perturbative approach in the next section.

Before moving on to the next section let us quickly note that the above discussion was in the limit of zero temperature. To obtain the equivalent results at finite temperatures one performs a Wick rotation $t \rightarrow -i\tau$, where the "imaginary time" τ is now defined on the finite interval $[0, \beta]$ with β denoting the inverse temperature. In this case one has to replace Fourier transforms by Fourier sums but the results presented above remain correct as long as one also replaces $\omega + i\eta$ by $i\omega_n$, where

$$\omega_n = \begin{cases} \frac{2n\pi}{\beta} & \text{bosons} \\ \frac{(2n+1)\pi}{\beta} & \text{fermions} \end{cases}, \quad (1.9)$$

with $n \in \mathbb{Z}$, are Matsubara frequencies. An alternative representation is to keep using real frequencies ω . In that case the (retarded) Green's function becomes somewhat more complicated and is given by

$$G_0(\omega, \mathbf{k}) = \frac{1}{\mathcal{Z}} \sum_{m,n} \frac{|\langle E_n | a_{\mathbf{k}}^\dagger | E_m \rangle|^2}{\omega - (\tilde{E}_n - \tilde{E}_m) + i\eta} \left(e^{-\beta\tilde{E}_m} - \zeta e^{-\beta\tilde{E}_n} \right). \quad (1.10)$$

Here β is the inverse temperature and E_n and \tilde{E}_n are defined through

$$H|E_n\rangle = E_n|E_n\rangle, \quad (1.11a)$$

$$(H - \mu N)|E_n\rangle = \tilde{E}_n|E_n\rangle, \quad (1.11b)$$

where μ is the chemical potential and N is the number operator. Finally

$$\mathcal{Z} = \sum_n e^{-\beta\tilde{E}_n}, \quad (1.12)$$

is the grand canonical partition function and

$$\zeta = \begin{cases} 1 & \text{bosons,} \\ -1 & \text{fermions,} \end{cases} \quad (1.13)$$

specifies the spin-statistics.

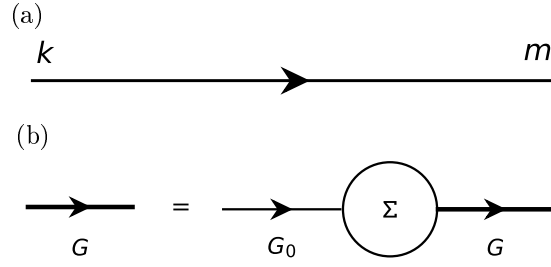


Figure 1.1: Diagrammatic representation of the contraction $\overline{A_k(t_n)A_m^\dagger(t_j)}$ and (b) diagrammatic representation of the Dyson equation (1.8). The thick line corresponds to the renormalized Green's function G , while the thin lines denote the bare Green's function G_0 .

1.1.2 Feynman diagrams

From the definition of the n -body Green's function (1.3) it is clear that it is necessary to evaluate the time-ordered product of several operators. To do this it is useful to use Wick's theorem. Wick's theorem states that the time-ordered product of n operators A_j , $j = 1 \dots n$ is given by

$$T(A_1 \dots A_n) =: A_1 \dots A_n : + \text{All possible contractions.} \quad (1.14)$$

Here the operators can be either fermionic or bosonic, and creation or annihilation operators. Moreover $: A_1 \dots A_n :$ denotes normal-ordering which places all annihilation operators to the right while a contraction of two operators is defined as

$$\overline{A_k(t_n)A_j(t_m)} = \langle T[A_k(t_n)A_j(t_m)] \rangle. \quad (1.15)$$

The usefulness of Wick's theorem thus lies in the possibility of rewriting time-ordered products of several operators as the sum of products of one-body Green's functions. To further simplify calculations one moreover introduces a graphical representation such that contractions are denoted by a solid line as shown in Figure 1.1(a).

To include interactions we write the full Hamiltonian as

$$H = H_0 + H_{\text{int}}, \quad (1.16)$$

with H_0 denoting the free part and H_{int} denoting the interactions. We then introduce the time-evolution operator $\mathcal{U}(t, t_0)$ as the formal solution to the interaction picture Schrödinger equation

$$i \frac{d}{dt} |\psi\rangle_I = H_{\text{int}}(t) |\psi\rangle_I. \quad (1.17)$$

According to the Dyson formula the time-evolution operator at zero temperature is then given by

$$\mathcal{U}(t, t_0) = T \exp \left(-i \int_{t_0}^t dt' H_{\text{int}}(t') \right), \quad (1.18)$$

where the time-ordering of the exponential is defined through its Taylor expansion. From this it can be shown that the full Green's function is given by

$$G(jt; j't') = -i \frac{\left\langle T \left(\mathcal{U}(\infty, -\infty) a_j(t) a_{j'}^\dagger(t') \right) \right\rangle_0}{\langle \mathcal{U}(\infty, -\infty) \rangle_0}, \quad (1.19)$$

where $\langle \dots \rangle_0$ denotes that the averaging is with respect to the free Hamiltonian H_0 . Expanding (1.19) in the interaction thus gives a perturbative way of calculating the full Green's function. Iterating the Dyson equation (1.8) likewise provides a perturbative method of finding the self-energy. As all the equations above contain time-ordered products of operators, Wick's theorem is again very useful. Like in the free case it is furthermore helpful here to introduce some diagrammatic notation. Contractions are then again denoted by a line and vertices by dots or simply by a different type of line. It should be noted however that the notation can vary depending on the theories one considers. Once the diagrams for a particular expansion have been drawn there exists a set of so-called Feynman rules that allows one to translate the diagrams into equations. As these rules also vary from theory to theory we shall refrain from citing them here and instead refer to suitable textbooks[1, 2, 4, 9]. The Feynman rules used in this thesis will be specified when we draw the relevant diagrams.

1.1.3 Functional representation

An alternative way of presenting the above is through generating functionals. We shall again skip details that can be found in various textbooks[1, 2, 3]. To begin our discussion we consider a general theory described by the action $S[\Phi]$, where, following the presentation in [1], Φ is a superfield which can contain fermionic or bosonic degrees of freedom. The partition function (with suitable normalisation) is then given by the path integral

$$Z = \int \mathcal{D}\Phi e^{-S[\Phi]}. \quad (1.20)$$

The n-body Green's function defined in (1.3) can be written as³

$$\langle \Phi_{\alpha_1} \dots \Phi_{\alpha_n} \rangle = \frac{1}{Z} \int \mathcal{D}\Phi e^{-S[\Phi]} \Phi_{\alpha_1} \dots \Phi_{\alpha_n}, \quad (1.21)$$

³In a similar way $\langle \dots \rangle_0$ appearing in (1.19) can be defined with functional integrals by replacing the action by its free counterpart $S_0[\Phi]$.

where the indices are superlabels containing both frequency and momentum. If we now define

$$\mathcal{G}[J] = \frac{1}{Z} \int \mathcal{D}\Phi e^{-S[\Phi] + \int_{\alpha} J_{\alpha} \Phi_{\alpha}}, \quad (1.22)$$

where \int_{α} denotes integration over the superlabels and J is called a source term, we see that the n-body Green's functions are given by the functional differentiation

$$\langle \Phi_{\alpha_1} \dots \Phi_{\alpha_n} \rangle = \left. \frac{\delta^n \mathcal{G}[J]}{\delta J_{\alpha_1} \dots \delta J_{\alpha_n}} \right|_{J=0}. \quad (1.23)$$

$\mathcal{G}[J]$ is called the generating functional for the Green's functions.

We finally note that, analogously, it is possible to define generating functionals for higher order vertices through expectation values of more fields. In particular we will be interested in the one-line irreducible vertices with n external legs below. These are then found from the generating functional $\Gamma[\bar{\Phi}]$ of one-line irreducible vertices which is defined through the Legendre transform

$$\Gamma[\bar{\Phi}] = \int_{\alpha} J_{\alpha}[\bar{\Phi}] \bar{\Phi}_{\alpha} - \mathcal{G}_c[[J[\bar{\Phi}]]] + \frac{1}{2} \int_{\alpha} \int_{\beta} \bar{\Phi}_{\alpha} [\mathbf{G}_0]_{\alpha\beta}^{-1} \bar{\Phi}_{\beta}, \quad (1.24)$$

with \mathbf{G}_0 being a matrix in the space of superlabels. $\Gamma[\bar{\Phi}]$ depends on the superfield $\bar{\Phi}$, defined as

$$\bar{\Phi}_{\alpha} = \langle \Phi_{\alpha} \rangle = \frac{\delta \mathcal{G}_c[J]}{\delta J_{\alpha}}. \quad (1.25)$$

Here $\mathcal{G}_c[J]$ denotes the generating functional of the connected Green's functions which is given by

$$\mathcal{G}_c[J] = \ln \frac{\int \mathcal{D}\Phi e^{-S[\Phi] + \int_{\alpha} J_{\alpha} \Phi_{\alpha}}}{\int \mathcal{D}\Phi e^{-S_0[\Phi]}}. \quad (1.26)$$

The connected diagrams are diagrammatically those expressions that are not split into two separate diagrams. It can be shown that the denominator in Equation (1.19) cancels out all disconnected diagrams (that is, those diagrams that consist of two separate diagrams) such that only the connected diagrams remain. Thus only considering the connected diagrams avoids a redundancy in the perturbation expansion. Once the generating functional $\Gamma[\bar{\Phi}]$ is obtained, the one-line irreducible vertices with n external legs is given by

$$\Gamma_{\alpha_1 \dots \alpha_n}^{(n)} = \left. \frac{\delta^n \Gamma[\bar{\Phi}]}{\delta \bar{\Phi}_{\alpha_1} \dots \delta \bar{\Phi}_{\alpha_n}} \right|_{\bar{\Phi}=0}, \quad (1.27)$$

as before. The one-line irreducible vertex with n external legs is shown in Figure 1.2. The name one-line irreducible means that none of the diagrams which

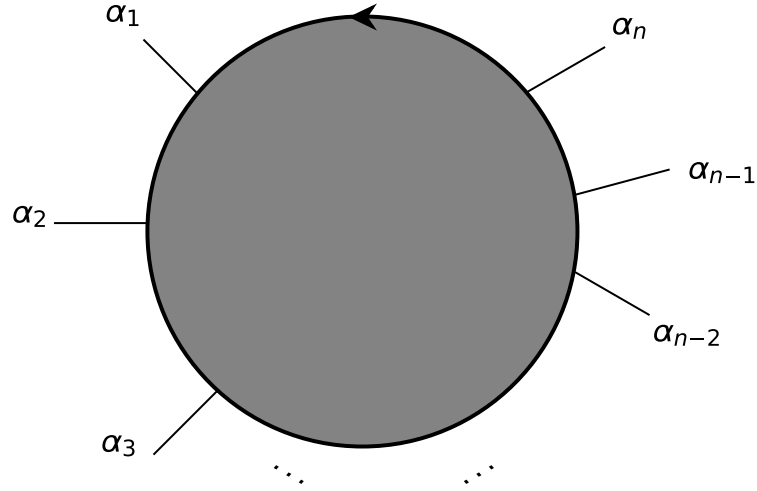


Figure 1.2: Diagrammatic representation of the one-particle irreducible vertex with n external legs given in Equation (1.27).

contribute to the vertices can be cut into two by cutting a single propagatorline in the diagram. Similarly two-line irreducible diagrams are those that cannot be cut into two by cutting two lines etc. For details we refer to [1] but let us just note that for $n = 2$ the one-line irreducible vertex defined above reduces to the self-energy.

1.1.4 Skeleton equations

In classical field theories Noether's theorem tells us that a continuous symmetry of the action implies that the system has a conserved current[9, 10]. Similarly continuous symmetries of the integral of generating functionals leads, by functional differentiation, to equations relating vertices of different order to each other[1, 9]. These equations are called skeleton or Dyson-Schwinger equations. To see how this works we shift the field in our expression for the generating functional (1.22) viz. $\Phi \rightarrow \Phi + \Delta$ and expand to first order in Δ . Doing this, using that the measure is invariant under the infinitesimal shift of the fields, yields[1]

$$\left(\zeta_\alpha J_\alpha - \frac{\delta S}{\delta \Phi_\alpha} \left[\frac{\delta}{\delta J} \right] \right) \mathcal{G}[J] = 0, \quad (1.28)$$

where ζ_α specifies the statistics of the superlabel α such that

$$\zeta_\alpha = \begin{cases} 1 & \text{if } \Phi_\alpha \text{ is bosonic,} \\ -1 & \text{if } \Phi_\alpha \text{ is fermionic.} \end{cases} \quad (1.29)$$

By taking further derivatives of this it is possible to derive relations between different order vertices. These skeleton equations will, together with a suitable truncation, be used to close the infinite hierarchy of functional renormalization group flow equations (see Section 1.2) in Chapter 2. In particular we will need

the skeleton equations for a mixed Fermi-Bose theory of fermions interacting via a real bosonic field through a Yukawa-type interaction, see Chapter 2. These are derived in [1] and are given by

$$\frac{\delta\Gamma}{\delta\phi_{\bar{K}\sigma}} - i \int_K \left[\bar{\psi}_{K+\bar{K},\sigma} \psi_{K\sigma} + \frac{\delta^2\mathcal{G}_c}{\delta\bar{j}_{K\sigma}\delta j_{K+\bar{K},\sigma}} \right] = 0, \quad (1.30a)$$

$$\frac{\delta\Gamma}{\delta\psi_{K\sigma}} - i \int_{\bar{K}} \left[\zeta \bar{\psi}_{K+\bar{K},\sigma} \phi_{\bar{K}\sigma} + \frac{\delta^2\mathcal{G}_c}{\delta j_{K+\bar{K},\sigma} \delta J_{-\bar{K}\sigma}} \right] = 0, \quad (1.30b)$$

$$\frac{\delta\Gamma}{\delta\bar{\psi}_{K\sigma}} - i \int_{\bar{K}} \left[\psi_{K-\bar{K},\sigma} \phi_{\bar{K}\sigma} + \frac{\delta^2\mathcal{G}_c}{\delta\bar{j}_{K-\bar{K},\sigma} \delta J_{-\bar{K}\sigma}} \right] = 0, \quad (1.30c)$$

where ϕ denotes the real bosonic field and ψ and $\bar{\psi}$ denote the fermionic fields. Moreover j and J are the source terms of the fields $\bar{\psi}$ and ϕ respectively, and we have again used the generating functional of the connected Green's functions \mathcal{G}_c . Finally Γ is the generating functional of irreducible vertices, introduced in the previous section. For more details and derivations we again refer to the literature[1, 9].

1.2 Functional Renormalization Group

In the last section we discussed, mainly, perturbative techniques to solve problems in field theories. However, in condensed matter, there are several examples of systems where such approaches are not permissible. For example for strongly coupled systems, an example of which will be considered in Chapter 2, there is simply no small parameter in which one can perform perturbation theory and whilst it is often possible to introduce such a variable by hand, as, for instance, in a $1/N$ expansion, such approaches also sometimes break down. Indeed as we shall see the system considered in Chapter 2 provides an example of this. In these cases a non-perturbative approach is needed. One such approach is the functional renormalization group (FRG) which will be introduced in this section. A complete introduction is, again, beyond the scope of this work and we will instead refer to other sources such as References [1, 11].

The FRG is a generalisation of the Wilsonian renormalization group developed by Wilson and collaborators[12, 13, 14, 15, 16, 17, 18]. While the Wilsonian renormalization group can be reproduced from the FRG it is also applicable in cases where the Wilsonian renormalization group is not used. In it a cutoff Λ is introduced in the bare propagator such that G_0 is replaced by a propagator which depends on the cutoff

$$G_{0,\Lambda}^{-1} = G_0^{-1} - R_\Lambda, \quad (1.31)$$

where R_Λ is a cutoff dependent regulator. The cutoff is usually taken to be some infrared cutoff, which disallows propagation below some energy scale, but

can in principle also be taken to be a physical parameter such as the magnetic field[19], out-scattering rate[20], etc. Common for any cutoff is the requirement that, as the cutoff is removed, the physical theory is recovered such that

$$G_{0,\Lambda} \rightarrow G_0, \quad \Lambda \rightarrow 0. \quad (1.32)$$

Moreover when the cutoff becomes large enough we require that the Gaussian propagator G_0 is suppressed. That is

$$G_{0,\Lambda} \rightarrow 0, \quad \Lambda \rightarrow \infty. \quad (1.33)$$

Let us point out that this latter condition implies that, as the cutoff is increased, the generating functional of the one-line irreducible vertices approaches the non-Gaussian part of the action, that is the interaction part. In this thesis we will exclusively be working with a sharp multiplicative cutoff in momentum which in its general form is

$$G_{0,\Lambda}(\mathbf{k}) = \Theta(|\mathbf{k}| - \Lambda)G_0(\mathbf{k}). \quad (1.34)$$

This type of regulator clearly satisfies (1.32) and (1.33) and is mainly useful for analytic calculations. For numerics it can often be more convenient to pick a regulator which is more smooth[21, 22, 23, 24].

Once the cutoff is introduced it is possible to write down a formally exact flow equation for the functionals. Many different formulations exist but the one we shall use uses the generating functionals of the one-line irreducible vertices [see also Equation (1.24)]. The formally exact flow equation for the (cutoff dependent) generating functional Γ_Λ of the one-particle irreducible vertices is then given by[25, 26]

$$\partial_\Lambda \Gamma_\Lambda = \frac{1}{2} \text{Str} \left(\frac{\partial_\Lambda R_\Lambda}{\Gamma_\Lambda^{(2)} + R_\Lambda} \right), \quad (1.35)$$

where $\Gamma_\Lambda^{(2)}$ denotes the second derivative of Γ_Λ with respect to the fields and Str is a supertrace over all degrees of freedom[8]. For the derivation of this equation we refer to the literature[1]. This equation is formally exact in that a solution would, in the limit $\Lambda \rightarrow 0$, yield the exact properties of the system considered. However, to solve it, it is almost always necessary to introduce certain approximations. Several different schemes exist in which these approximations can be implemented but the main two are the derivative expansion in which the generating functionals are expanded in gradients of the fields[22, 27, 28], and the vertex expansion[29]. As we will be using the latter we will simply refer to the literature for a discussion of the derivative expansion and turn instead to the vertex expansion. Here we expand the generating functional of the one-line irreducible vertices with respect to the fields using the functional Taylor expansion

$$\Gamma[\bar{\Phi}] = \sum_{n=0}^{\infty} \frac{1}{n!} \int_{\alpha_1} \dots \int_{\alpha_n} \Gamma_{\alpha_1 \dots \alpha_n}^{(n)} \bar{\Phi}_{\alpha_1} \dots \bar{\Phi}_{\alpha_n}. \quad (1.36)$$

Substituting this into Equation (1.35) and comparing terms that contain the same number of fields, one then obtains equations that relate the flow of the (cutoff dependent) one-line irreducible vertices with a certain numbers of external legs to one-line irreducible vertices with a different number of external legs. These equations will only contain a finite number of vertices and so can in principle be solved. However, the different equations are all coupled and moreover integro-differential equations so in practice a solution is usually complicated. For example the flow equation for the two-legged one-line irreducible vertex (the self-energy) will depend on the three- and four-legged one-line irreducible vertices, whilst the flow equation for the three-legged one-line irreducible vertex will in turn depend on the three-, four-, and five-legged one-line irreducible vertices. This hierarchy, in principle, continues to infinity and so has to be truncated at some order. For most practical purposes it is sufficient to truncate at the level of the four-legged one-line irreducible vertex but the truncation strategy may differ if it is possible to draw on some prior physical insight. Indeed in Chapter 2 we will truncate the flow already at the level of the three-legged vertices. This will be justified using results obtained with other methods.

1.3 Fermi liquid theory

Fermi liquid theory, originally developed by Landau[5, 30, 31] to explain the behaviour of liquid ${}^3\text{He}$ [32, 33, 34], has been immensely successful in explaining a wide range of phenomena including electron interactions in metals. As this thesis will be dealing with exactly electron interactions in a metal both within regimes where Fermi liquid theory is valid and where it breaks down, we will end this introductory chapter with a brief review of this theory. For details we will again refer to the literature[2, 4, 5, 30, 31].

Fermi liquid theory is based on the concept of adiabatic continuity. One starts with a non-interacting ground state and then adiabatically turns on interactions. The elementary excitations of the non-interacting ground state are then approximate excitations of the interacting ground state, that is the excitations of the interacting ground state can be labelled by the same quantum numbers as the excitations of the non-interacting ground state. This then means that the interacting Green's function takes the same form as the non-interacting Green's function [see Eq. (1.7)] and is expected to have similar thermodynamic properties (although see Chapter 3), albeit with renormalized parameters such as a renormalized mass and velocity. These excitations are called quasi-particles. The quasi-particles will have the same spin-statistics

as the free elementary excitations of the non-interacting system⁴ but will be damped. For the concept to make sense it is then essential for this damping to be small. In particular defining the distance to the Fermi surface as $\xi_{\mathbf{k}} = E_{\mathbf{k}} - E_{\mathbf{k}_F}$, we note that $1/|\xi_{\mathbf{k}}|$ is the minimal time required to create a quasi-particle. For Fermi liquid theory to be valid we must thus require that the lifetime of quasi-particles $\tau_{\mathbf{k}}$ satisfies

$$\frac{1}{\tau_{\mathbf{k}}} \ll |\xi_{\mathbf{k}}|, \quad (1.37)$$

as we approach the Fermi surface. Notice that there is no requirement about the damping of the quasi-particles far from the Fermi surface. In three dimensions it can be shown, using energy conservation, the Pauli principle and phase-space arguments[5, 30, 31], that at zero temperature

$$\frac{1}{\tau_{\mathbf{k}}} = \mathcal{O}((|\mathbf{k}| - k_F)^2), \quad (1.38)$$

where k_F is the Fermi momentum. Because we may expand close to the Fermi surface

$$\xi_{\mathbf{k}} = v_F(|\mathbf{k}| - k_F) + \mathcal{O}((|\mathbf{k}| - k_F)^2), \quad (1.39)$$

with

$$v_F = v_{\mathbf{k}_F} = \nabla_{\mathbf{k}} E_{\mathbf{k}}|_{\mathbf{k}=\mathbf{k}_F}, \quad (1.40)$$

denoting the Fermi velocity, and where we have assumed a regular Fermi surface, we see that the criterion (1.37) is always satisfied close enough to the Fermi surface.

Consider now two quasi-particle states labelled by their momenta and spin close to a (for convenience circular) Fermi surface as shown in Figure 1.3. Unlike the non-interacting case the energy is not a simple linear combination of the single-particle energies and we must include interactions between quasi-particles. The effect of these interactions is phenomenologically to alter the distribution of quasi-particles by an amount $\delta n_{\mathbf{k}\sigma} = n_{\mathbf{k}\sigma} - n_{\mathbf{k}\sigma,0}$, with $n_{\mathbf{k}\sigma}$ and $n_{\mathbf{k}\sigma,0}$ denoting the distribution of interacting and free particles respectively (the latter is of course simply given by a step function at zero temperature). Thus the energy is

$$E = E_0 + \sum_{\mathbf{k}\sigma} E_{\mathbf{k}} \delta n_{\mathbf{k}\sigma} + \frac{1}{2V} \sum_{\substack{\mathbf{k}\mathbf{k}' \\ \sigma\sigma'}} f_{\sigma\sigma'}(\mathbf{k}, \mathbf{k}') \delta n_{\mathbf{k}\sigma} \delta n_{\mathbf{k}'\sigma'} + \mathcal{O}(\delta n_{\mathbf{k}}^3), \quad (1.41)$$

⁴Fermi liquid theory is usually only applied to fermionic systems, but lately there have been examples of bosonic systems which can be said to exhibit similar behaviour. Such ‘‘Bose liquids’’ are then defined around an analogue of a Fermi surface, where the energy dispersion has a minimum. For more details see for example References [35], [36], and [37].

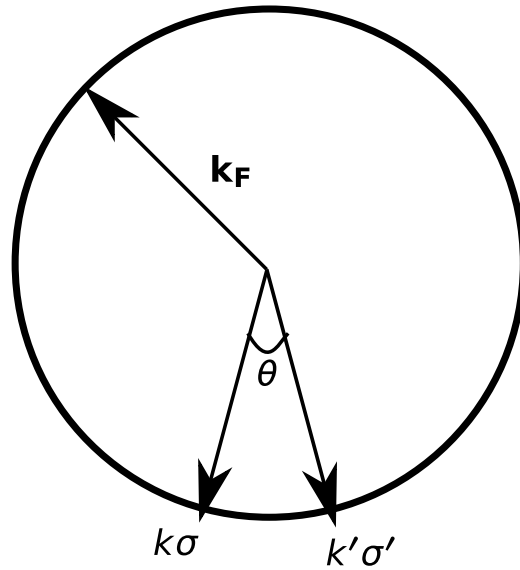


Figure 1.3: An example of a circular Fermi surface with two states separated by an angle θ .

where $f_{\sigma\sigma'}(\mathbf{k}, \mathbf{k}')$ is a Landau function. Close to the Fermi surface these Landau functions become only dependent on the angle separating the momenta of the two quasi-particle states such that they may be expanded in Legendre polynomials. Making the coefficient of such an expansion dimensionless finally yields Landau parameters F_l ($l = 0, 1, \dots$). There are several of these which take into account, phenomenologically, the interaction between quasi-particles. Knowing the Landau parameters one can then deduce various physical quantities such as the renormalized mass, compressibility, sound velocity, spin susceptibility, etc.

The discussion above was all based on a phenomenological approach. To quantify this and introduce some terms that will be used later it is useful to discuss also the microscopic basis for Fermi liquid theory which was developed later (see for example [38]). First of all we note that the excitations in D dimensions are quasi-particles above a sharp $(D - 1)$ -dimensional manifold in momentum space defined as the surface where the energy of excitations changes sign, that is when

$$E_{\mathbf{k}_F} - \mu + \Sigma(0, \mathbf{k}_F) = 0, \quad (1.42)$$

where μ is again the chemical potential. This surface, which thus separates the occupied from the unoccupied states, is the Fermi surface and the solution \mathbf{k}_F to (1.42) is the Fermi momentum. Consider now the Green's function as written in Eq. (1.8) but dividing the self-energy into its real and imaginary parts. Then

$$G(\omega, \mathbf{k}) = \frac{1}{\omega - [\xi_{\mathbf{k}} + \text{Re}\Sigma(\omega, \mathbf{k})] - i\text{Im}\Sigma(\omega, \mathbf{k})}. \quad (1.43)$$

If we further consider the spectral function, which is a measure of how well an excitation can be described as being non-interacting (this becomes obvious when we give the form of the spectral function for a free particle), we find that

$$\begin{aligned} A(\omega, \mathbf{k}) &= -\frac{1}{\pi} \text{Im}G(\omega + i\eta, \mathbf{k}) \\ &= -\frac{1}{\pi} \frac{\text{Im}\Sigma(\omega, \mathbf{k})}{[\omega - \xi_{\mathbf{k}} - \text{Re}\Sigma(\omega, \mathbf{k})]^2 + [\text{Im}\Sigma(\omega, \mathbf{k})]^2}, \end{aligned} \quad (1.44)$$

where we recall that $\eta > 0$ is a positive infinitesimal. The spectral function as a function of the frequency thus takes the form of a Lorentzian centred around $\tilde{\xi}_{\mathbf{k}} = \xi_{\mathbf{k}} + \text{Re}\Sigma(\omega, \mathbf{k})$ and with a width of

$$\frac{1}{2\tau_{\mathbf{k}}} = -Z_{\mathbf{k}} \text{Im}\Sigma(\tilde{\xi}_{\mathbf{k}}, \mathbf{k}), \quad (1.45)$$

where

$$Z_{\mathbf{k}} = \frac{1}{1 - \left. \frac{\partial}{\partial \omega} \text{Re}\Sigma(\omega, \mathbf{k}) \right|_{\omega=\tilde{\xi}_{\mathbf{k}}}}, \quad (1.46)$$

is the quasi-particle residue. At $\mathbf{k} = \mathbf{k}_{\mathbf{F}}$ it measures the discontinuity in the momentum distribution at the Fermi momentum. A vanishing quasi-particle residue at the Fermi surface ($\tilde{\xi}_{\mathbf{k}_{\mathbf{F}}} = 0$) signals a destruction of the Fermi liquid state. $\tau_{\mathbf{k}}$ can furthermore be identified as the quasi-particle life-time. The quasi-particle residue on the Fermi surface (which we simply denote by Z) may also be defined in an alternative way through an expansion of the self-energy around the Fermi surface. Indeed such an expansion may be written as

$$\Sigma(\omega, \mathbf{k}) = \Sigma(0, \mathbf{k}_{\mathbf{F}}) + (1 - Z^{-1}) i\omega - (1 - Y^{-1}) \tilde{\xi}_{\mathbf{k}} + \dots, \quad (1.47)$$

such that we see that the quasi-particle residue on the Fermi surface acts as a renormalization of the frequency-dependent part of the self-energy. In this expansion we have also defined a second renormalization parameter Y , which renormalizes the momentum dependence of the self-energy and is defined through this expansion, although we may also define it for momenta away from the Fermi surface in an analogous way to Z . A large part of this thesis will be devoted to calculating Z and Y .

Returning to the spectral function we note that, for a free particle with a Green's function given by (1.7), it follows from the Dirac identity

$$\lim_{\eta \rightarrow 0^+} \frac{1}{x \pm i\eta} = \mp i\pi\delta(x) + \mathcal{P}\frac{1}{x}, \quad (1.48)$$

where \mathcal{P} stands for the principal part, that the spectral function would become a δ -function centred around the unrenormalized dispersion. For the concept of a quasi-particle to be well-defined one should therefore require that the damping fulfils $1/\tau_{\mathbf{k}} \ll |\tilde{\xi}_{\mathbf{k}}|$ as we approach the Fermi surface. This is of course the same criterion as (1.37) but obtained in a different way. Microscopically it corresponds to a sharp peak in the spectral function and is the defining property of a Fermi liquid. For a normal Fermi liquid in three dimensions, and in fact for all dimensions $2 < D \leq 3$, it can be shown that (we refer to textbooks such as [4] and [5] for the derivation)

$$\text{Im}\Sigma(\omega, \mathbf{k}_{\mathbf{F}}) \propto -(\omega^2 + \pi^2 T^2). \quad (1.49)$$

At zero temperature it then follows that

$$1/\tau_{\mathbf{k}} \propto (|\mathbf{k}| - k_F)^2, \quad (1.50)$$

which is exactly Equation (1.38). Thus the criterion (1.37) is always satisfied close enough to the Fermi surface where

$$\tilde{\xi}_{\mathbf{k}} \sim (|\mathbf{k}| - k_F), \quad (1.51)$$

as we discussed earlier. Let us here note that the condition,

$$\text{Im}\Sigma(\omega, \mathbf{k}_{\mathbf{F}}) \propto \omega^2, \quad (1.52)$$

at $T = 0$, while sufficient to have Fermi liquid behaviour, is not necessary. Indeed the condition (1.37) is clearly satisfied whenever the self-energy has the following imaginary part[39]

$$\text{Im}\Sigma(\omega, \mathbf{k}_{\mathbf{F}}) \propto \omega^{1+a}, \quad (1.53)$$

where $a > 0$. Indeed it is known[39] that in two dimensions one typically finds

$$\text{Im}\Sigma(\omega, \mathbf{k}_{\mathbf{F}}) \propto \omega^2 \ln |\omega|, \quad (1.54)$$

while in dimensions $1 < D < 2$

$$\text{Im}\Sigma(\omega, \mathbf{k}_{\mathbf{F}}) \propto \omega^D. \quad (1.55)$$

Systems with self-energies that satisfy these two relations still have well-defined quasi-particles and can be described within Fermi liquid theory.

Moreover we should stress that the above conditions only make statements about the quasi-particles close to the Fermi surface. At higher energies the quasi-particles could in principle be damped out, but Fermi liquid theory would still be sufficient to describe the low-energy excitations.

Let us finally note that the breakdown of Fermi liquid theory has been widely discussed in recent years. This has amongst other reasons been motivated by the discovery of non-Fermi liquid behaviour of some high- T_c superconductors and other materials (see for example [40, 41]). In Chapter 2 we will discuss an example of a specific quantum critical point where Fermi liquid theory breaks down.

Chapter 2

The Ising-nematic quantum critical point in two-dimensional metals

2.1 Introduction

The discovery of the presence of nematic order in materials such as the cuprates and ruthenates[42, 43, 44, 45, 46, 47, 48] has led to significant theoretical activity in attempting to understand nematic transitions[49, 50, 51, 52, 53, 54, 55, 56, 57, 58, 59, 60, 61]. Such transitions, in which the rotational order of the lattice is broken while the translational symmetries are preserved, often come with the breakdown of the Fermi liquid theory discussed in Section 1.3. Such “non-Fermi liquids” have themselves been the subject of intense investigations[54, 55, 62, 63, 64, 65, 66, 67, 68, 69, 70].

One way to achieve a nematic transition together with the breakdown of Fermi liquid theory is by coupling a Fermi surface to a gapless bosonic scalar order parameter[54, 55, 65, 71, 72, 73, 74, 75, 76, 77]. Indeed the idea that the Fermi liquid picture breaks down when coupling fermions near a Fermi surface to gapless bosons has been promoted for quite some time[73, 78, 79]. In this chapter we discuss an example of such a system, namely a Pomeranchuk[80] transition of electrons in a two-dimensional metal, into a nematic phase. This is a quantum phase transition where the lattice is distorted in some direction and an example of a nematic phase transition (see Figure 2.1). We consider only the quantum critical point and begin by reviewing the standard approach used to describe quantum criticality of electrons in metals, as developed by Hertz[82] and Millis[83] in the 70’s and 90’s. We then discuss how complications arise in the $1/N$ expansion for this problem and how anomalous dimensions appear. We finally calculate the anomalous dimensions using the FRG. The work presented in this chapter was done with Lorenz Bartosch, Aldo Isidori, and Peter Kopietz, and has been published in [84].

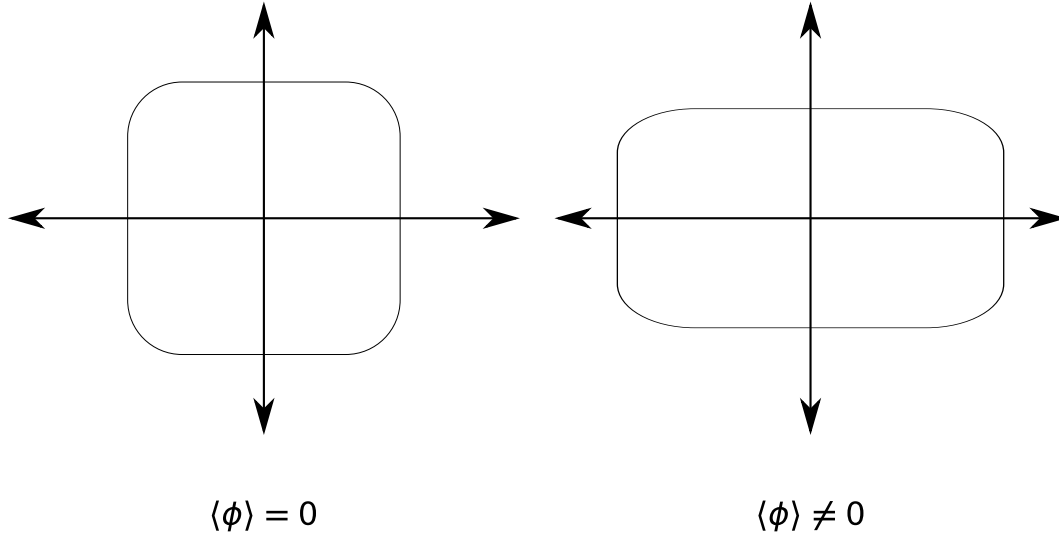


Figure 2.1: An example illustrating a nematic phase transition. When the order parameter vanishes the lattice has rotational symmetry. When the order parameter is turned on such that $\langle \phi \rangle \neq 0$ this symmetry is broken while the translational symmetry is retained. The sign of $\langle \phi \rangle$ governs the direction in which the lattice is distorted.

2.1.1 Hertz-Millis theory

The Hertz-Millis theory[82, 83, 85] has been the canonical approach to describe the quantum critical behaviour of electrons in metals for several years. In it the interaction between the electrons is decoupled via a bosonic Hubbard-Stratonovich transformation. One then ends up with a theory containing both fermionic and bosonic degrees of freedom. The latter are treated using Landau theory and the theory is thus specified by the following action in two dimensions

$$S[\bar{\psi}, \psi, \phi] = S_\psi[\bar{\psi}, \psi] + S_\phi[\phi] + S_{\text{int}}[\bar{\psi}, \psi, \phi], \quad (2.1a)$$

$$S_\psi[\bar{\psi}, \psi] = \int d^{2+1}x \bar{\psi} (\partial_\tau - \xi) \psi, \quad (2.1b)$$

$$S_\phi[\phi] = \int d^{2+1}x \left(\frac{1}{2} (\partial\phi)^2 + \frac{r}{2} \phi^2 + g\phi^4 \right), \quad (2.1c)$$

$$S_{\text{int}}[\bar{\psi}, \psi, \phi] = \int d^{2+1}x \Gamma_0 \bar{\psi} \psi \phi, \quad (2.1d)$$

where ψ and ϕ are fermionic and bosonic fields respectively, Γ_0 is the bare interaction vertex between fermions and bosons, $\xi = E - E_F$, with E_F being the Fermi energy, is the dispersion of electrons and the parameters in the bosonic part of the action are the usual couplings in Landau theory. The integration is performed over two-dimensional space and over time. Notice

that the bosonic part of the action is truncated at the quartic level. This is justified using scaling arguments, see below. In this work we shall be discussing a specific type of phase transition, namely the Ising-nematic phase transition. In this case the bosonic field ϕ will be an Ising-nematic order parameter which does not transfer momentum (if the order parameter is allowed to transfer momentum, spin-density wave instabilities occur[65]) and is non-zero only in the ordered phase. It is thus, in its most general form, given by (see e.g. [54])

$$\phi \sim \int d^2k (\cos k_x - \cos k_y) a_{\mathbf{k}\sigma}^\dagger a_{\mathbf{k}\sigma}, \quad (2.2)$$

where $a_{\mathbf{k}\sigma}^\dagger$ and $a_{\mathbf{k}\sigma}$ are respectively creation and annihilation operators. The theory governing the Ising-nematic quantum critical point is closely related to the theory of a $U(1)$ gauge field interacting with a Fermi surface[86, 87, 88]. Thus, in principle ϕ could also describe an emergent $U(1)$ gauge-field which couples to the Fermi surface. Such models are relevant, for example, in spin-liquids where the spinons can form a “spinon Fermi-surface”[89, 90]. To see how this happens consider a Mott insulator with Hamiltonian

$$H = J \sum_{\langle ij \rangle} \mathbf{S}_i \cdot \mathbf{S}_j, \quad (2.3)$$

where \mathbf{S}_i is the usual spin-operator at site i , J is the exchange coupling, and the summation is performed over nearest neighbours. The emergent gauge symmetry comes from the $U(1)$ gauge invariance of the spinon operators f_i which appear when fractionalising the spin operators as

$$S_i^a = \frac{1}{2} \sum_{\alpha\beta} f_{i\alpha} \sigma_{\alpha\beta}^a f_{i\beta}, \quad (2.4)$$

where $\sigma_{\alpha\beta}^a$ is a component of the vector of spin half Pauli matrices. An other example is in the theory of the half-filled Landau levels where the emergent gauge-field is a Chern-Simons gauge-field used to attach a flux[91]. Gauge theories of this sort have been studied excessively in the past.

Returning to Hertz-Millis theory, in the next step one integrates out the fermionic degrees of freedom. Doing this we end up with a $(2+1)$ -dimensional purely bosonic field theory described by the effective action

$$S_{\text{eff}}[\phi] = \frac{1}{2} \int \frac{d^2k d\omega}{(2\pi)^3} \phi(-\omega, -\mathbf{k}) \left(b_0 \frac{|\omega|}{|\mathbf{k}|} + c_0 k^2 \right) \phi(\omega, \mathbf{k}) + g \int d^2k d\omega \phi(\omega, \mathbf{k})^4, \quad (2.5)$$

where to lowest order $b_0 = c_0 = 1/(4\pi)^1$ and we have performed a Fourier transform. Notice the Landau damping term $|\omega|/|\mathbf{k}|$ which will turn out to

¹In the next section we will extend the theory to contain N flavours of fermions. In this case the right-hand side of b_0 and c_0 is multiplied by N .

be crucial for the dynamics of the system. Indeed if we perform the rescaling $k \rightarrow \Lambda k$, the presence of the Landau damping requires that $\omega \rightarrow \Lambda^3 \omega$, that is the bosonic field has a dynamic exponent of three. To achieve a consistent scaling we then must let $\phi \rightarrow \Lambda^{3/2} \phi$. From this we see that $g \rightarrow \Lambda g$ such that, under this rescaling, the ϕ^4 term is irrelevant in the renormalization group sense². The same is true for the higher order terms which justifies the truncation of the bosonic part of the action (2.1c) and allows one to describe the quantum critical point using a Gaussian theory. A more complete discussion of the scaling can be found in Reference [93]. Because we will be using the FRG which does not rely on the existence of a small parameter, the scaling behaviour and classification into relevant and irrelevant couplings is not crucial to us. In any case we shall see later that such a rescaling is not sufficient in two dimensions and that one should also keep higher order terms in the action. The reason for this is that the gapless electrons give rise to highly singular interactions in both frequency and momenta³. It is therefore better to not integrate out the bosonic degrees of freedom and instead consider a mixed Fermi-Bose theory. Let us finally point out that if one does apply Hertz-Millis theory, scaling arguments yield in two dimensions

$$\Sigma(\omega, \mathbf{k}) \sim -i \text{sgn}(\omega) |\omega|^{2/3}. \quad (2.6)$$

The 2/3 exponent implies non-Fermi liquid behaviour which arises due to fluctuations of the field ϕ . Since this term is more singular than the bare frequency dependence, the renormalized Green's function can thus be written as

$$G(\omega + i\eta, \mathbf{k}) \propto \frac{1}{A|\omega|^{2/3} - \xi_{\mathbf{k}}}, \quad (2.7)$$

where A is a complex constant which depends on the sign of ω and η is a positive infinitesimal. We shall see later that anomalous dimensions modify the 2/3 exponent and the power of the dispersion.

2.1.2 $1/N$ -expansion

The discussion in the previous section was largely based on a scaling analysis of the Hertz-Millis action (2.5). In this section we will review how it is possible to arrive at the same results using a more stringent approach. In particular, as the theory turns out to be strongly coupled, there is no small parameter to do perturbation theory in. Therefore the $1/N$ expansion has often been

²The general scaling dimension of g in D dimensions with a dynamic bosonic critical exponent z_b is $\text{dim}[g] = 4 - D - z_b$ [92]. The result in the main text is reproduced for $D = 2$ and $z_b = 3$.

³It should be noted, however, that this is a special property of two dimensions. In three dimensions, for example, Hertz-Millis theory gives the correct results. The reason for this is that the patch construction discussed later in this section needs to be modified in $D = 3$. Indeed here the patches on opposite sides of the Fermi surface become great circles and the bosonic order parameter no longer couples strongly to the electrons on the Fermi surface.

used[63, 72, 73] to confirm the Hertz-Millis results from the previous section. We shall do the same in this section and then comment on when this approach breaks down[54, 77].

To begin let us return to the mixed Fermi-Bose theory (2.1). Due to the Landau damping, the bosonic fluctuations can only be properly absorbed if their momentum is almost tangent to the Fermi surface[72, 73]. To see this note that, as discussed above, from the Landau damping term in Equation (2.5) it follows that the frequency scales as $\omega \sim |\mathbf{k}|^3$. Because we are only interested in states close to the Fermi surface we expand the dispersion around a point on the Fermi surface

$$\xi_{\mathbf{k}} = E_{\mathbf{k}_F + \mathbf{k}} - E_{\mathbf{k}_F} \approx v_F k_{\parallel} + \frac{k_{\perp}^2}{2m}, \quad (2.8)$$

where k_{\parallel} and k_{\perp} denote the components of momentum parallel and perpendicular to the Fermi surface normal respectively, m denotes the electron mass and v_F is the local Fermi velocity (although note that, if the Fermi surface is not circular, this does not necessarily correspond to the physical Fermi velocity). In principle one should now expand around every point on the Fermi surface. However we now note that, if the fluctuations are not tangent to the Fermi surface, the first term dominates and the energy needed to absorb a fluctuation goes as $v_F |\mathbf{k}| \sim \omega^{1/3}$. On the other hand we saw, in the previous section, that $\Sigma(\omega, \mathbf{k}) \sim \omega^{2/3}$ and so there is a mismatch between the self-energy and the energy required to absorb a fluctuation. This is not the case when the fluctuations are nearly tangent to the Fermi surface in which case the energy needed to absorb the fluctuation instead scales as $|\mathbf{k}|^2 \sim \omega^{2/3}$. This precisely matches the self-energy. We hence conclude that the electrons couple strongly to the bosonic fluctuations when the momentum of the bosonic fluctuations is almost tangent to the Fermi surface. For a closed Fermi surface, in two dimensions, this happens at exactly two patches as illustrated in Figure 2.2. The essential low-energy physics is therefore captured by expanding the dispersion of the electrons near two patches of the Fermi surface. An other way to see this is to notice that the mismatch between the scaling behaviour of k_{\parallel} and k_{\perp} in Equation (2.8) leads, after a renormalization group procedure, to a non-compact Fermi surface consisting of the two patches. We will therefore focus on the two patches of the Fermi surface shown in Figure 2.2 and arrive at[63, 72, 73, 54]

$$\xi_{\mathbf{k}}^{\alpha} = E_{\mathbf{k}_F^{\alpha} + \mathbf{k}} - E_{\mathbf{k}_F^{\alpha}} \approx \alpha k_{\parallel} + k_{\perp}^2, \quad (2.9)$$

where α denotes the patch index, \mathbf{k}_F^{α} is the Fermi momentum corresponding to the patch labelled by α , and k_{\parallel} and k_{\perp} are again the components of momentum parallel and perpendicular to the Fermi surface normal but at a given patch (see also Figure 2.2). The patch index α appears in front of the parallel component of momentum because the Fermi momenta on the two

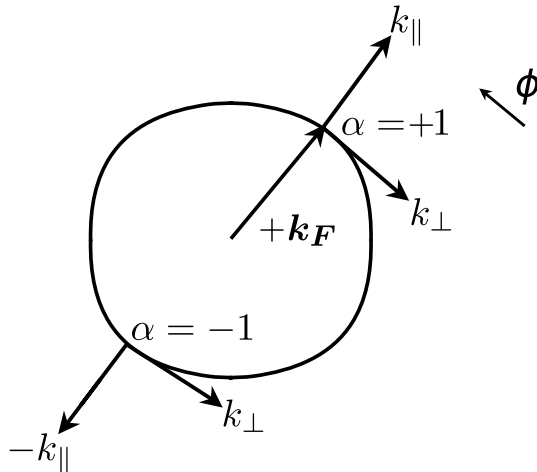


Figure 2.2: This is an illustration of the patch construction. The order parameter couples strongly to two patches on the Fermi surfaces (labelled by $\alpha = \pm 1$) to which it is tangent. A local coordinate system is then defined at each patch with k_{\parallel} denoting the momentum parallel to the Fermi momentum and k_{\perp} denoting the momentum perpendicular to the Fermi momentum.

opposite patches have different signs. The two components of momentum have further been made dimensionless through the rescaling $k_{\parallel} \rightarrow 2mv_F k_{\parallel}$ and $k_{\perp} \rightarrow 2mv_F k_{\perp}$. Finally anticipating that we will, in this section, moreover be discussing the $1/N$ expansion we further introduce N flavours of the electrons (for the theory of the Ising-nematic quantum critical point $N = 2$, corresponding to the two physical spin states). In this approximation we should then sum all fermionic degrees of freedom over both all fermionic flavours and the patch index and we should introduce a cutoff Λ_{\perp} in the perpendicular component of the momentum to take into account the finite size of a patch. Such a cutoff should be proportional to the angular extension of a patch, but as all integrals over perpendicular components of momentum will turn out to be ultraviolet convergent we may send the cutoff to infinity. Let us here remark that there are different ways of regularizing the theory. The low-energy singular behaviour of the theory should however not depend on which regularization is chosen.

With this we can now consider the one-loop contribution to the self-energy shown in Figure 2.3(a) and show that it reproduces the Hertz-Millis result. First let us, however, calculate the polarization at one-loop order. This is simply given by (see, for example, Reference [92] for details)

$$\begin{aligned} \Pi(\omega, \mathbf{k}) &= N \int \frac{d^2q d\Omega}{(2\pi)^3} \frac{1}{-i\eta\Omega + \alpha q_{\parallel} + q_{\perp}^2} \\ &\times \frac{1}{-i\eta(\omega + \Omega) + \alpha(k_{\parallel} + q_{\parallel}) + (k_{\perp} + q_{\perp})^2}, \end{aligned} \quad (2.10)$$

where we use free fermionic propagators with dispersion given in Equation (2.9), rescale frequencies viz. $\omega \rightarrow 2mv_F^2\omega$, and have introduced the positive infinitesimal factor η in the dynamic part of the propagators to take into account the fact that the dynamic part is formally irrelevant under a renormalization group treatment of the action. At the end of the calculation we therefore send η to zero. The polarization is shown in Figure 2.3(b). Because we are only interested in the singular contribution to the polarization we may perform the integrations in whichever order we wish. If we then moreover separate the momentum integration into integrals over q_{\perp} and q_{\parallel} it turns out that it is convenient to perform the latter first. This can be done using the method of residues with the result

$$\Pi(\omega, \mathbf{k}) = \frac{N}{2} \int \frac{dq_{\perp}}{2\pi} \frac{i\alpha}{i\omega - \alpha k_{\parallel} - k_{\perp}^2 - 2q_{\perp}k_{\perp}} \int \frac{d\Omega}{2\pi} [\Theta(\alpha(\omega + \Omega)) - \Theta(\alpha\Omega)]. \quad (2.11)$$

Finally the frequency integration is trivial and equal to $\alpha\omega$ such that only the integration over q_{\perp} remains. This integrand goes as $1/q_{\perp}$ in the ultraviolet and is therefore divergent. It can however be regularized by noticing that we should also be summing over the patch index. Doing this corresponds to adding the same term but with the sign of all parallel components of momentum interchanged. Because the integrand is moreover symmetric under the simultaneous shift of $k_{\perp} \rightarrow -k_{\perp}$ and $q_{\perp} \rightarrow -q_{\perp}$ we see that summing over the patch index simply amounts to symmetrising the integrand with respect to \mathbf{k} [54]. Then the integrand goes as $1/k_{\perp}^2$ in the ultraviolet and the integral is convergent. The final integration can then be performed using the method of residues. The result is

$$\Pi(\omega, \mathbf{k}) = b_0 \frac{|\omega|}{|k_{\perp}|}, \quad (2.12)$$

where $b_0 = N/(4\pi)$ to first order. We see that this is independent of k_{\parallel} . The reason for this is that this component of momentum can be eliminated by performing a shift of momenta in the dispersion. Since, from scaling, we expect $k_{\perp} \gg k_{\parallel}$ (indeed if the parallel and perpendicular components of momentum were not of different orders of magnitude we would not be able to separate the integration over momenta) we thus reproduce the Landau damping form of the bosonic part of the Hertz-Millis action, Equation (2.5).

The fermionic self-energy is now given by[92]

$$\Sigma(\omega, \mathbf{k}) = \frac{-1}{N} \int \frac{d^2q d\Omega}{(2\pi)^3} \frac{1}{c_0 q_\perp^2 + b_0 \frac{|\Omega|}{|q_\perp|}} \frac{1}{-i\eta(\omega - \Omega) + \alpha(k_\parallel - q_\parallel) + (k_\perp - q_\perp)^2}, \quad (2.13)$$

where we have dressed the boson propagator while using the free fermion propagator. Separating, again, the momentum integral into integrals over q_\perp and q_\parallel , we see that the latter is again ultraviolet divergent. This divergence can be regularized by subtracting the self-energy on the Fermi surface. Doing thus the q_\parallel integration can once more be done using the method of residues such that

$$\Sigma(\omega, \mathbf{k}) = \frac{-i}{2N} \int \frac{dq_\perp d\Omega}{(2\pi)^2} \frac{1}{b_0 \frac{|\Omega|}{|q_\perp|} + c_0 q_\perp^2} \text{sgn}(\omega - \Omega). \quad (2.14)$$

Notice that η has dropped out at this stage such that there will be no problem with taking the $\eta \rightarrow 0$ limit. The last two integrations are now standard integrals and can be performed such that we finally find

$$\Sigma(\omega, \mathbf{k}) \sim -i \frac{1}{N} \text{sgn}(\omega) |\omega|^{2/3}, \quad (2.15)$$

which confirms the Hertz-Millis result (2.6). Calculations have also been done at two-loop order[72, 73, 79]. In this case the $\omega^{2/3}$ form of the self-energy was retained and it was found (see also Reference [95]) that, in the limit of large N , the N -dependence of the prefactor of the $\omega^{2/3}$ term becomes

$$\left(\frac{\ln N}{N}\right)^2 \ll 1. \quad (2.16)$$

Because of this and for scaling reasons it was for a long time believed that the theory could be controlled in a $1/N$ -expansion and that the exponent of $2/3$ remained exact at higher loops. We will show in the next section that this is not the whole story, however.

2.1.3 The genus expansion and breakdown of large- N counting

When we did the large- N expansion in the previous section all calculations were done with free fermionic propagators. It turns out that this causes problems when including vertex corrections[77]. To see this note that the frequency in the free fermionic propagator, within the large- N expansion of this problem, always comes with a factor of η . If we therefore send η to zero from the beginning of the calculation, the free fermionic propagator is frequency independent. In that case the integration over frequencies is not well-defined. This manifests itself in divergences in the self-energy. Indeed, whilst we saw in the previous section that η drops out of the self-energy at one-loop order

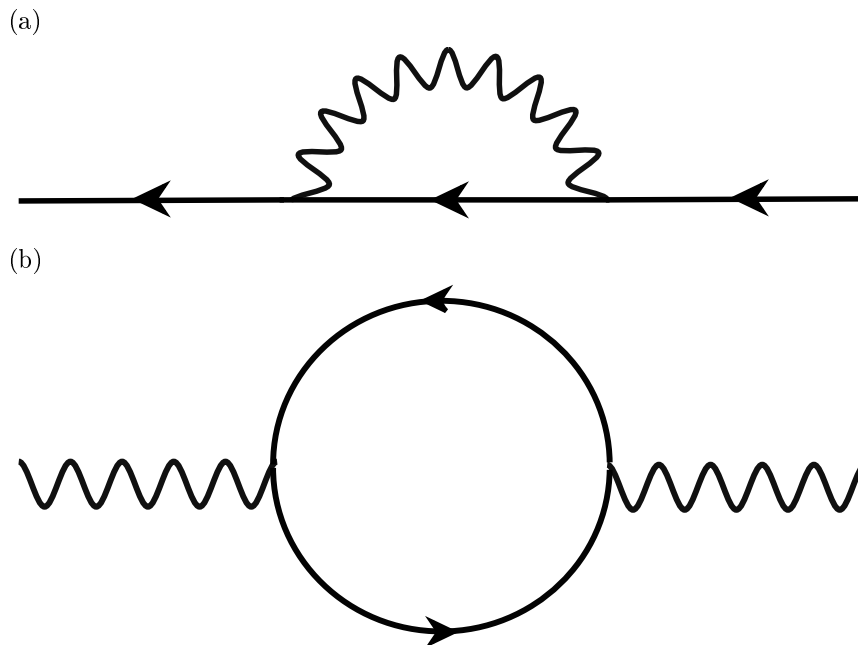


Figure 2.3: (a) One-loop fermionic self-energy and (b) one-loop bosonic self-energy (polarization). The solid lines denote fermionic propagators, while the wavy lines are bosonic propagators. A bare vertex is represented by an intersection of two lines.

this does not happen at higher orders where one encounters divergences as $\eta \rightarrow 0$ [77]. Examples of diagrams that have this kind of behaviour are shown in Figure 2.4. All of the divergences are regularized if one dresses the fermionic propagators by including self-energy corrections such as (2.15). Because, for small frequencies, the one-loop self-energy correction is more singular than the bare frequency part of the fermionic propagator we may replace the latter with the one-loop self-energy which is independent of η . The fermionic propagator then no longer becomes frequency independent as $\eta \rightarrow 0$. The fact that this is the case shows that the divergences obtained in the naive large- N expansion are unphysical.

Replacing the $\eta\omega$ terms in the propagators by (2.15) however not only regularizes the divergences but also comes at the price that it is necessary to modify which order a given diagram is in N . In fact it can be seen from the form of the self-energy that each factor of η should be replaced by a factor of $1/N$ in the final result. A more general scheme for calculating this enhancement of the N -counting, was developed by Lee[77] for a one-patch model. In this scheme diagrams are redrawn using a double-line formalism where bosonic lines are denoted by double-lines symbolising the interaction between two fermions on the Fermi surface and where the lines are not allowed to cross (see Figure 2.5). If one then imagines the diagrams lying on a two-dimensional surface and “glues” sides made from single-lines together, the diagrams form distinct

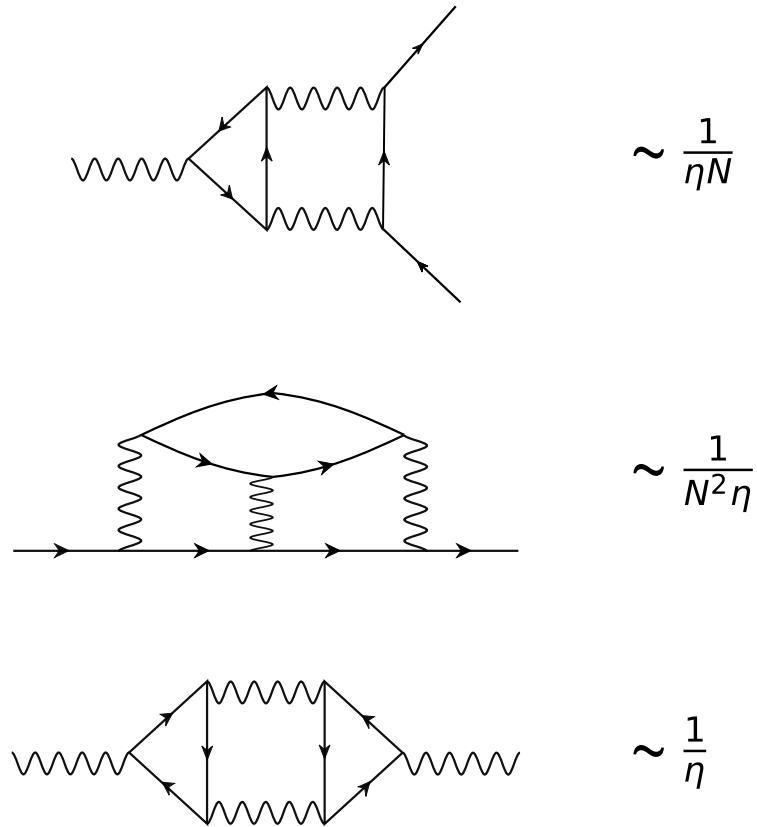


Figure 2.4: *Examples of ill-defined diagrams within the large N expansion in a one-patch model.*

topological surfaces in two dimensions. The enhancement of the N -counting for a certain diagram is then uniquely related to the genus of the surface it forms in this way. Performing such a “genus expansion” leads to a certain class of diagrams. These, so-called planar diagrams, are the ones that can be drawn lying on a flat surface and it was shown by Lee[77], for a one-patch model, that they lead to a breakdown of the $1/N$ -expansion in that all planar diagrams are as important as the one-loop diagrams. Later Metlitski and Sachdev[54] considered the full two-patch model and showed that not only the planar diagrams give rise to a breakdown of the $1/N$ -expansion. The reason for this is that there is a cancellation of curvature terms in the propagator which come with a factor of N . In particular they considered the three-loop diagrams shown in Figure 2.6. They showed that the diagrams contributing to the fermionic self-energy [Figure 2.6(a)] give rise to anomalous dimensions which modify the $\omega^{2/3}$ behaviour of the self-energy. Moreover, they found that the sum of the two Aslamazov-Larkin[94] diagrams [Figure 2.6(b)] are of order $N^{3/2}$. As the one-loop polarization given in Equation (2.12) is only of order N this indicates a breakdown of the $1/N$ -expansion. In the next section we will develop an alternative way of studying this problem and will

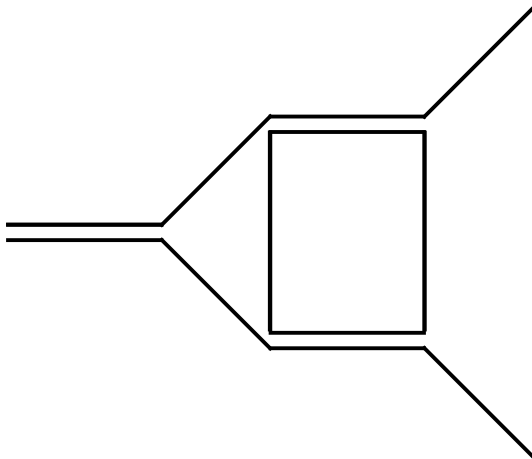


Figure 2.5: *The top diagram of Figure 2.4 drawn in the double-line formalism.*

explicitly calculate the anomalous dimensions found by Metlitski and Sachdev.

Before finishing this introductory section let us mention that there have been attempts at putting the $1/N$ -expansion under control[55, 71]. These attempts have been based on introducing an extra control parameter. For example, it is possible to perform an ϵ -expansion at finite N [71] or one can perform a $1/N$ -expansion, keeping $(z_b - 2)N$, where z_b is the bosonic dynamic exponent, finite[55]. In the latter case the bosonic part of our action should be replaced by

$$S_\phi[\phi] = \frac{1}{2} \int_{\bar{K}} c_0 |\bar{k}_\perp|^{z_b-1} |\phi_{\bar{K}}|^2, \quad (2.17)$$

with $2 < z_b \leq 3$ and where $\int_{\bar{K}} = (\beta V)^{-1} \sum_{\bar{\omega}} \sum_{\bar{\mathbf{k}}}$ denotes a sum over bosonic frequencies and momenta, with $\bar{K} = (i\bar{\omega}, \bar{\mathbf{k}})$ denoting a rescaled (using the same rescaling procedure as for the fermions) dimensionless bosonic $(D+1)$ -momentum in D dimensions. For the Ising-nematic quantum critical point we recall that scaling yields $z_b = 3$ while for example at an antiferromagnetic quantum critical point one would have $z_b = 2$ if this was allowed for. The reason using z_b as a control parameter works, is that it is not expected to be renormalized by a non-local interaction. Indeed it has been checked by Metlitski and Sachdev[54] that this holds true up to at least three-loop order. Using this strategy Mross et al.[55] were able to also calculate the anomalous dimensions discussed above. However, their method relies on being able to extrapolate to $z_b = 3$ at the end of the calculation and whilst both Mross et al. and Metlitski and Sachdev find that anomalous dimensions appear such that the Green's function in Equation (2.7) should be replaced by

$$G(\omega + i\eta, \mathbf{k}) \propto \frac{1}{(A|\omega|^{2/z_b} - \xi_{\mathbf{k}})^{1-\eta_\psi/2}}, \quad (2.18)$$

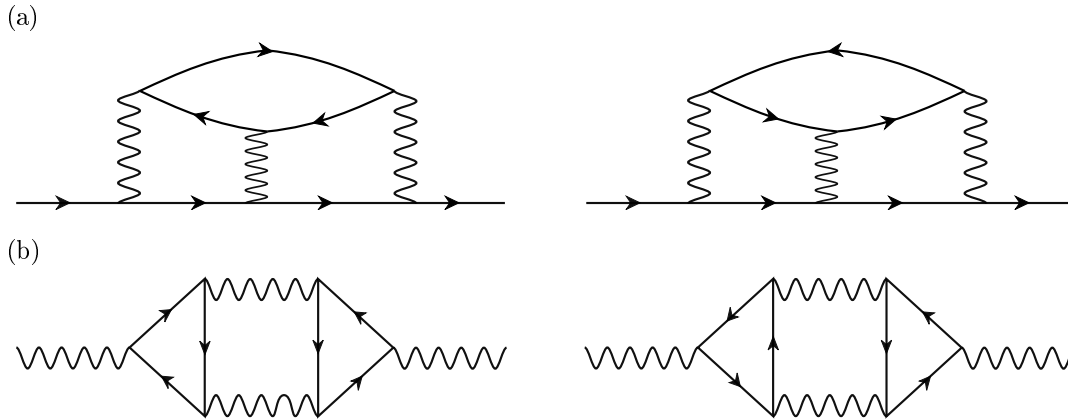


Figure 2.6: *These are the three-loop diagrams identified by Metlitski and Sachdev. (a) is the fermionic self-energy at three loops, while (b) represents the so-called Aslamazov-Larkin contribution to the bosonic self-energy.*

they find different values for the anomalous dimension: $\eta_\psi \approx 0.068$ [54] and $\eta_\psi \approx 0.6$ [55] for the results obtained by Metlitski and Sachdev, and Mross et al. respectively. To obtain the latter we have extrapolated the result of Mross et al. to $z_b = 3$. In the next section we will discuss an alternative scheme to calculate η_ψ which uses the FRG.

2.2 Functional Renormalization Group approach to the Ising-nematic quantum-critical point in two-dimensional metals

We now come to the main part of this chapter. In the previous section we saw that the $1/N$ -expansion breaks down for the theory of a two-dimensional Fermi surface strongly coupled to a bosonic field and that anomalous dimensions appear at three-loop order. Moreover, while there exist attempts at putting the theory under control, we saw that the results for the anomalous dimension vary significantly depending on the method used. We shall therefore in this section develop an alternative way, based on the FRG, of calculating the anomalous dimension η_ψ , defined in Equation (2.18). In contrast to previous work we will explicitly calculate both the anomalous dimension coming from the momentum dependence of the self-energy (which arises at three-loop order) and the anomalous dimension coming from the frequency dependence of the self-energy (which arises at four-loop order[95]). Only the former has been calculated explicitly by previous authors[54, 55] and this is the value we cited at the end of the previous section.

2.2.1 Model

It turns out that the interaction between fermions and bosons is highly singular and it is therefore more convenient not to integrate out the bosonic degrees of freedom from the initial action. Our starting point is hence the mixed Fermi-Bose model given in Equation (2.1) but with rescaled, dimensionless variables, an, in general, momentum dependent interaction between the fermions and bosons, and extended to $2 < z_b \leq 3$ through replacing the bosonic part of the action with Equation (2.17). We finally extend the theory to N flavours and expand the dispersion around two patches on the Fermi surface, as in Equation (2.9). The full action is then given by

$$S[\bar{\psi}, \psi, \phi] = S_\psi[\bar{\psi}, \psi] + S_\phi[\phi] + S_{\text{int}}[\bar{\psi}, \psi, \phi], \quad (2.19a)$$

$$S_\psi[\bar{\psi}, \psi] = - \int_K \sum_{\sigma=1}^N \sum_{\alpha=\pm} (i\omega - \xi_{\mathbf{k}}^\alpha) \bar{\psi}_{K\sigma}^\alpha \psi_{K\sigma}^\alpha, \quad (2.19b)$$

$$S_\phi[\phi] = \frac{1}{2} \int_{\bar{K}} (r_0 + c_0 |\bar{k}_\perp|^{z_b-1}) \phi_{-\bar{K}} \phi_{\bar{K}}, \quad (2.19c)$$

$$S_{\text{int}}[\bar{\psi}, \psi, \phi] = \int_{K_1} \int_{K_2} \int_{\bar{K}_3} \sum_{\sigma=1}^N \sum_{\alpha=\pm} \delta_{K_1, K_2 + \bar{K}_3} \times \Gamma_0^{\bar{\psi}^\alpha \psi^\alpha \phi}(K_1; K_2; \bar{K}_3) \bar{\psi}_{K_1\sigma}^\alpha \psi_{K_2\sigma}^\alpha \phi_{\bar{K}_3}, \quad (2.19d)$$

where again $\xi_{\mathbf{k}}^\alpha$ is given in Equation (2.9), but now with the extra label σ which labels the different electron flavours, r_0 denotes the distance to the quantum critical point (as we will be working at the quantum critical point we will set $r_0 = 0$ in the end), and $\Gamma_0^{\bar{\psi}^\alpha \psi^\alpha \phi}(K_1; K_2; \bar{K}_3)$ is the bare interaction vertex between fermions and bosons. We will normalise the fields such that

$$\Gamma_0^{\bar{\psi}^\alpha \psi^\alpha \phi}(K_1; K_2; \bar{K}_3) = \Gamma_0^\alpha = \begin{cases} 1 & (\text{Ising-nematic}), \\ \alpha & (U(1) \text{ gauge-field}), \end{cases} \quad (2.20)$$

with the upper line holding in the case of the Ising-nematic quantum critical point and the lower line holding for the case where the bosonic field represents a $U(1)$ gauge-field. We shall be focusing on the former and so the bare vertex will be set to unity. We will however renormalize the vertex such that it acquires a frequency- and momentum dependence. As before the integration symbols, furthermore, denote a sum over frequencies and momenta and where we now distinguish between fermionic and bosonic degrees of freedom by putting a bar over the latter as in Equation (2.17). Finally we will be working at zero temperature and in the limit of infinite volume, such that the frequency and momentum sums become integrals.

Apart from the mixed fermion-boson vertex appearing in Equation (2.19d), higher order vertices will also be generated as part of the FRG flow. In particular we will generate a three-boson vertex $\Gamma^{\phi\phi\phi}(\bar{K}_1, \bar{K}_2, \bar{K}_3)$ representing the

interaction between three bosons mediated by fermions. Whilst a scaling analysis shows that this vertex has scaling dimension $z_b - 3$ such that it is formally irrelevant for $z_b < 3$ and marginal in the physical case of $z_b = 3$, we will show that the vertex is crucial in order to generate the diagrams needed to get an anomalous dimension beyond first order. Indeed it is important to emphasise here that the FRG, unlike the field theoretical renormalization group, does not itself require a small parameter. It is thus only out of convenience that we rescale variables.

2.2.2 FRG flow equations

Having defined the model in the previous section we are now ready to write down our FRG flow equations. Our starting point will be the flow equation given in Equation (1.35) and the vertex expansion described thereafter. As mentioned in Section 1.2, a general solution of the flow equations leads to an infinite hierarchy of coupled partial-integro-differential equations. These therefore have to be truncated in some way. In this chapter our strategy will be to truncate the flow equations in such a way that we include the diagrams identified by Metlitski and Sachdev[54] (see Figure 2.6). This can be achieved using the following truncation strategy:

- The flow of the (fermionic and bosonic) self-energies are truncated at the level of three-legged vertices.
- The three-legged vertices in the flow equations for the self-energies are themselves renormalized but have their flow equations truncated at the same level as the flow equations for the self-energies.

Within this truncation the flow equation for the fermionic self-energy $\Sigma^\alpha(K)$ is given by

$$\begin{aligned} \partial_\Lambda \Sigma^\alpha(K) = & \int_{\bar{K}} \left[\dot{F}(\bar{K}) G^\alpha(K + \bar{K}) + F(\bar{K}) \dot{G}^\alpha(K + \bar{K}) \right] \\ & \times \Gamma^{\bar{\psi}^\alpha \psi^\alpha \phi}(K + \bar{K}; K; \bar{K}) \Gamma^{\bar{\psi}^\alpha \psi^\alpha \phi}(K; K + \bar{K}; -\bar{K}), \end{aligned} \quad (2.21)$$

while the flow equation for the bosonic self-energy $\Pi(\bar{K})$ is

$$\begin{aligned} \partial_\Lambda \Pi(\bar{K}) = & \int_K \sum_{\sigma=1}^N \sum_{\alpha=\pm} \left[\dot{G}^\alpha(K) G^\alpha(K + \bar{K}) + G^\alpha(K) \dot{G}^\alpha(K + \bar{K}) \right] \\ & \times \Gamma^{\bar{\psi}^\alpha \psi^\alpha \phi}(K + \bar{K}; K; \bar{K}) \Gamma^{\bar{\psi}^\alpha \psi^\alpha \phi}(K; K + \bar{K}; -\bar{K}) \\ & - \int_{\bar{K}'} \dot{F}(\bar{K}') F(\bar{K}' + \bar{K}) \Gamma^{\phi\phi\phi}(-\bar{K}, -\bar{K}', \bar{K} + \bar{K}'). \end{aligned} \quad (2.22)$$

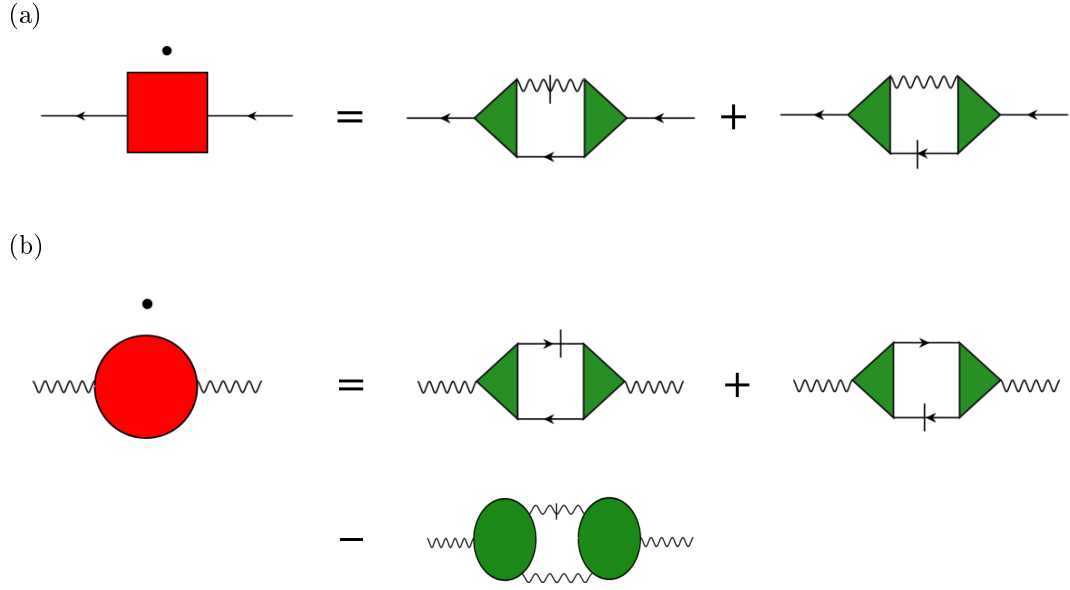


Figure 2.7: Pictorial representation of the flow equations (2.21) (a) and (2.22) (b). As usual solid lines denote fermionic propagators while the wavy lines denote bosonic propagators. A line with a dash represents the single-scale propagators defined in (2.24). The red square denotes the (flowing) fermionic self-energy whilst the red circle is the (flowing) bosonic self-energy. Green triangles and circles represent respectively the renormalized mixed fermion-boson vertex and the renormalized three-boson vertex.

In these flow equations we have introduced the renormalized fermionic and bosonic propagators which are given by

$$G^\alpha(K) = \frac{1}{[G_{0,\Lambda}^\alpha(K)]^{-1} - \Sigma^\alpha(K)}, \quad (2.23a)$$

$$F(\bar{K}) = \frac{1}{[F_{0,\Lambda}(\bar{K})]^{-1} + \Pi(\bar{K})}, \quad (2.23b)$$

respectively, where $G_{0,\Lambda}^\alpha(K)$ and $F_{0,\Lambda}(\bar{K})$ are the fermionic and bosonic bare, cutoff dependent (we will discuss the cutoff dependence of the propagators below) propagators. Furthermore propagators with dots denote single-scale propagators[1] which are defined as

$$\dot{G}^\alpha(K) = -[G^\alpha(K)]^2 \partial_\Lambda [G_{0,\Lambda}^\alpha(K)]^{-1}, \quad (2.24a)$$

$$\dot{F}(\bar{K}) = -[F(\bar{K})]^2 \partial_\Lambda [F_{0,\Lambda}(\bar{K})]^{-1}. \quad (2.24b)$$

The flow equations are shown diagrammatically in Figure 2.7.

The mixed fermion-boson vertex, describing the interaction between two fermions and one boson, satisfies the following flow equation

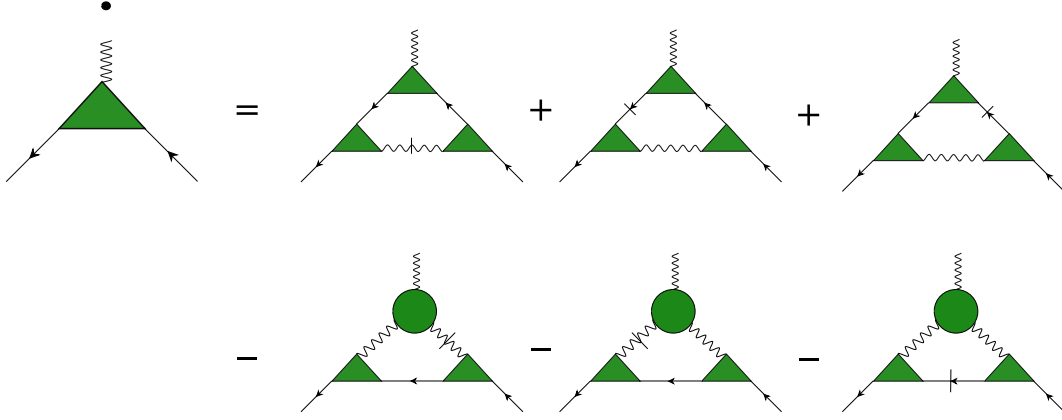


Figure 2.8: Diagrammatic representation of the flow equation for the mixed fermion-boson vertex (2.25) describing the interaction between two fermions and one boson.

$$\begin{aligned}
 \partial_{\Lambda} \Gamma^{\bar{\psi}^{\alpha} \psi^{\alpha} \phi}(K + \bar{K}; K; \bar{K}) &= \int_{\bar{K}'} \left[\dot{F}(\bar{K}') G^{\alpha}(K + \bar{K}') G^{\alpha}(K + \bar{K} + \bar{K}') \right. \\
 &\quad + F(\bar{K}') \dot{G}^{\alpha}(K + \bar{K}') G^{\alpha}(K + \bar{K} + \bar{K}') \\
 &\quad \left. + F(\bar{K}') G^{\alpha}(K + \bar{K}') \dot{G}^{\alpha}(K + \bar{K} + \bar{K}') \right] \\
 &\quad \times \Gamma^{\bar{\psi}^{\alpha} \psi^{\alpha} \phi}(K + \bar{K}'; K; \bar{K}') \\
 &\quad \times \Gamma^{\bar{\psi}^{\alpha} \psi^{\alpha} \phi}(K + \bar{K}; K + \bar{K} + \bar{K}'; -\bar{K}') \\
 &\quad \times \Gamma^{\bar{\psi}^{\alpha} \psi^{\alpha} \phi}(K + \bar{K} + \bar{K}'; K + \bar{K}'; \bar{K}) \\
 &\quad - \int_{\bar{K}'} \left[\dot{F}(\bar{K}') F(\bar{K} + \bar{K}') G^{\alpha}(K + \bar{K} + \bar{K}') \right. \\
 &\quad + F(\bar{K}') \dot{F}(\bar{K} + \bar{K}') G^{\alpha}(K + \bar{K} + \bar{K}') \\
 &\quad \left. + F(\bar{K}') F(\bar{K} + \bar{K}') \dot{G}^{\alpha}(K + \bar{K} + \bar{K}') \right] \\
 &\quad \times \Gamma^{\phi \phi \phi}(-\bar{K} - \bar{K}', \bar{K}, \bar{K}') \\
 &\quad \times \Gamma^{\bar{\psi}^{\alpha} \psi^{\alpha} \phi}(K + \bar{K}; K + \bar{K} + \bar{K}'; -\bar{K}') \\
 &\quad \times \Gamma^{\bar{\psi}^{\alpha} \psi^{\alpha} \phi}(K + \bar{K} + \bar{K}'; K; \bar{K} + \bar{K}'), \quad (2.25)
 \end{aligned}$$

which is shown diagrammatically in Figure 2.8.

Finally the flow equation for the three-boson vertex, which describes the interaction of three bosons mediated by fermions, is given by

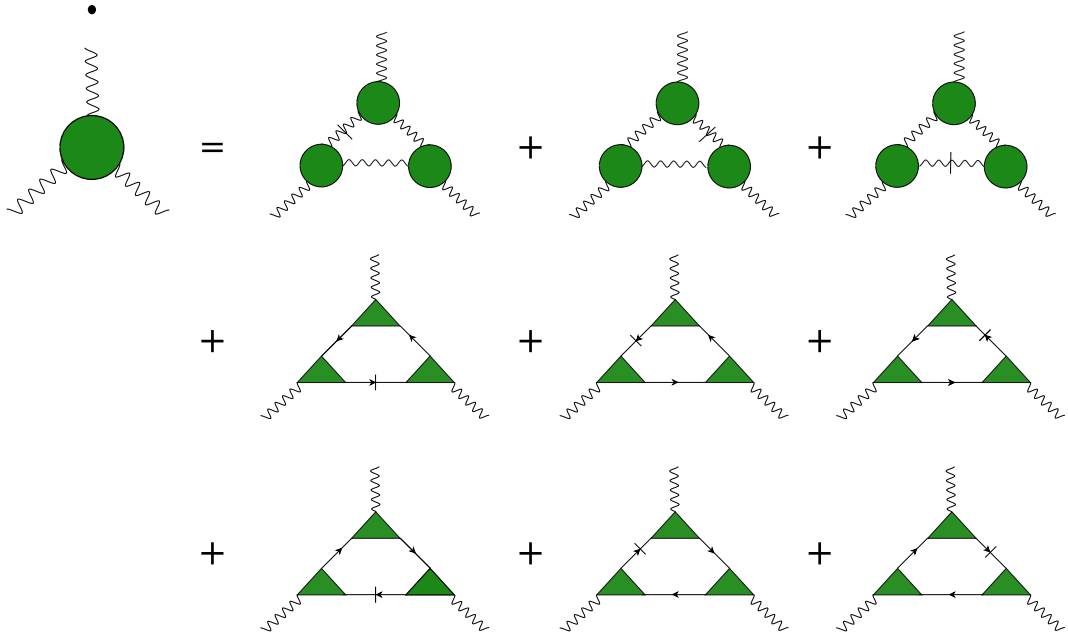


Figure 2.9: Diagrammatic representation of the flow equation for three-boson vertex (2.26) describing the interaction of three bosons mediated by fermions.

$$\begin{aligned}
 \partial_\Lambda \Gamma^{\phi\phi\phi}(\bar{K}_1, \bar{K}_2, -\bar{K}_1 - \bar{K}_2) &= \int_{\bar{K}} \left[\dot{F}(\bar{K}) F(\bar{K} - \bar{K}_1) F(\bar{K} + \bar{K}_2) \right. \\
 &\quad + F(\bar{K}) \dot{F}(\bar{K} - \bar{K}_1) F(\bar{K} + \bar{K}_2) \\
 &\quad \left. + F(\bar{K}) F(\bar{K} - \bar{K}_1) \dot{F}(\bar{K} + \bar{K}_2) \right] \\
 &\quad \times \Gamma^{\phi\phi\phi}(\bar{K}_1, \bar{K} - \bar{K}_1, -\bar{K}) \Gamma^{\phi\phi\phi}(\bar{K}_2, -\bar{K} - \bar{K}_2, \bar{K}) \\
 &\quad \times \Gamma^{\phi\phi\phi}(-\bar{K}_1 - \bar{K}_2, -\bar{K} + \bar{K}_1, \bar{K} + \bar{K}_2) \\
 &\quad + \int_K \sum_{\sigma=1}^N \sum_{\alpha=\pm} \left\{ \left[\dot{G}^\alpha(K) G^\alpha(K + \bar{K}_1) G^\alpha(K + \bar{K}_1 + \bar{K}_2) \right. \right. \\
 &\quad + G^\alpha(K) \dot{G}^\alpha(K + \bar{K}_1) G^\alpha(K + \bar{K}_1 + \bar{K}_2) \\
 &\quad \left. \left. + G^\alpha(K) G^\alpha(K + \bar{K}_1) \dot{G}^\alpha(K + \bar{K}_1 + \bar{K}_2) \right] \right. \\
 &\quad \times \Gamma^{\bar{\psi}^\alpha \psi^\alpha \phi}(K + \bar{K}_1; K; \bar{K}_1) \\
 &\quad \times \Gamma^{\bar{\psi}^\alpha \psi^\alpha \phi}(K + \bar{K}_1 + \bar{K}_2; K + \bar{K}_1; \bar{K}_2) \\
 &\quad \times \Gamma^{\bar{\psi}^\alpha \psi^\alpha \phi}(K; K + \bar{K}_1 + \bar{K}_2; -\bar{K}_1 - \bar{K}_2) \\
 &\quad \left. + (\bar{K}_1 \leftrightarrow \bar{K}_2) \right\}. \tag{2.26}
 \end{aligned}$$

This is shown pictorially in Figure 2.9.

As it stands the flow equations are too complicated to solve so as the last step in our truncation we shall approximate all mixed fermion-boson vertices

on the right-hand sides of Equations (2.25) and (2.26) by their bare values. This finally forms a set of closed coupled integro-differential equations one can attempt to solve numerically. To moreover see that this truncation contains the 3-loop diagrams considered by Metlitski and Sachdev it is only necessary to consider the last six diagrams in the flow equation for the three-boson vertex (2.26) (see also Figure 2.9). Integrating up these contributions to the flow and substituting them in the flow of the bosonic self-energy (2.22) [also Figure 2.7(b)] indeed leads to the Aslamazov-Larkin diagrams in Figure 2.6(b) whilst substituting the same diagrams into the flow of the mixed fermion-boson vertex (2.25) (Figure 2.8) and performing an other integration over the flow parameter Λ yields the fermionic 3-loop diagram in Figure 2.6(a) after substituting the resulting expression into the flow of the fermionic self-energy.

Before concluding this section let us discuss the cutoff procedure. In general the (cutoff dependent) bare propagators are given by

$$[G_{0,\Lambda}^\alpha(K)]^{-1} = i\omega - \xi_{\mathbf{k}}^\alpha - R_\Lambda(K), \quad (2.27a)$$

$$[F_{0,\Lambda}(\bar{K})]^{-1} = r_0 + c_0|\bar{k}_\perp|^{z_b-1} + \bar{R}_\Lambda(\bar{K}), \quad (2.27b)$$

where $R_\Lambda(K)$ and $\bar{R}_\Lambda(\bar{K})$ are fermionic and bosonic regulators respectively. In principle it is possible to use an additive regulator in both the fermionic and bosonic sector but it turns out to be more convenient to only consider a regulator in the bosonic sector and make it a sharp momentum cutoff. Such a “momentum-transfer cutoff” has been used before in other systems such as the Tomonaga-Luttinger model[96]. We thus set the fermionic regulator to zero whilst in the bosonic sector

$$\bar{R}_\Lambda(\bar{K}) = (r_0 + c_0|\bar{k}_\perp|^{z_b-1}) [\Theta^{-1}(|\bar{k}_\perp| - \Lambda) - 1]. \quad (2.28)$$

The renormalized propagators introduced earlier in Equations (2.23) are hence given by

$$G^\alpha(K) = \frac{1}{i\omega - \xi_{\mathbf{k}}^\alpha - \Sigma^\alpha(K)}, \quad (2.29a)$$

$$F(\bar{K}) = \frac{\Theta(|\bar{k}_\perp| - \Lambda)}{r_0 + c_0|\bar{k}_\perp|^{z_b-1} + \Theta(|\bar{k}_\perp| - \Lambda)\Pi(\bar{K})}, \quad (2.29b)$$

whilst the corresponding single-scale propagators [see Equations (2.24)] are given by

$$\dot{G}^\alpha(K) = 0, \quad (2.30a)$$

$$\dot{F}(\bar{K}) = -\frac{\delta(|\bar{k}_\perp| - \Lambda)}{r_0 + c_0\Lambda^{z_b-1} + \Pi(\bar{K})}. \quad (2.30b)$$

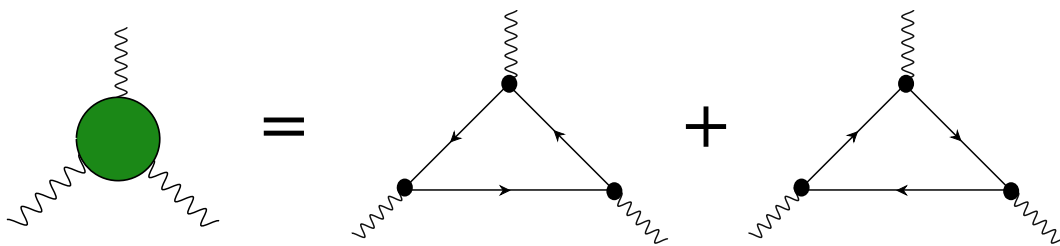


Figure 2.10: Pictorial representation of the symmetrised three-loop. To more easily distinguish flowing from bare vertices in our FRG flow diagrams, black dots will represent the latter whenever both are present.

Using such a cutoff procedure thus allows us to only consider terms containing bosonic single-scale propagators in our flow equations. Diagrammatically this corresponds to neglecting all diagrams that contain a fermionic propagator with a slash.

2.2.3 Skeleton equations

While the FRG flow equations discussed in the previous section form a closed set of equations that recover the relevant diagrams, they are unfortunately still too complicated to be solved, even numerically. To proceed we therefore introduce the further approximation that the flow equation for the three-boson vertex $\Gamma^{\phi\phi\phi}(\bar{K}_1, \bar{K}_2, \bar{K}_3)$ is replaced by the symmetrised three-loop diagram shown in Figure 2.10.

While we will calculate the symmetrised three-loop explicitly later (see Section 2.2.6), let us here briefly discuss the justification for doing this. Indeed similar approaches have been used previously[57] but it turns out that, in order to get the correct scaling behaviour, it is crucial to use one-loop renormalized propagators in the calculation. The resulting expression for the symmetrised three-loop then becomes equivalent to a truncated skeleton equation for the three-boson vertex $\Gamma^{\phi\phi\phi}(\bar{K}_1, \bar{K}_2, \bar{K}_3)$. Such an approach has been used to truncate FRG flow equations with success in previous studies such as Reference [97]. As discussed in Section 1.1.4 the skeleton equations relate vertices of different order and come from the invariance of the measure in functional integrals. The relevant skeleton equation, in this case, can be derived by differentiating Equation (1.30a) twice with respect to the bosonic fields. Doing this leads, after some manipulations, to the following expression for the three-boson vertex

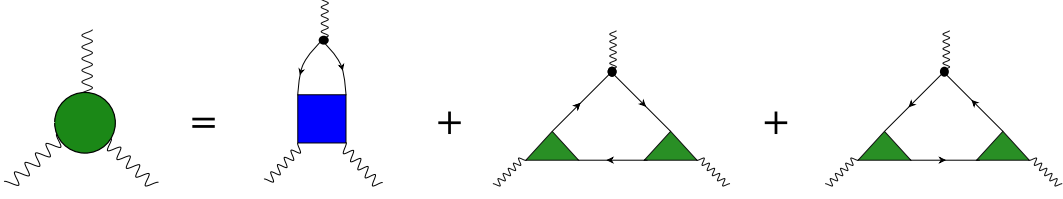


Figure 2.11: Representation of the exact skeleton equation for the three-boson vertex.

$$\begin{aligned}
\Gamma^{\phi\phi\phi}(\bar{K}_1, \bar{K}_2, -\bar{K}_1 - \bar{K}_2) &= N \sum_{\alpha=\pm} \Gamma_0^\alpha \left[\int_K G^\alpha(K) G^\alpha(K + \bar{K}_1) \right. \\
&\quad \times \Gamma^{\bar{\psi}^\alpha \psi^\alpha \phi\phi}(K; K + \bar{K}_1; \bar{K}_2, -\bar{K}_1 - \bar{K}_2) \\
&\quad + \int_K G^\alpha(K) G^\alpha(K + \bar{K}_1) G^\alpha(K + \bar{K}_1 + \bar{K}_2) \\
&\quad \times \Gamma^{\bar{\psi}^\alpha \psi^\alpha \phi\phi}(K + \bar{K}_1 + \bar{K}_2; K + \bar{K}_1; \bar{K}_2) \\
&\quad \times \Gamma^{\bar{\psi}^\alpha \psi^\alpha \phi\phi}(K; K + \bar{K}_1 + \bar{K}_2; -\bar{K}_1 - \bar{K}_2) \\
&\quad + \int_K G^\alpha(K) G^\alpha(K + \bar{K}_1) G^\alpha(K - \bar{K}_2) \\
&\quad \times \Gamma^{\bar{\psi}^\alpha \psi^\alpha \phi\phi}(K - \bar{K}_2; K + \bar{K}_1; -\bar{K}_1 - \bar{K}_2) \\
&\quad \left. \times \Gamma^{\bar{\psi}^\alpha \psi^\alpha \phi\phi}(K; K - \bar{K}_2; \bar{K}_2), \right. \quad (2.31)
\end{aligned}$$

where $\Gamma^{\bar{\psi}^\alpha \psi^\alpha \phi\phi}(K; K + \bar{K}_1; \bar{K}_2, -\bar{K}_1 - \bar{K}_2)$ denotes a four-point vertex between two fermions and two bosons and where we have imposed momentum conservation. Equation (2.31) is shown diagrammatically in Figure 2.11.

From this, the symmetrised three-loop shown in Figure 2.10, with one-loop renormalized propagators, is then obtained by simply replacing all vertices on the right-hand side with their bare values. Within our truncation scheme, the four-point vertex then vanishes and we are left with

$$\Gamma_0^{\phi\phi\phi}(\bar{K}_1, \bar{K}_2, \bar{K}_3) = 2!N \sum_{\alpha=\pm} (\Gamma_0^\alpha)^3 L_3^\alpha(-\bar{K}_1, -\bar{K}_2, -\bar{K}_3), \quad (2.32)$$

where we have defined the symmetrised three-loop as

$$\begin{aligned}
L_3^\alpha(\bar{K}_1, \bar{K}_2, \bar{K}_3) &= \frac{1}{3!} \left[\bar{L}_3^\alpha(\bar{K}_1, \bar{K}_1 + \bar{K}_2, 0) + \bar{L}_3^\alpha(\bar{K}_2, \bar{K}_1 + \bar{K}_2, 0) \right. \\
&\quad + \bar{L}_3^\alpha(\bar{K}_2, \bar{K}_2 + \bar{K}_3, 0) + \bar{L}_3^\alpha(\bar{K}_3, \bar{K}_2 + \bar{K}_3, 0) \\
&\quad \left. + \bar{L}_3^\alpha(\bar{K}_1, \bar{K}_1 + \bar{K}_3, 0) + \bar{L}_3^\alpha(\bar{K}_3, \bar{K}_1 + \bar{K}_3, 0) \right], \quad (2.33)
\end{aligned}$$

with

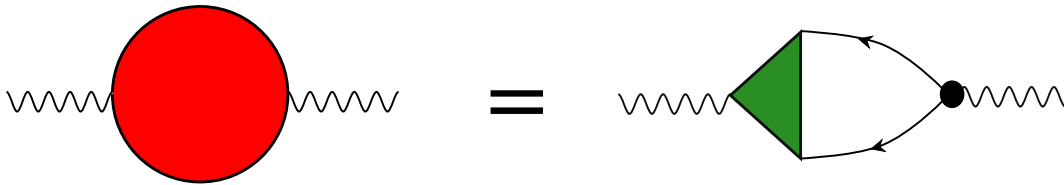


Figure 2.12: Diagrammatic representation of the exact skeleton equation for the polarization.

$$\bar{L}_3^\alpha(\bar{K}_1, \bar{K}_2, \bar{K}_3) = \int_K G^\alpha(K - \bar{K}_1)G^\alpha(K - \bar{K}_2)G^\alpha(K - \bar{K}_3) \quad (2.34)$$

denoting the unsymmetrised three-loop and where we have again imposed momentum conservation. We will calculate the three-boson vertex within this approximation in Section 2.2.6.

With the truncation strategy discussed above for the three-boson vertex it is natural to consider a similar approach for the bosonic self-energy. In this case differentiating Equation (1.30a) once with respect to the bosonic field yields[1, 97]

$$\Pi(\bar{K}) = \int_K \sum_{\sigma=1}^N \sum_{\alpha=\pm} G^\alpha(K)G^\alpha(K + \bar{K})\Gamma_0^\alpha \Gamma^{\bar{\psi}^\alpha \psi^\alpha \phi}(K; K + \bar{K}; -\bar{K}), \quad (2.35)$$

which is shown in Figure 2.12.

2.2.4 Obtaining the anomalous dimensions

The truncated FRG flow equations discussed in the previous two sections allow for a very direct calculation of the anomalous dimension η_ψ defined in Equation (2.18). Before performing this calculation explicitly we therefore first show how this is done in a more general way. The approach will mainly follow the one outlined in Reference [1].

First note that there are, in principle, two anomalous dimensions in this problem, related to the frequency- and momentum dependence of the self-energy respectively. We will show in this section that these relate to the anomalous dimension η_ψ and the fermionic dynamic exponent z which in Equation (2.18) was taken to be equal to $z = z_b/2$. This was shown by Metlitski and Sachdev[54] to remain true up to at least three-loop order. A more general form of Equation (2.18) would however be

$$G(\omega + i0^+, \mathbf{k}) \propto \frac{1}{(A|\omega|^{1/z} - \xi_{\mathbf{k}})^{1-\eta_\psi/2}}, \quad (2.36)$$

where, in principle, z can also be renormalized. From the FRG we now define anomalous dimensions from the quasi-particle residue Z and from the momentum-renormalization factor of the self-energy Y (see Section 1.3, and Equations (2.39) and (2.53) below) as follows

$$\eta_\Lambda = \Lambda \partial_\Lambda \ln Z_\Lambda, \quad (2.37a)$$

$$\tilde{\eta}_\Lambda = \Lambda \partial_\Lambda \ln Y_\Lambda, \quad (2.37b)$$

where we allow for a cutoff dependence of the quasi-particle residue and the momentum-renormalization factor such that also the anomalous dimensions depend on the cutoff. To recover the physical anomalous dimensions we then take the limit $\Lambda \rightarrow 0$,

$$\eta = \lim_{\Lambda \rightarrow 0} \eta_\Lambda, \quad (2.38a)$$

$$\tilde{\eta} = \lim_{\Lambda \rightarrow 0} \tilde{\eta}_\Lambda. \quad (2.38b)$$

From the definitions of Z and Y it now follows that⁴

$$Z_\Lambda = 1 - \lim_{\omega \rightarrow 0} \frac{\partial \Sigma_\Lambda^\alpha(i\omega, 0)}{\partial(i\omega)}, \quad (2.39a)$$

$$Y_\Lambda = 1 + \lim_{\mathbf{k} \rightarrow 0} \frac{\partial \Sigma_\Lambda^\alpha(0, \mathbf{k})}{\partial \xi_{\mathbf{k}}^\alpha}, \quad (2.39b)$$

where we have explicitly included the subscript Λ to make it clear that the self-energy depends on the cutoff. From this it is then easy to see that the anomalous dimensions as defined in Equations (2.37) can be related to the cutoff derivative of the self-energy in the following way

$$\eta_\Lambda = Z_\Lambda \Lambda \lim_{\omega \rightarrow 0} \frac{\partial}{\partial(i\omega)} \partial_\Lambda \Sigma_\Lambda^\alpha(i\omega, 0), \quad (2.40a)$$

$$\tilde{\eta}_\Lambda = -Y_\Lambda \Lambda \lim_{\mathbf{k} \rightarrow 0} \frac{\partial}{\partial \xi_{\mathbf{k}}^\alpha} \partial_\Lambda \Sigma_\Lambda^\alpha(0, \mathbf{k}). \quad (2.40b)$$

In order to calculate the anomalous dimensions we are thus interested in the right-hand side of the flow equation (2.21). In particular substituting this flow equation into Equations (2.40) we see that

⁴The momentum is defined with respect to the Fermi surface such that $\mathbf{k} = 0$ corresponds to the Fermi momentum. The fact that we can measure K relative to the Fermi surface comes from the fact that the fermionic propagator only depends on momenta via $\xi_{\mathbf{k}}^\alpha$ such that $G^\alpha(K) = G^\alpha(i\omega, \xi_{\mathbf{k}}^\alpha)$. The latter is guaranteed by a Ward identity and is a consequence of the invariance of our action under a local rotation of the Fermi surface[54].

$$\begin{aligned} \eta_\Lambda &= Z_\Lambda \Lambda \lim_{\bar{K} \rightarrow 0} \frac{\partial}{\partial(i\omega)} \int_{\bar{K}} \dot{F}(\bar{K}) G^\alpha(\bar{K} + K) \left[\Gamma^{\bar{\psi}^\alpha \psi^\alpha \phi}(\bar{K}; 0; \bar{K}) \right]^2 \\ &\quad + 2Z_\Lambda \Lambda \int_{\bar{K}} \dot{F}(\bar{K}) G^\alpha(\bar{K}) \Gamma^{\bar{\psi}^\alpha \psi^\alpha \phi}(\bar{K}; 0; \bar{K}) \lim_{\bar{K} \rightarrow 0} \frac{\partial \Gamma^{\bar{\psi}^\alpha \psi^\alpha \phi}(\bar{K} + K; K; \bar{K})}{\partial(i\omega)}, \end{aligned} \quad (2.41a)$$

$$\begin{aligned} \tilde{\eta}_\Lambda &= -Y_\Lambda \Lambda \lim_{\bar{K} \rightarrow 0} \frac{\partial}{\partial(\alpha k_\parallel)} \int_{\bar{K}} \dot{F}(\bar{K}) G^\alpha(\bar{K} + K) \left[\Gamma^{\bar{\psi}^\alpha \psi^\alpha \phi}(\bar{K}; 0; \bar{K}) \right]^2 \\ &\quad - 2Y_\Lambda \Lambda \int_{\bar{K}} \dot{F}(\bar{K}) G^\alpha(\bar{K}) \Gamma^{\bar{\psi}^\alpha \psi^\alpha \phi}(\bar{K}; 0; \bar{K}) \lim_{\bar{K} \rightarrow 0} \frac{\partial \Gamma^{\bar{\psi}^\alpha \psi^\alpha \phi}(\bar{K} + K; K; \bar{K})}{\partial(\alpha k_\parallel)}, \end{aligned} \quad (2.41b)$$

where we have used that the momentum dependence always appears through the dispersion $\xi_{\mathbf{k}}^\alpha = \alpha k_\parallel + k_\perp^2$ such that we may replace the derivative with respect to $\xi_{\mathbf{k}}^\alpha$ with a derivative with respect to αk_\parallel . Whilst these are very complicated expressions let us here note that we only need the mixed fermion-boson vertex and its frequency- and momentum derivatives at vanishing fermionic frequencies and momenta.

To now establish the connection between the anomalous dimensions η and $\tilde{\eta}$, and the anomalous dimension η_ψ and the fermionic dynamic exponent z notice that setting $\omega = k_\perp = 0$ in Equation (2.36) yields

$$G(i0^+, k_\parallel) \propto k_\parallel^{-1+\eta_\psi/2}, \quad (2.42)$$

where 0^+ denotes a positive infinitesimal (we do not use η here so as to not confuse it with the anomalous dimensions). From Equation (2.37b) however, it follows, using that $k_\parallel \propto \Lambda^2$, that

$$Y_\Lambda \propto \Lambda^{\tilde{\eta}} \propto k_\parallel^{\tilde{\eta}/2}. \quad (2.43)$$

Hence (see Section 1.3, and Equation (2.54) below)

$$G(i0^+, k_\parallel) \propto \frac{Y_\Lambda}{k_\parallel} \propto k_\parallel^{-1+\tilde{\eta}/2}. \quad (2.44)$$

Comparing Equations (2.42) and (2.44) thus yields

$$\tilde{\eta} = \eta_\psi. \quad (2.45)$$

On the other hand, setting $\mathbf{k} = 0$ in Equation (2.36) gives

$$G(\omega + i0^+, 0) \propto \omega^{-(1-\eta_\psi/2)/z}. \quad (2.46)$$

Now, from (2.37a)

$$Z_\Lambda \propto \Lambda^\eta \propto \omega^{\eta/(2z)}, \quad (2.47)$$

where we have used that the frequency goes as $\omega \propto \Lambda^{2z}$. In that case

$$G(\omega + i0^+, 0) \propto \frac{Z_\Lambda}{\omega} \propto \omega^{-(1-\eta/(2z))}, \quad (2.48)$$

such that we get, by comparing Equations (2.46) and (2.48), that the fermionic dynamic exponent is given by

$$z = 1 + \frac{\eta - \tilde{\eta}}{2}. \quad (2.49)$$

Our two anomalous dimensions η and $\tilde{\eta}$ thus fully correspond to the anomalous dimension η_ψ and the fermionic dynamic exponent z . We therefore focus on calculating η and $\tilde{\eta}$. It should finally be noted that the exponent η (related to the renormalization of the frequency dependent part of the propagator and needed to extract the renormalization of the fermionic dynamic exponent) was not previously calculated and is not expected to appear before four-loop order[95]. Instead, the results previously obtained[54, 55] are inferred from a calculation of the exponent $\tilde{\eta}$ (corresponding to η_ψ) which indeed appears at three-loop order. This can be done if one expects the bosonic and fermionic dynamic exponents to renormalize in the same way which is the case here.

2.2.5 Recovering one loop

Before calculating the anomalous dimensions identified by Metlitski and Sachdev let us first show that it is possible to recover the one-loop results that were discussed in Section 2.1.2 from our FRG flow equations. Doing this we will also explicitly derive expressions for the (cutoff dependent, one-loop renormalized) quasi-particle residue and for the momentum renormalization factor (see Section 1.3 and below) which will be used later as well.

To obtain the one-loop results from our FRG flow equation it is sufficient to neglect vertex corrections. In this case the vertex describing interactions between two fermions and one boson simply takes its bare value as given in Equation (2.20) whilst the three-boson vertex vanishes. Within our truncation scheme, where, as described in the previous section, we replace flow equations for vertices only containing bosonic external legs with corresponding (truncated) skeleton equations, the equations we have to solve simplify to

$$\partial_\Lambda \Sigma^\alpha(K) = \int_{\bar{K}} \dot{F}(\bar{K}) G^\alpha(\bar{K} + K), \quad (2.50a)$$

$$\Pi(\bar{K}) = \frac{1}{2} \int_K \sum_{\sigma=1}^N \sum_{\alpha=\pm} G^\alpha(K) [G^\alpha(K + \bar{K}) + G^\alpha(K - \bar{K})], \quad (2.50b)$$

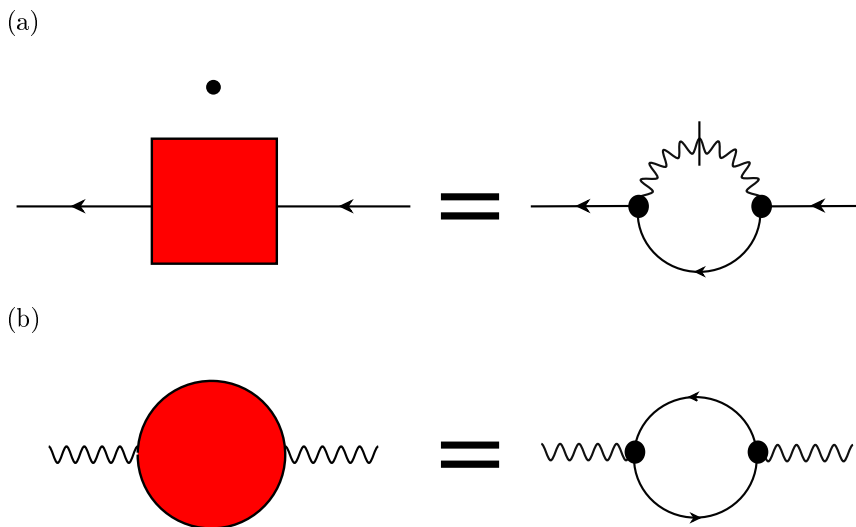


Figure 2.13: Diagrammatic representation of Equations (2.50) for the flow of the fermionic self-energy (a) and the skeleton equation for the bosonic self-energy (b) without vertex corrections.

where we have also symmetrised the bosonic self-energy and used that $(\Gamma_0^\alpha)^2 = 1$. These two equations are shown diagrammatically in Figure 2.13.

It now turns out that the integral on the right-hand side of the flow equation for the fermionic self-energy is ultraviolet divergent. To regularize this divergence we note that, since we have expanded our dispersion $\xi_{\mathbf{k}}^\alpha$ around the Fermi surface, the self-energy in the fermionic propagator (2.29a) should actually be replaced by the self-energy relative to the Fermi surface. As we moreover do not keep track of the shape of the renormalized Fermi surface, defined through Equation (1.42) but where the self-energy now flows (the physical Fermi surface is recovered by letting $\Lambda \rightarrow 0$), we may in general replace the self-energy $\Sigma^\alpha(K)$ by the subtracted self-energy

$$\Delta^\alpha(K) = \Sigma^\alpha(K) - \Sigma^\alpha(0), \quad (2.51)$$

where we recall that K is measured relative to the Fermi surface such that $|\mathbf{k}| = 0$ corresponds to the Fermi momentum. In an analogous fashion to the self-energy itself, the subtracted self-energy then satisfies the following flow equation

$$\partial_\Lambda \Delta^\alpha(K) = \int_{\bar{K}} \dot{F}(\bar{K}) [G^\alpha(\bar{K} + K) - G^\alpha(\bar{K})], \quad (2.52)$$

which is ultraviolet convergent.

In order to solve our truncated flow equations and calculate the anomalous

dimensions we now expand the subtracted self-energy around the Fermi surface (see also Section 1.3). Then

$$\Delta^\alpha(K) = (1 - Z_\Lambda^{-1}) i\omega - (1 - Y_\Lambda^{-1}) \xi_{\mathbf{k}}^\alpha + \dots, \quad (2.53)$$

where we have introduced Λ as a subscript to make it clear that the quasi-particle residue and momentum-renormalization factor depend on the cutoff. The physical values of Z and Y are obtained by taking the limit $\Lambda \rightarrow 0$. The fermionic propagator given in Equation (2.29a) thus takes on the following Fermi liquid form

$$G^\alpha(K) = \frac{1}{Z_\Lambda^{-1}i\omega - Y_\Lambda^{-1}\xi_{\mathbf{k}}^\alpha} = \frac{Z_\Lambda}{i\omega - (Z_\Lambda/Y_\Lambda)\xi_{\mathbf{k}}^\alpha}. \quad (2.54)$$

With this it is now possible to perform all integrations on the right-hand sides of Equations (2.50b) and (2.52). Starting with the former we see that it is given by

$$\begin{aligned} \Pi(\bar{K}) &= \frac{1}{2} \int_K \sum_{\sigma=1}^N \sum_{\alpha=\pm} \left[\frac{Z_\Lambda}{i\omega - (Z_\Lambda/Y_\Lambda)(\alpha k_\parallel + k_\perp^2)} \right. \\ &\quad \left. \times \frac{Z_\Lambda}{i(\omega + \bar{\omega}) - (Z_\Lambda/Y_\Lambda)[\alpha(k_\parallel + \bar{k}_\parallel) + (k_\perp + \bar{k}_\perp)^2]} + (\bar{K} \rightarrow -\bar{K}) \right]. \end{aligned} \quad (2.55)$$

This has exactly the same structure as Equation (2.10). In that case we saw that a divergence in the ultraviolet appeared. This divergence can be traced back to the integral being ill defined for vanishing external frequencies. Indeed changing the order of integration will give different results. The origin of this is with the patch construction which decompactifies the Fermi surface. This, as we discussed earlier, implies that we should introduce an angular cutoff, limiting the momentum integration to take place in the vicinity of the patches. To obtain well defined integrals such a cutoff has to be introduced in a way that respects all symmetries of the underlying microscopic theory[55]. However, as was also discussed earlier, we are only interested in the singular low-energy behaviour of the theory, and this cannot depend on how the theory is regularized in the ultraviolet. We may thus perform the same steps as after (2.10) and arrive at the result

$$\Pi(\bar{K}) = b_\Lambda \frac{|\bar{\omega}|}{|\bar{k}_\perp|}, \quad (2.56)$$

where now $b_\Lambda = NY_\Lambda^2/(4\pi)$ which should be compared to $b_0 = N/(4\pi)$ as given below (2.12). We now insert this result for the bosonic self-energy into the bosonic propagator (2.29b). For the fermionic self-energy, however, we only need the bosonic single-scale propagator (2.30b) which becomes

$$\dot{F}(\bar{K}) \approx -\frac{\delta(|\bar{k}_\perp| - \Lambda)}{r_0 + c_0\Lambda^{z_b-1} + b_\Lambda|\bar{\omega}|/\Lambda}. \quad (2.57)$$

Substituting this into the flow equation for the (subtracted) self-energy (2.52), the integration over \bar{k}_\perp on the right-hand side becomes trivial due to the δ -function. Furthermore the k_\parallel integration can be performed using the method of residues whilst the remaining frequency integration is a standard integral. We finally arrive at

$$\partial_\Lambda \Delta^\alpha(K) = Y_\Lambda \frac{i \operatorname{sgn}(\omega)\Lambda}{2\pi^2 b_\Lambda} \ln \left[1 + \frac{b_\Lambda|\omega|/\Lambda}{r_0 + c_0\Lambda^{z_b-1}} \right]. \quad (2.58)$$

As this is independent of momentum we immediately see, using Equations (2.37b) [or equivalently (2.40b)] and (2.39b), that $Y_\Lambda = 1$ and $\tilde{\eta} = 0$ within this approximation. Hence we recover the one-loop results $\eta_\psi = 0$ and $b_\Lambda = b_0$ derived in Section 2.1.2. Moreover substituting Equation (2.58) into Equation (2.40a) it follows that

$$\eta_\Lambda = \frac{\Lambda Z_\Lambda Y_\Lambda}{2\pi^2 (r_0 + c_0\Lambda^{z_b-1})} = \frac{Z_\Lambda}{2\pi^2 c_0 \Lambda^{z_b-2}}, \quad (2.59)$$

where, in the last equality, we have used that $Y_\Lambda = 1$ and set $r_0 = 0$ as we only consider the behaviour at the quantum critical point. With this, Equation (2.37a) becomes a differential equation for Z_Λ which can be integrated up to give

$$Z_\Lambda = \frac{Z_{\Lambda_0}}{1 + \frac{Z_{\Lambda_0}}{2\pi^2 c_0 (z_b-2)} (\Lambda^{2-z_b} - \Lambda_0^{2-z_b})}, \quad (2.60)$$

where Λ_0 is the initial cutoff scale. Since now $z_b > 2$ we find that, sending $\Lambda \rightarrow 0$ this goes as

$$Z_\Lambda \sim 2\pi^2 c_0 (z_b - 2) \Lambda^{z_b-2}. \quad (2.61)$$

We therefore see that, as expected, the quasi-particle residue vanishes such that the quasi-particles decohere and the Fermi liquid behaviour is broken. Furthermore, substituting back into Equation (2.37a) and sending $\Lambda \rightarrow 0$ yields the anomalous dimension

$$\eta = z_b - 2. \quad (2.62)$$

Hence, from Equation (2.49)

$$z = \frac{z_b}{2}, \quad (2.63)$$

as also previously obtained[54, 55, 65, 72, 73, 92, 95], to one-loop order.

Finally as $Y_\Lambda = 1$ we may integrate up the flow equation for the self-energy (2.58) and obtain, at the quantum critical point,

$$\Delta_{\Lambda}^{\alpha}(K) - \Delta_{\Lambda_0}^{\alpha}(K) = -\frac{i\text{sgn}(\omega)}{2\pi^2 b_0} \int_{\Lambda}^{\Lambda_0} d\lambda \lambda \ln \left[1 + \frac{b_0 |\omega|}{c_0 \lambda^{z_b}} \right], \quad (2.64)$$

where we have included the cutoff dependence of the self-energy explicitly to make it clear that they are evaluated at different scales. Because this is ultraviolet convergent we may now let $\Lambda_0 \rightarrow \infty$. In this case $\Delta_{\Lambda_0}^{\alpha}(K)$ vanishes and, sending also $\Lambda \rightarrow 0$ to recover the physical self-energy, the frequency dependence may be scaled out. In fact the remaining integral can also be performed such that we obtain

$$\lim_{\Lambda \rightarrow 0} \Delta_{\Lambda}^{\alpha}(K) = -i\text{sgn}(\omega) \frac{a_0}{b_0} \left(\frac{b_0 |\omega|}{c_0} \right)^{2/z_b}, \quad (2.65)$$

with

$$a_0 = \frac{1}{2\pi^2 z_b} \int_0^{\infty} dx \frac{\ln(1+x)}{x^{1+2/z_b}} = \frac{1}{4\pi \sin(2\pi/z_b)}. \quad (2.66)$$

Setting $z_b = 3$ we thus recover the, at one-loop order, expected form of the self-energy[54, 55, 65, 72, 73, 92, 95].

In the following sections we will include vertex corrections in order to calculate the corrections to the anomalous dimensions. Doing this, we will use the results from this section by using one-loop renormalized propagators. The dressing of the propagators will therefore be done through the one-loop results for the renormalization factors Y_{Λ} and Z_{Λ} discussed above.

2.2.6 The symmetrised three-loop

To include vertex corrections we again consider the flow equation for the self-energy (2.21), but now do not replace the fermion-boson vertex $\Gamma^{\bar{\psi}^{\alpha}\psi^{\alpha}\phi}(K_1; K_2; \bar{K}_3)$ with its bare value. Instead the vertex is calculated from the flow Equation (2.25) with the truncation discussed in Section 2.2.2. We therefore replace all fermion-boson vertices on the right-hand side of Equation (2.25) by their bare values and arrive at

$$\begin{aligned} \partial_{\Lambda} \Gamma^{\bar{\psi}^{\alpha}\psi^{\alpha}\phi}(K + \bar{K}; K; \bar{K}) &= \Gamma_0^{\alpha} \int_{\bar{K}'} \dot{F}(\bar{K}') G^{\alpha}(K + \bar{K}') G^{\alpha}(K + \bar{K} + \bar{K}') \\ &\quad - \int_{\bar{K}'} \dot{F}(\bar{K}') F(\bar{K} + \bar{K}') [G^{\alpha}(K + \bar{K} + \bar{K}') \\ &\quad + G^{\alpha}(K - \bar{K}')] \Gamma^{\phi\phi\phi}(\bar{K}, \bar{K}', -\bar{K} - \bar{K}'), \end{aligned} \quad (2.67)$$

where we have used that $(\Gamma_0^{\alpha})^2 = 1$ and neglected all terms containing fermionic single-scale propagators as these vanish with the cutoff procedure used. Equation (2.67) is shown diagrammatically in Figure 2.14.

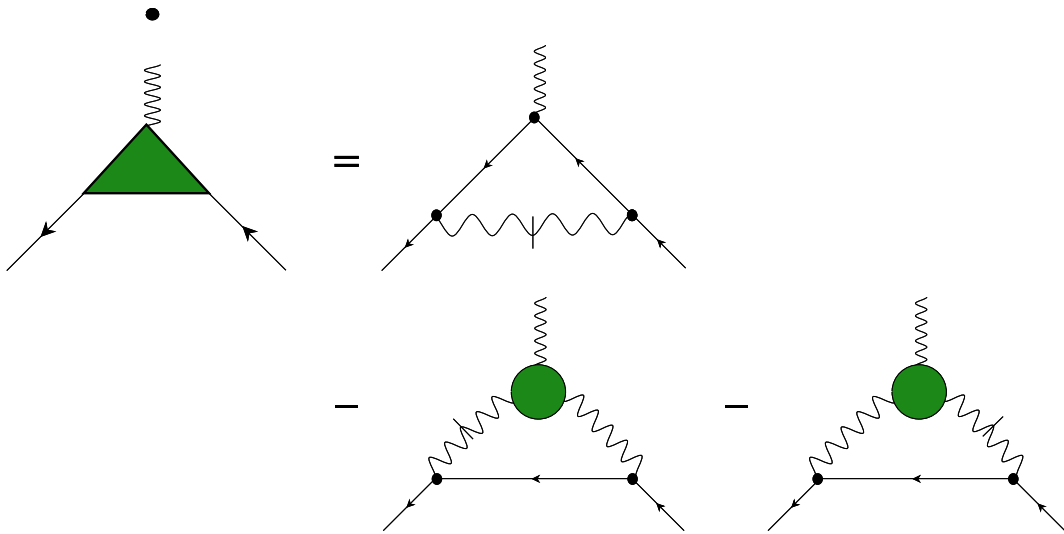


Figure 2.14: Diagrammatic representation of the truncated flow Equation (2.67) for the mixed fermion-boson vertex.

From Equation (2.67) it is clear that, in order to calculate the fermion-boson vertex, we first need an expression for the three-boson vertex. Within our truncation this is given by truncating the skeleton equation (2.31). In Section 2.2.3 we then argued that this is equivalent to calculating the symmetrised three-loop (2.33) which in turn depends on the unsymmetrised three-loop (2.34) with the caveat that, to get the correct scaling, all propagators have to be dressed to one-loop order. Within one-loop the latter can be done simply by multiplying all external frequencies in the propagators by Z_Λ^{-1} , where Z_Λ is the one-loop result for the quasi-particle residue given in Equation (2.60). We therefore temporarily make the replacements $Z_\Lambda^{-1}\bar{\omega} \rightarrow \bar{\omega}$, $Z_\Lambda^{-1}\omega \rightarrow \omega$ in the integral. Doing this we then need to multiply the three-loop by an overall factor of Z_Λ (to take into account that the measure of the integration over frequency also has dimensions of frequency). Hence the unsymmetrised three-loop can be calculated (similar calculations have been performed for other systems, see e.g. References [98, 99]). First the k_\parallel integration can be performed using the method of residues

$$\begin{aligned}
\bar{L}_3^\alpha(\bar{K}_1, \bar{K}_2, \bar{K}_3) &= Z_\Lambda \int_K \frac{1}{i\omega - i\bar{\omega}_1 - \alpha(k_{\parallel} - \bar{k}_{\parallel 1}) - (k_{\perp} - \bar{k}_{\perp 1})^2} \\
&\times \frac{1}{i\omega - i\bar{\omega}_2 - \alpha(k_{\parallel} - \bar{k}_{\parallel 2}) - (k_{\perp} - \bar{k}_{\perp 2})^2} \\
&\times \frac{1}{i\omega - i\bar{\omega}_3 - \alpha(k_{\parallel} - \bar{k}_{\parallel 3}) - (k_{\perp} - \bar{k}_{\perp 3})^2} \\
&= Z_\Lambda \int \frac{dk_{\perp} d\omega}{(2\pi)^3} 2\pi i \sum_{i=1}^3 \prod_{\substack{j=1 \\ j \neq i}}^3 \frac{1}{\Omega_{ij}(k_{\perp})} \Theta(\bar{\omega}_i - \omega), \quad (2.68)
\end{aligned}$$

where $\bar{\omega}_i$, $\bar{k}_{\parallel i}$, and $\bar{k}_{\perp i}$ are respectively the frequency and momentum components of \bar{K}_i , and where we have defined

$$\Omega_{ij}(k_{\perp}) = i(\bar{\omega}_i - \bar{\omega}_j) + \xi_{\mathbf{k}-\bar{\mathbf{k}}_i}^\alpha - \xi_{\mathbf{k}-\bar{\mathbf{k}}_j}^\alpha = -2\bar{k}_{ij}(k_{\perp} - k_{ij}), \quad (2.69)$$

with

$$\bar{k}_{ij} = \bar{k}_{\perp i} - \bar{k}_{\perp j}, \quad (2.70a)$$

$$\bar{\omega}_{ij} = \bar{\omega}_i - \bar{\omega}_j, \quad (2.70b)$$

$$k_{ij} = \frac{\bar{k}_{\perp i} + \bar{k}_{\perp j}}{2} + \frac{i\bar{\omega}_{ij} - \alpha(\bar{k}_{\parallel i} - \bar{k}_{\parallel j})}{2\bar{k}_{ij}}. \quad (2.70c)$$

The frequency integral is now trivial whilst the k_{\perp} integration can again be performed using the method of residues. The result for the unsymmetrised three-loop is

$$\begin{aligned}
\bar{L}_3^\alpha(\bar{K}_1, \bar{K}_2, \bar{K}_3) &= \frac{-Z_\Lambda}{8\pi} \left[\frac{\bar{\omega}_1}{\bar{k}_{12}\bar{k}_{13}} \frac{\Theta(\text{Im}k_{12}) - \Theta(\text{Im}k_{13})}{k_{12} - k_{13}} \right. \\
&+ \frac{\bar{\omega}_2}{\bar{k}_{21}\bar{k}_{23}} \frac{\Theta(\text{Im}k_{23}) - \Theta(\text{Im}k_{21})}{k_{23} - k_{21}} \\
&\left. + \frac{\bar{\omega}_3}{\bar{k}_{31}\bar{k}_{32}} \frac{\Theta(\text{Im}k_{31}) - \Theta(\text{Im}k_{32})}{k_{31} - k_{32}} \right]. \quad (2.71)
\end{aligned}$$

What now remains is to symmetrise the three-loop as given in Equation (2.33). First of all we impose momentum conservation and set $\bar{K}_3 = -\bar{K}_1 - \bar{K}_2$. Moreover we use the identity

$$\Theta(x) - \Theta(y) = \text{sgn}(x)\Theta(-xy), \quad (2.72)$$

which can be verified by simply comparing both sides for different values of x and y , and (using the shorthand notation: $-\omega_i = \omega_{-i}$, $-\bar{k}_{\perp i} = \bar{k}_{\perp, -i}$, and $-\bar{k}_{\parallel i} = \bar{k}_{\parallel, -i}$) the relations

$$\omega_{ij} = -\omega_{ji}, \quad (2.73a)$$

$$\bar{k}_{ij} = -\bar{k}_{ji}, \quad (2.73b)$$

$$k_{-i, -j} = k_{ij} - (\bar{k}_{\perp i} + \bar{k}_{\perp j}), \quad (2.73c)$$

$$\text{Im}k_{-i, -j} = \text{Im}k_{ij}, \quad (2.73d)$$

$$k_{ij} - k_{ik} = \frac{\bar{k}_{jk}}{2} + \frac{i(\bar{k}_{\perp k}\omega_{ji} + \bar{k}_{\perp i}\omega_{kj} + \bar{k}_{\perp j}\omega_{ik}) - \alpha(\bar{k}_{\perp k}\bar{k}_{ji}^{\parallel} + \bar{k}_{\perp i}\bar{k}_{kj}^{\parallel} + \bar{k}_{\perp j}\bar{k}_{ik}^{\parallel})}{\bar{k}_{ij}\bar{k}_{ik}}, \quad (2.73e)$$

where we have defined also

$$\bar{k}_{ij}^{\parallel} = \bar{k}_{\parallel i} - \bar{k}_{\parallel j}. \quad (2.74)$$

Equations (2.73) can be readily proven from the definitions (2.70). With all this we add all terms together, rescale back to usual frequencies $\bar{\omega} \rightarrow Z_{\Lambda}^{-1}\bar{\omega}$, and arrive at the following expression for the symmetrised three-loop, taking momentum conservation into account,

$$L_3^{\alpha}(\bar{K}_1, \bar{K}_2, -\bar{K}_1 - \bar{K}_2) = \frac{1}{4\pi} \left(\frac{1}{\bar{k}_{\perp 1}} + \frac{1}{\bar{k}_{\perp 2}} \right) \times \frac{\bar{\omega}_1 \Theta\left(\frac{\bar{\omega}_1}{\bar{k}_{\perp 1}}\right) + \bar{\omega}_2 \Theta\left(\frac{\bar{\omega}_2}{\bar{k}_{\perp 2}}\right) - (\bar{\omega}_1 + \bar{\omega}_2) \Theta\left(\frac{\bar{\omega}_1 + \bar{\omega}_2}{\bar{k}_{\perp 1} + \bar{k}_{\perp 2}}\right)}{\left[\frac{\bar{k}_{\parallel 1}}{\bar{k}_{\perp 1}} - \frac{\bar{k}_{\parallel 2}}{\bar{k}_{\perp 2}} - \frac{i\alpha}{Z_{\Lambda}} \left(\frac{\bar{\omega}_1}{\bar{k}_{\perp 1}} - \frac{\bar{\omega}_2}{\bar{k}_{\perp 2}} \right) \right]^2 - (\bar{k}_{\perp 1} + \bar{k}_{\perp 2})^2}, \quad (2.75)$$

which yields an expression for the value of the three-boson vertex viz. Equation (2.32). This expression should be contrasted with the three-boson vertex used in Hertz-Millis theory (see Section 2.1.1) where it is simply given by a frequency- and momentum independent constant. It is clear from Equation (2.75), which is highly singular in both momenta and frequencies, that such an approximation is not sufficient.

2.2.7 The mixed fermion-boson vertex

With the results from the previous section we are now ready to calculate the mixed fermion-boson vertex which, within our truncation scheme, satisfies the

flow equation (2.67). As can be seen from the flow equation the vertex receives two distinct contributions, namely a contribution where no vertices on the right-hand side of the flow equation are renormalized (the first line of Equation (2.67) corresponding to the first diagram on the right-hand side in Figure 2.14), and a contribution where the three-boson vertex is renormalized as described in the previous section (the second term in Equation (2.67) and last two diagrams in Figure 2.14). We will treat these two contributions separately as they require different approaches. Starting with the first contribution, without renormalized vertices on the right-hand side, we get

$$\partial_\Lambda \Gamma^{\bar{\psi}^\alpha \psi^\alpha \phi}(K + \bar{K}; K; \bar{K})^{(1)} = \Gamma_0^\alpha \int_{\bar{K}'} \dot{F}(\bar{K}') G^\alpha(K + \bar{K}') G^\alpha(K + \bar{K} + \bar{K}'), \quad (2.76)$$

where all propagators are renormalized to one-loop order using the results of Section 2.2.5. We now perform the frequency and momentum integration on the right-hand side. The \bar{k}_\perp integration is trivial due to the δ -function in the single-scale propagator $\dot{F}(\bar{K}')$, while the \bar{k}_\parallel integral can be performed using the method of residues. Finally the frequency integral is a standard integral and we arrive at

$$\begin{aligned} \Lambda \partial_\Lambda \Gamma^{\bar{\psi}^\alpha \psi^\alpha \phi}(K + \bar{K}; K; \bar{K})^{(1)} &= -\frac{\Gamma_0^\alpha}{(2\pi)^2} \frac{Z_\Lambda}{b_0} \left[\frac{\Lambda^2}{i\bar{\omega} - Z_\Lambda [\alpha \bar{k}_\parallel + \bar{k}_\perp^2 + 2\bar{k}_\perp (k_\perp + \Lambda)]} \right. \\ &\quad \left. + (\Lambda \rightarrow -\Lambda) \right] \left[i \operatorname{sgn}(\omega + \bar{\omega}) \ln \left(1 + \frac{b_0 |\omega + \bar{\omega}|}{r_0 \Lambda + c_0 \Lambda^{z_b}} \right) \right. \\ &\quad \left. - i \operatorname{sgn}(\omega) \ln \left(1 + \frac{b_0 |\omega|}{r_0 \Lambda + c_0 \Lambda^{z_b}} \right) \right], \quad (2.77) \end{aligned}$$

where we have, for now, allowed for $r_0 \neq 0$. In the end we will set $r_0 = 0$ in order to describe the quantum critical point.

We now recall that, in order to calculate the anomalous dimensions, it follows from Equations (2.41) that we only need the fermion-boson vertex and its derivatives with respect to momentum and frequency at $K = 0$. For the vertex itself we may hence set $K = 0$ in the flow equations whilst for the derivatives we may differentiate both sides of the flow equations with respect to either frequency or momentum. Swapping the order of differentiation we then arrive at three flow-equations which can be written in the following scaling form

$$\Lambda \partial_\Lambda \Gamma^{\bar{\psi}^\alpha \psi^\alpha \phi}(\bar{K}; 0; \bar{K})^{(1)} = -I_\Lambda^{(1)} \left(\frac{\bar{\omega}}{\Lambda^{z_b}}, \frac{\bar{k}_\parallel}{\Lambda^2}, \frac{\bar{k}_\perp}{\Lambda} \right), \quad (2.78a)$$

$$\Lambda \partial_\Lambda \left. \frac{\partial \Gamma^{\bar{\psi}^\alpha \psi^\alpha \phi}(K + \bar{K}; K; \bar{K})^{(1)}}{\partial(i\omega)} \right|_{K=0} = -\frac{1}{\Lambda^{z_b}} I_\Lambda^{(1\omega)} \left(\frac{\bar{\omega}}{\Lambda^{z_b}}, \frac{\bar{k}_\parallel}{\Lambda^2}, \frac{\bar{k}_\perp}{\Lambda} \right), \quad (2.78b)$$

$$\Lambda \partial_\Lambda \left. \frac{\partial \Gamma^{\bar{\psi}^\alpha \psi^\alpha \phi}(K + \bar{K}; K; \bar{K})^{(1)}}{\partial(\alpha k_\parallel)} \right|_{K=0} = -\frac{1}{\Lambda^2} I_\Lambda^{(1k)} \left(\frac{\bar{\omega}}{\Lambda^{z_b}}, \frac{\bar{k}_\parallel}{\Lambda^2}, \frac{\bar{k}_\perp}{\Lambda} \right), \quad (2.78c)$$

where the dimensionless scaling functions are obtained from the right-hand side of Equation (2.77) by setting $K = 0$, differentiating with respect to $i\omega$ and setting $K = 0$, and differentiating with respect to αk_\parallel and setting $K = 0$ respectively, and writing everything in terms of rescaled variables such that they are given by

$$I_\Lambda^{(1)}(\bar{\epsilon}, \bar{q}_\parallel, \bar{q}_\perp) = \frac{\gamma_\Lambda}{(2\pi)^2 b_0} i \text{sgn}(\bar{\epsilon}) \ln \left(1 + \frac{b_0 |\bar{\epsilon}|}{r_\Lambda + c_0} \right) \times \left[\frac{1}{i\bar{\epsilon} - \gamma_\Lambda [\alpha \bar{q}_\parallel + \bar{q}_\perp^2 + 2\bar{q}_\perp]} + (\bar{q}_\perp \rightarrow -\bar{q}_\perp) \right], \quad (2.79a)$$

$$I_\Lambda^{(1\omega)}(\bar{\epsilon}, \bar{q}_\parallel, \bar{q}_\perp) = -\frac{\gamma_\Lambda}{(2\pi)^2 (r_\Lambda + c_0)^2} \frac{b_0}{1 + \frac{b_0}{r_\Lambda + c_0} |\bar{\epsilon}|} \times \left[\frac{|\bar{\epsilon}|}{i\bar{\epsilon} - \gamma_\Lambda [\alpha \bar{q}_\parallel + \bar{q}_\perp^2 + 2\bar{q}_\perp]} + (\bar{q}_\perp \rightarrow -\bar{q}_\perp) \right], \quad (2.79b)$$

$$I_\Lambda^{(1k)}(\bar{\epsilon}, \bar{q}_\parallel, \bar{q}_\perp) = 0, \quad (2.79c)$$

where we have now focused on the case of the Ising-nematic quantum critical point and set $\Gamma_0^\alpha = 1$, where $r_\Lambda = r_0 \Lambda^{1-z_b}$ and we have defined the dimensionless flowing parameter

$$\gamma_\Lambda = \frac{Z_\Lambda}{\Lambda^{z_b-2}} = \frac{2\pi^2 c_0 (z_b - 2)}{1 - \Lambda^{z_b-2} \left[\frac{2\pi^2 c_0 (z_b-2)}{Z_{\Lambda_0}} - \Lambda_0^{2-z_b} \right]}. \quad (2.80)$$

In this we have used the one-loop result for the quasi-particle residue (2.60). We note that in the limit $\Lambda \rightarrow 0$

$$\gamma = \lim_{\Lambda \rightarrow 0} \gamma_\Lambda = 2\pi^2 c_0 (z_b - 2) = \frac{\pi}{2} N (z_b - 2), \quad (2.81)$$

using that $c_0 = N/(4\pi)$ at lowest order. This, we recall, is of course proportional to the expansion parameter used by Mross et al[55]. Finally notice that the formal reason for the absence of a scaling function for the derivative with respect to momentum, $I_\Lambda^{(1k)}(\bar{\epsilon}, \bar{q}_\parallel, \bar{q}_\perp)$, is that the right-hand side of Equation (2.77) is independent of k_\parallel , which in turn is due to the fact that it can be

subsumed in a shift of the momentum in the dispersion.

Let us now turn to the second contribution to the flow of the mixed fermion-boson vertex. This contribution, which is shown in the last two diagrams in Figure 2.14, contains the renormalized three-boson vertex and is given by

$$\begin{aligned} \partial_\Lambda \Gamma^{\bar{\psi}^\alpha \psi^\alpha \phi}(K + \bar{K}; K; \bar{K})^{(2)} = & - \int_{\bar{K}'} \dot{F}(\bar{K}') F(\bar{K} + \bar{K}') \left[G^\alpha(K + \bar{K} + \bar{K}') \right. \\ & \left. + G^\alpha(K - \bar{K}') \right] \Gamma^{\phi\phi\phi}(\bar{K}, \bar{K}', -\bar{K} - \bar{K}'). \end{aligned} \quad (2.82)$$

Because the three-boson vertex has the very complicated form given in Equations (2.32) and (2.75), the integrations involved on the right-hand side of this are quite cumbersome. The \bar{k}_\perp integration, however, is still trivial due to the δ -function in $\dot{F}(\bar{K}')$ and we may still do the k'_\parallel integration using the method of residues. We are then left with a frequency integral given by

$$\begin{aligned} \partial_\Lambda \Gamma^{\bar{\psi}^\alpha \psi^\alpha \phi}(K + \bar{K}; K; \bar{K})^{(2)} = & - \frac{i\alpha N \Lambda^2}{(2\pi)^2} \int_{-\infty}^{\infty} \frac{d\bar{\omega}'}{2\pi} \frac{1}{r_0 + c_0 \Lambda^{z_b-1} + b_0 \frac{|\bar{\omega}'|}{\Lambda}} \\ & \times \sum_{s=\pm} F(\bar{\omega} + \bar{\omega}', \bar{k}_\perp + s\Lambda) J(\bar{\omega}, \bar{k}_\perp, \bar{\omega}', s\Lambda) \\ & \times \sum_{\alpha'=\pm} \Gamma_0^{\alpha'} \left[\frac{\Theta(\text{Im}z_1) - \Theta(\text{Im}z_3)}{(z_1 - z_3)^2 - z_4^2} \right. \\ & \left. - \frac{\Theta(\text{Im}z_2) - \Theta(\text{Im}z_3)}{(z_2 - z_3)^2 - z_4^2} \right], \end{aligned} \quad (2.83)$$

with

$$\begin{aligned} J(\bar{\omega}, \bar{k}_\perp, \bar{\omega}', \bar{k}'_\perp) = & \left(\frac{1}{\bar{k}_\perp} + \frac{1}{\bar{k}'_\perp} \right) \left[\bar{\omega} \Theta \left(\frac{\bar{\omega}}{\bar{k}_\perp} \right) + \bar{\omega}' \Theta \left(\frac{\bar{\omega}'}{\bar{k}'_\perp} \right) \right. \\ & \left. - (\bar{\omega} + \bar{\omega}') \Theta \left(\frac{\bar{\omega} + \bar{\omega}'}{\bar{k}_\perp + \bar{k}'_\perp} \right) \right], \end{aligned} \quad (2.84a)$$

$$\begin{aligned} z_1 = & - (k_\parallel + \bar{k}_\parallel) - \alpha [\Lambda + s(k_\perp + \bar{k}_\perp)]^2 \\ & + \frac{i\bar{\omega}' + i\bar{\omega} + i\omega}{Z_\Lambda}, \end{aligned} \quad (2.84b)$$

$$z_2 = k_\parallel + \alpha (\Lambda - s k_\perp)^2 + \alpha \frac{i\bar{\omega}' - i\omega}{Z_\Lambda}, \quad (2.84c)$$

$$z_3 = \Lambda \left[\frac{\bar{k}_\parallel}{s\bar{k}_\perp} - \frac{\alpha'}{Z_\Lambda} \left(\frac{i\bar{\omega}}{s\bar{k}_\perp} - \frac{i\bar{\omega}'}{\Lambda} \right) \right], \quad (2.84d)$$

$$z_4 = \Lambda (\Lambda + s\bar{k}_\perp). \quad (2.84e)$$

Whilst Equations (2.83) and (2.84) constitute a very complicated expression for the fermion-boson vertex, it is in principle possible to perform the final frequency integration exactly. To do this one would first notice that the integrand in Equation (2.83) is symmetric under the simultaneous sign change of all frequencies and complex conjugation. This is clearly the case for z_1, z_2, z_3 , and z_4 while for $J(\bar{\omega}, \bar{k}_\perp, \bar{\omega}', \bar{k}'_\perp)$ it is seen by rewriting

$$\begin{aligned}
 & \bar{\omega} \Theta \left(\frac{\bar{\omega}}{\bar{k}_\perp} \right) + \bar{\omega}' \Theta \left(\frac{\bar{\omega}'}{\bar{k}'_\perp} \right) - (\bar{\omega} + \bar{\omega}') \Theta \left(\frac{\bar{\omega} + \bar{\omega}'}{\bar{k}_\perp + \bar{k}'_\perp} \right) \\
 &= \bar{\omega} \left[\Theta \left(\frac{\bar{\omega}}{\bar{k}_\perp} \right) - \Theta \left(\frac{\bar{\omega} + \bar{\omega}'}{\bar{k}_\perp + \bar{k}'_\perp} \right) \right] \\
 &+ \bar{\omega}' \left[\Theta \left(\frac{\bar{\omega}'}{\bar{k}'_\perp} \right) - \Theta \left(\frac{\bar{\omega} + \bar{\omega}'}{\bar{k}_\perp + \bar{k}'_\perp} \right) \right] \\
 &= \bar{\omega} \operatorname{sgn} \left(\frac{\bar{\omega}}{\bar{k}_\perp} \frac{\bar{\omega} + \bar{\omega}'}{\bar{k}_\perp + \bar{k}'_\perp} \right) \Theta \left(-\frac{\bar{\omega}}{\bar{k}_\perp} \frac{\bar{\omega} + \bar{\omega}'}{\bar{k}_\perp + \bar{k}'_\perp} \right) \\
 &+ \bar{\omega}' \operatorname{sgn} \left(\frac{\bar{\omega}'}{\bar{k}'_\perp} \frac{\bar{\omega} + \bar{\omega}'}{\bar{k}_\perp + \bar{k}'_\perp} \right) \Theta \left(-\frac{\bar{\omega}'}{\bar{k}'_\perp} \frac{\bar{\omega} + \bar{\omega}'}{\bar{k}_\perp + \bar{k}'_\perp} \right), \quad (2.85)
 \end{aligned}$$

where, in the last equality, we have used the identity (2.72). It is thus readily seen that $J(\bar{\omega}, \bar{k}_\perp, \bar{\omega}', \bar{k}'_\perp) = -J(-\bar{\omega}, \bar{k}_\perp, -\bar{\omega}', \bar{k}'_\perp)$. This asymmetry is however cancelled by the factor of i in Equation (2.83). Therefore the integrand is symmetric as stated above. Using this, the frequency integral can then be done by splitting the integrand into partial fractions which reduces the integral to a sum of standard integrals which can be solved in a tedious but straightforward way. The result, however, is fairly involved and it is not simple to extract any physical insight from it. We therefore write down scaling relations analogously to the previous calculation such that

$$\Lambda \partial_\Lambda \Gamma^{\bar{\psi}^\alpha \psi^\alpha \phi}(\bar{K}; 0; \bar{K})^{(2)} = -I_\Lambda^{(2)} \left(\frac{\bar{\omega}}{\Lambda^{z_b}}, \frac{\bar{k}_\parallel}{\Lambda^2}, \frac{\bar{k}_\perp}{\Lambda} \right), \quad (2.86a)$$

$$\Lambda \partial_\Lambda \left. \frac{\partial \Gamma^{\bar{\psi}^\alpha \psi^\alpha \phi}(K + \bar{K}; K; \bar{K})^{(2)}}{\partial(i\omega)} \right|_{K=0} = -\frac{1}{\Lambda^{z_b}} I_\Lambda^{(2\omega)} \left(\frac{\bar{\omega}}{\Lambda^{z_b}}, \frac{\bar{k}_\parallel}{\Lambda^2}, \frac{\bar{k}_\perp}{\Lambda} \right), \quad (2.86b)$$

$$\Lambda \partial_\Lambda \left. \frac{\partial \Gamma^{\bar{\psi}^\alpha \psi^\alpha \phi}(K + \bar{K}; K; \bar{K})^{(2)}}{\partial(\alpha k_\parallel)} \right|_{K=0} = -\frac{1}{\Lambda^2} I_\Lambda^{(2k)} \left(\frac{\bar{\omega}}{\Lambda^{z_b}}, \frac{\bar{k}_\parallel}{\Lambda^2}, \frac{\bar{k}_\perp}{\Lambda} \right). \quad (2.86c)$$

Naturally the scaling functions appearing on the right-hand side of Equations (2.86) will be far more complicated than their counterparts in (2.78). To proceed let us therefore assume that the cutoff Λ is the largest scale in the problem. This corresponds to assuming that the arguments of the scaling functions are much smaller than unity. Then the frequency integration can be performed without much trouble, yielding for the scaling functions

$$I_{\Lambda}^{(2)}(\bar{\epsilon}, \bar{q}_{\parallel}, \bar{q}_{\perp}) \approx \frac{\gamma_{\Lambda} |\bar{\epsilon}| N}{2(2\pi)^3 (r_{\Lambda} + c_0)^2} \left[\frac{1}{|\bar{q}_{\perp}| - w} - \frac{|\bar{q}_{\perp}|}{(|\bar{q}_{\perp}| - w)^2} \ln \left(\frac{|\bar{q}_{\perp}|}{w} \right) \right], \quad (2.87a)$$

$$I_{\Lambda}^{(2\omega)}(\bar{\epsilon}, \bar{q}_{\parallel}, \bar{q}_{\perp}) \approx \frac{\gamma_{\Lambda} N}{(2\pi)^3 (r_{\Lambda} + c_0)^2} \left[\frac{\alpha \gamma_{\Lambda} \bar{q}_{\parallel} |\bar{\epsilon}|}{\bar{\epsilon}^2 + \gamma_{\Lambda}^2 \bar{q}_{\parallel}^2} - i \operatorname{sgn}(\bar{\epsilon}) |\bar{q}_{\perp}| \frac{\bar{\epsilon}^2 (\bar{\epsilon}^2 - \gamma_{\Lambda}^2 \bar{q}_{\parallel}^2)}{(\bar{\epsilon}^2 + \gamma_{\Lambda}^2 \bar{q}_{\parallel}^2)^2} \right], \quad (2.87b)$$

$$I_{\Lambda}^{(2k)}(\bar{\epsilon}, \bar{q}_{\parallel}, \bar{q}_{\perp}) \approx \frac{i \operatorname{sgn}(\bar{\epsilon}) \gamma_{\Lambda}^2 |\bar{q}_{\perp}| N}{(2\pi)^3 (r_{\Lambda} + c_0)^2} \frac{\bar{\epsilon}^2 (\bar{\epsilon}^2 - \gamma_{\Lambda}^2 \bar{q}_{\parallel}^2)}{(\bar{\epsilon}^2 + \gamma_{\Lambda}^2 \bar{q}_{\parallel}^2)^2}, \quad (2.87c)$$

where γ_{Λ} and r_{Λ} have been defined below Equation (2.79) and we have introduced

$$w = \frac{b_0}{2(r_{\Lambda} + c_0)} [|\bar{\epsilon}| - i\alpha\gamma_{\Lambda}\bar{q}_{\parallel}\operatorname{sgn}(\bar{\epsilon})]. \quad (2.88)$$

Now that we have the scaling functions for both contributions to the flow equation for the fermion-boson vertex we may add these to get scaling relations for the full vertex. However, as we have approximated the contributions from the second part (Equations (2.87) above) for small frequencies and momenta, we should do the same for the first part in order to be consistent. Doing thus and adding terms together we then arrive at

$$\begin{aligned}
 I_\Lambda(\bar{\epsilon}, \bar{q}_\parallel, \bar{q}_\perp) &= I_\Lambda^{(1)}(\bar{\epsilon}, \bar{q}_\parallel, \bar{q}_\perp) + I_\Lambda^{(2)}(\bar{\epsilon}, \bar{q}_\parallel, \bar{q}_\perp) \\
 &\approx \frac{\gamma_\Lambda}{(2\pi)^2 (r_\Lambda + c_0)} \left\{ \frac{i\bar{\epsilon}}{i\bar{\epsilon} - \gamma_\Lambda [\alpha\bar{q}_\parallel + \bar{q}_\perp^2 + 2\bar{q}_\perp]} \right. \\
 &\quad + \frac{i\bar{\epsilon}}{i\bar{\epsilon} - \gamma_\Lambda [\alpha\bar{q}_\parallel + \bar{q}_\perp^2 - 2\bar{q}_\perp]} \\
 &\quad \left. + \frac{N}{4\pi (r_\Lambda + c_0)} \left[\frac{|\bar{\epsilon}|}{|\bar{q}_\perp| - w} - \frac{|\bar{q}_\perp|\bar{\epsilon}}{(|\bar{q}_\perp| - w)^2} \ln \left(\frac{|\bar{q}_\perp|}{w} \right) \right] \right\}, \quad (2.89a)
 \end{aligned}$$

$$\begin{aligned}
 I_\Lambda^{(\omega)}(\bar{\epsilon}, \bar{q}_\parallel, \bar{q}_\perp) &= I_\Lambda^{(1\omega)}(\bar{\epsilon}, \bar{q}_\parallel, \bar{q}_\perp) + I_\Lambda^{(2\omega)}(\bar{\epsilon}, \bar{q}_\parallel, \bar{q}_\perp) \\
 &\approx \frac{\gamma_\Lambda b_0}{(2\pi)^2 (r_\Lambda + c_0)^2} \left\{ - \frac{|\bar{\epsilon}|}{i\bar{\epsilon} - \gamma_\Lambda [\alpha\bar{q}_\parallel + \bar{q}_\perp + 2\bar{q}_\perp]} \right. \\
 &\quad - \frac{|\bar{\epsilon}|}{i\bar{\epsilon} - \gamma_\Lambda [\alpha\bar{q}_\parallel + \bar{q}_\perp - 2\bar{q}_\perp]} \\
 &\quad \left. + \frac{N}{2\pi b_0} \left[\frac{\alpha\gamma_\Lambda \bar{q}_\parallel |\bar{\epsilon}|}{\bar{\epsilon}^2 + \gamma_\Lambda^2 \bar{q}_\parallel^2} - |\bar{q}_\perp| \frac{i\bar{\epsilon}|\bar{\epsilon}| (\bar{\epsilon}^2 - \gamma_\Lambda^2 \bar{q}_\parallel^2)}{(\bar{\epsilon}^2 + \gamma_\Lambda^2 \bar{q}_\parallel^2)^2} \right] \right\}, \quad (2.89b)
 \end{aligned}$$

$$\begin{aligned}
 I_\Lambda^{(k)}(\bar{\epsilon}, \bar{q}_\parallel, \bar{q}_\perp) &= I_\Lambda^{(1k)}(\bar{\epsilon}, \bar{q}_\parallel, \bar{q}_\perp) + I_\Lambda^{(2k)}(\bar{\epsilon}, \bar{q}_\parallel, \bar{q}_\perp) \\
 &\approx \frac{\gamma_\Lambda^2 |\bar{q}_\perp| N}{(2\pi)^3 (r_\Lambda + c_0)^2} \frac{i\bar{\epsilon}|\bar{\epsilon}| (\bar{\epsilon}^2 - \gamma_\Lambda^2 \bar{q}_\parallel^2)}{(\bar{\epsilon}^2 + \gamma_\Lambda^2 \bar{q}_\parallel^2)^2}. \quad (2.89c)
 \end{aligned}$$

What remains is now to integrate up the flow of the fermion-boson vertex and its derivatives at $K = 0$. Formally the solutions after integrating up may be written as

$$\Gamma^{\bar{\psi}^\alpha \psi^\alpha \phi}(\bar{K}; 0; \bar{K}) = \tilde{\Gamma}_\Lambda(\bar{\epsilon}, \bar{q}_\parallel, \bar{q}_\perp), \quad (2.90a)$$

$$\left. \frac{\partial \Gamma^{\bar{\psi}^\alpha \psi^\alpha \phi}(K + \bar{K}; K; \bar{K})}{\partial(i\omega)} \right|_{K=0} = \frac{1}{\Lambda^{z_b}} \tilde{\Gamma}_\Lambda^\omega(\bar{\epsilon}, \bar{q}_\parallel, \bar{q}_\perp), \quad (2.90b)$$

$$\left. \frac{\partial \Gamma^{\bar{\psi}^\alpha \psi^\alpha \phi}(K + \bar{K}; K; \bar{K})}{\partial(\alpha k_\parallel)} \right|_{K=0} = \frac{1}{\Lambda^2} \tilde{\Gamma}_\Lambda^k(\bar{\epsilon}, \bar{q}_\parallel, \bar{q}_\perp), \quad (2.90c)$$

with the scaling functions defined as

$$\tilde{\Gamma}_\Lambda(\bar{\epsilon}, \bar{q}_\parallel, \bar{q}_\perp) = 1 + \int_{\Lambda/\Lambda_0}^1 \frac{ds}{s} I_{\Lambda/s}(s^{z_b} \bar{\epsilon}, s^2 \bar{q}_\parallel, s \bar{q}_\perp), \quad (2.91a)$$

$$\tilde{\Gamma}_\Lambda^\omega(\bar{\epsilon}, \bar{q}_\parallel, \bar{q}_\perp) = \int_{\Lambda/\Lambda_0}^1 ds s^{z_b-1} I_{\Lambda/s}^{(\omega)}(s^{z_b} \bar{\epsilon}, s^2 \bar{q}_\parallel, s \bar{q}_\perp), \quad (2.91b)$$

$$\tilde{\Gamma}_\Lambda^k(\bar{\epsilon}, \bar{q}_\parallel, \bar{q}_\perp) = \int_{\Lambda/\Lambda_0}^1 ds s I_{\Lambda/s}^{(k)}(s^{z_b} \bar{\epsilon}, s^2 \bar{q}_\parallel, s \bar{q}_\perp). \quad (2.91c)$$

Let us at this stage stress that, in order to write down these formal solutions for the vertex, no approximations other than the ones inherent in our truncation scheme are needed, and in principle we could have used the expression for the fermion-boson vertex with full frequency- and momentum dependence included. However, to proceed further analytically and to extract the essential physical content it is convenient to use the low-energy approximation discussed above. Moreover to simplify the expressions in Equations (2.91) note that these depend on our dimensionless parameter γ_Λ , defined in (2.80). As already noted this becomes proportional to $N(z_b - 2)$ as the cutoff is sent to zero. This however is exactly the small parameter used by Mross et al[55] to put the $1/N$ -expansion under control. It is therefore natural to also use this parameter as an expansion parameter in our case, although it should be stressed again that it is, in principle, not necessary for the theory to be under control in our case. Before actually performing the integral let us furthermore note that we are only interested in the vertex scaling functions at $\bar{q}_\perp = 1$ (corresponding to $\bar{k}_\perp = \Lambda$). This is due to the δ -function which appears in the expressions for the anomalous dimensions (2.41) through the bosonic single-scale propagator $\dot{F}(\bar{K})$. Taking this into account, the relevant integrals in (2.91) yield, in the physical limit $\Lambda \rightarrow 0$,

$$\begin{aligned} \lim_{\Lambda \rightarrow 0} \tilde{\Gamma}_\Lambda(\bar{\epsilon}, \bar{q}_\parallel, 1) = 1 + \frac{\gamma}{(2\pi)^2(c_0 + r_0)} & \left\{ \frac{i\bar{\epsilon}}{i\bar{\epsilon} - \alpha\gamma\bar{q}_\parallel - \gamma} \ln \left[1 - \left(\frac{i\bar{\epsilon} - \alpha\gamma\bar{q}_\parallel - \gamma}{2\gamma} \right)^2 \right] \right. \\ & \left. - \frac{i\bar{\epsilon}N}{2\pi(c_0 + r_0)} \left[\frac{\ln \left[\frac{2i\text{sgn}(\bar{\epsilon})}{i\bar{\epsilon} + \alpha\gamma\bar{q}_\parallel} \right]}{2i\text{sgn}(\bar{\epsilon}) - (i\bar{\epsilon} + \alpha\gamma\bar{q}_\parallel)} + 2 \frac{\ln \left[1 - \frac{i\bar{\epsilon} + \alpha\gamma\bar{q}_\parallel}{2i\text{sgn}(\bar{\epsilon})} \right]}{i\bar{\epsilon} + \alpha\gamma\bar{q}_\parallel} \right] \right\}, \end{aligned} \quad (2.92a)$$

$$\begin{aligned} \lim_{\Lambda \rightarrow 0} \tilde{\Gamma}_\Lambda^\omega(\bar{\epsilon}, \bar{q}_\parallel, 1) = \frac{\gamma}{(2\pi)^2(c_0 + r_0)} & \left\{ - \frac{|\bar{\epsilon}|}{i\bar{\epsilon} - \alpha\gamma\bar{q}_\parallel} + \frac{N}{2\pi(c_0 + r_0)} \left[\frac{|\bar{\epsilon}|\alpha\gamma\bar{q}_\parallel}{\bar{\epsilon}^2 + \gamma^2\bar{q}_\parallel^2} \right. \right. \\ & \left. \left. - \frac{i\bar{\epsilon}|\bar{\epsilon}|(\bar{\epsilon}^2 - \gamma^2\bar{q}_\parallel^2)}{3(\bar{\epsilon}^2 + \gamma^2\bar{q}_\parallel^2)^2} \right] \right\}, \end{aligned} \quad (2.92b)$$

$$\lim_{\Lambda \rightarrow 0} \tilde{\Gamma}_\Lambda^k(\bar{\epsilon}, \bar{q}_\parallel, 1) = \frac{\gamma^2 N}{(2\pi)^3(c_0 + r_0)^2} \frac{i\bar{\epsilon}|\bar{\epsilon}|(\bar{\epsilon}^2 - \gamma^2\bar{q}_\parallel^2)}{3(\bar{\epsilon}^2 + \gamma^2\bar{q}_\parallel^2)^2}. \quad (2.92c)$$

In all these expressions we have evaluated the integrals to leading order in γ only.

The above expressions constitute our final result for the fermion-boson vertex and its derivatives with respect to frequency and momentum at $K = 0$. In the next section we will use them to explicitly calculate the anomalous dimensions.

2.2.8 Results for the anomalous dimensions

With the results of the previous sections we are now ready to calculate the anomalous dimensions. We thus insert Equations (2.90) into (2.41). To ensure ultraviolet convergence of the \bar{k}_\parallel integration we moreover regularize the integral by subtracting the self-energy at the Fermi surface (see also Section 2.2.5). After performing the straightforward \bar{k}_\perp integration, switching to the rescaled, dimensionless variables $\bar{q}_\parallel = \bar{k}_\parallel/\Lambda^2$, $\bar{\epsilon} = \bar{\omega}/\Lambda^{z_b}$, and defining $p = \gamma_\Lambda \alpha \bar{q}_\parallel$ we arrive at the following two-dimensional integrals

$$\begin{aligned} \eta_\Lambda &= -\frac{\gamma_\Lambda}{2\pi} \lim_{\omega \rightarrow 0} \frac{\partial}{\partial(i\omega)} \int_{-\lambda_0}^{\lambda_0} \frac{d\bar{\epsilon}}{2\pi} \int_{-\infty}^{\infty} \frac{dp}{2\pi} \frac{1}{r_\Lambda + c_0 + b_0|\bar{\epsilon}|} \\ &\times \left[\frac{1}{i\bar{\epsilon} + i\omega - p - \gamma_\Lambda} - \frac{1}{i\bar{\epsilon} - p - \gamma_\Lambda} \right] \left[\tilde{\Gamma}_\Lambda \left(\bar{\epsilon}, \frac{p}{\alpha\gamma_\Lambda}, 1 \right) \right]^2 \\ &- \frac{\gamma_\Lambda}{\pi} \int_{-\lambda_0}^{\lambda_0} \frac{d\bar{\epsilon}}{2\pi} \int_{-\infty}^{\infty} \frac{dp}{2\pi} \frac{1}{r_\Lambda + c_0 + b_0|\bar{\epsilon}|} \frac{1}{i\bar{\epsilon} - p - \gamma_\Lambda} \\ &\times \tilde{\Gamma}_\Lambda \left(\bar{\epsilon}, \frac{p}{\alpha\gamma_\Lambda}, 1 \right) \tilde{\Gamma}_\Lambda^\omega \left(\bar{\epsilon}, \frac{p}{\alpha\gamma_\Lambda}, 1 \right), \end{aligned} \quad (2.93a)$$

$$\begin{aligned} \tilde{\eta}_\Lambda &= \frac{\gamma_\Lambda}{2\pi} \lim_{k \rightarrow 0} \frac{\partial}{\partial k} \int_{-\lambda_0}^{\lambda_0} \frac{d\bar{\epsilon}}{2\pi} \int_{-\infty}^{\infty} \frac{dp}{2\pi} \frac{1}{r_\Lambda + c_0 + b_0|\bar{\epsilon}|} \\ &\times \left[\frac{1}{i\bar{\epsilon} - p - k - \gamma_\Lambda} - \frac{1}{i\bar{\epsilon} - p - \gamma_\Lambda} \right] \left[\tilde{\Gamma}_\Lambda \left(\bar{\epsilon}, \frac{p}{\alpha\gamma_\Lambda}, 1 \right) \right]^2 \\ &+ \frac{1}{\pi} \int_{-\lambda_0}^{\lambda_0} \frac{d\bar{\epsilon}}{2\pi} \int_{-\infty}^{\infty} \frac{dp}{2\pi} \frac{1}{r_\Lambda + c_0 + b_0|\bar{\epsilon}|} \frac{1}{i\bar{\epsilon} - p - \gamma_\Lambda} \\ &\times \tilde{\Gamma}_\Lambda \left(\bar{\epsilon}, \frac{p}{\alpha\gamma_\Lambda}, 1 \right) \tilde{\Gamma}_\Lambda^k \left(\bar{\epsilon}, \frac{p}{\alpha\gamma_\Lambda}, 1 \right). \end{aligned} \quad (2.93b)$$

The presence of the ultraviolet cutoff λ_0 is due to the fact that we will be using the expressions for the vertices which were derived in the previous section. These were all derived in the limit where frequencies and momenta are much smaller than the flow parameter Λ . Because of these approximations, the expressions above for the anomalous dimensions would be logarithmically divergent in the ultraviolet without the cutoff. If we had used, instead, the full expression for the vertices and not made any approximations in the previous

section we would have arrived at ultraviolet convergent integrals. It should in principle be possible to evaluate these numerically although this has not yet been attempted. Instead we simply take λ_0 to be of the order of unity and keep working with the vertices derived in the previous section. For $\Lambda \rightarrow 0$ we therefore substitute Equations (2.92) into (2.93). The p integral can then be performed using the method of residues. Before explicitly doing this though it is worth noting that the first term in the curly brackets of (2.92a) and the first term in the curly brackets of (2.92b) do not yield any contribution to the anomalous dimensions. The reason for this is that, for these terms, all poles are situated in the same half of the complex plane. Closing the contour in the opposite half then yields a vanishing contribution. Tracking the origin of these terms we see that they are generated from the first contribution to the flow of the fermion-boson vertex, namely from $\Gamma^{\bar{\psi}^\alpha \psi^\alpha \phi}(K + \bar{K}; K; \bar{K})^{(1)}$ whose flow equation is given in (2.77). We thus see that only the terms that receive a contribution from the renormalized three-boson vertex contribute. The renormalization of the three-boson vertex is therefore critical in order to calculate the anomalous dimensions beyond one-loop order. For these terms we then find, after performing the p integral and setting $r_0 = 0$ in order to consider the quantum critical point,

$$\eta = z_b - 2 + \frac{(z_b - 2)^2}{2} C(\lambda_0) + \mathcal{O}((z_b - 2)^3), \quad (2.94a)$$

$$\tilde{\eta} = \frac{(z_b - 2)^2}{2} \tilde{C}(\lambda_0) + \mathcal{O}((z_b - 2)^3), \quad (2.94b)$$

where we have introduced the cutoff functions

$$C(\lambda_0) = \int_0^{\lambda_0} \frac{dy}{1+y} \left[\frac{7}{6} + \frac{1}{1-y} + \frac{y \ln y}{(1-y)^2} \right], \quad (2.95a)$$

$$\begin{aligned} \tilde{C}(\lambda_0) &= \int_0^{\lambda_0} \frac{dy}{1+y} \left[\frac{1}{6} + \frac{1}{1-y} + \frac{y \ln y}{(1-y)^2} \right] \\ &= C(\lambda_0) - \ln(1 + \lambda_0), \end{aligned} \quad (2.95b)$$

which are both shown in Figure 2.15. Both cutoff functions diverge logarithmically as $\lambda_0 \rightarrow \infty$. We also note that the one-loop results are recovered as the leading terms in the expansion above, namely $\eta = z_b - 2$ and $\tilde{\eta} = 0$.

As was discussed above, it is in principle possible to arrive at ultraviolet convergent expressions for the anomalous dimensions. To achieve this, however, it would be necessary to retain the full frequency- and momentum dependence of the fermion-boson vertex. This would require some numerical effort and has not been attempted. It is however important to stress that our theory does not implicitly rely on the smallness of momenta or frequencies. Likewise the fact that we have expanded in $N(z_b - 2)$ is not a requirement to

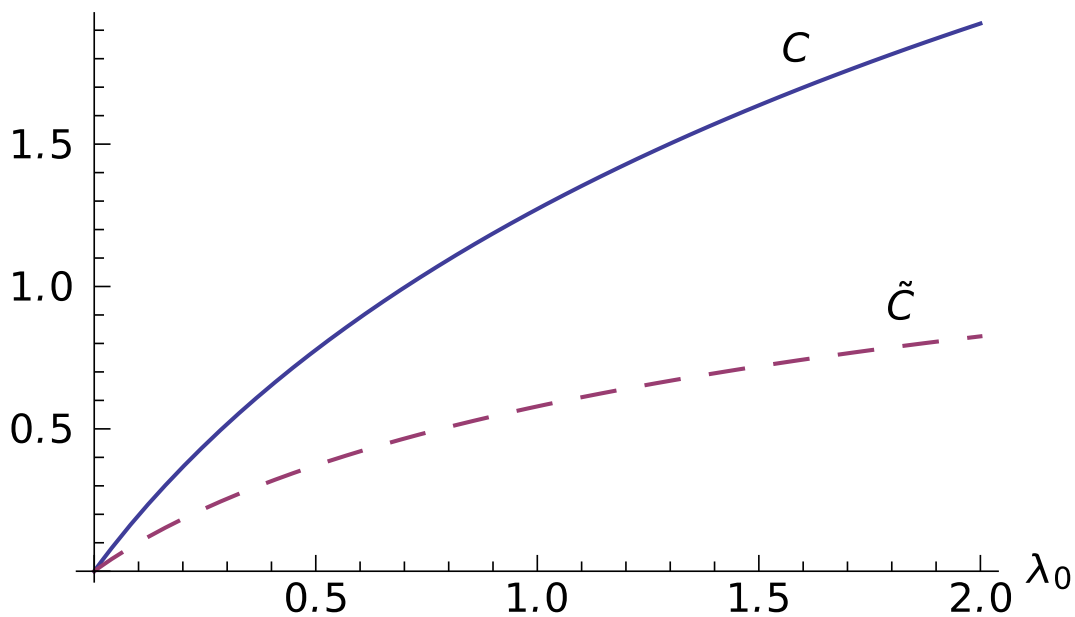


Figure 2.15: Plot of the cutoff functions $C(\lambda_0)$ and $\tilde{C}(\lambda_0)$ given by Equations (2.95).

put the theory under control and it should be possible to obtain values for the anomalous dimensions without making this approximation as well. For now, however, we simply take Equations (2.94) as our final results for the anomalous dimensions and extrapolate to $z_b = 3$. As the ultraviolet divergence is moreover only logarithmic we choose the sensible value $\lambda_0 = 1$ for the ultraviolet cutoff. In that case we arrive at $C \approx 1.27$ and $\tilde{C} \approx 0.58$. Using Equations (2.45) and (2.49) we hence find

$$\begin{aligned} \eta_\psi &= \frac{(z_b - 2)^2}{2} \tilde{C}(\lambda_0) + \mathcal{O}((z_b - 2)^3) \\ &\approx 0.3(z_b - 2)^2 + \mathcal{O}((z_b - 2)^3), \end{aligned} \quad (2.96a)$$

$$\begin{aligned} z &= \frac{z_b}{2} + \frac{(z_b - 2)^2}{4} [C(\lambda_0) - \tilde{C}(\lambda_0)] + \mathcal{O}((z_b - 2)^3) \\ &\approx \frac{z_b}{2} + 0.2(z_b - 2)^2 + \mathcal{O}((z_b - 2)^3). \end{aligned} \quad (2.96b)$$

Extrapolating to $z_b = 3$ we thus get $\eta_\psi \approx 0.3$ which is greater than the result obtained by Metlitski and Sachdev[54] but smaller than the results obtained by extrapolating the results of Mross et al.[55]. This discrepancy is not surprising given the different approximations used in the various calculations. It is however reassuring that we also find a non-zero value of η_ψ .

We also note that, in our calculation, we obtain a small renormalization of the fermionic dynamic exponent z which was expected[54] to remain unrenormalized up to three-loop order. Indeed this is also what we would have expected. If the fermionic dynamic exponent is allowed to renormalize, while the bosonic

dynamic exponent z_b remains unrenormalized (recall that we expect this as the dynamic exponent is not expected to renormalize because the interaction is non-local), it would imply that the fermionic and bosonic degrees of freedom decouple at some point. As our theory is strongly coupled however this should not happen. The reason we find a small renormalization of z is likely that our truncation misses some diagrams which are important for this calculation. Indeed the diagrams which contribute to the anomalous dimension corresponding to the frequency dependence of the self-energy (η in our notation) are not expected to arise before four-loop order[95]. The exponent calculated by Metlitski and Sachdev[54] is instead calculated via the anomalous dimension corresponding to the momentum dependence of the self-energy ($\tilde{\eta}$ in our notation), which arises at three-loop order as discussed in Section 2.1.3. η is then deduced by expecting that the frequency and momentum dependence of the self-energy should renormalize in the same way. Since our calculation, on the other hand, is not perturbative in the loop order, we have implicitly also taken into account diagrams with more than three loops, albeit only a certain class of these diagrams, namely the ones generated in our flow. This is also the reason why we are able to explicitly calculate η from our flow equations.

2.3 Implications for experiments

Before ending this chapter, let us briefly discuss consequences of a finite value of η_ψ that can be determined in experiments[55, 64]. Because the anomalous dimension modifies the scaling of the fermionic propagator, it will also appear in the spectral function $A(K)$, defined in general in the first equality of Equation (1.44). From the spectral function we may now calculate the frequency-dependent tunnelling density of states by

$$\nu(\omega) = \int \frac{d^2k}{(2\pi)^2} A(\omega, \mathbf{k}). \quad (2.97)$$

The integral may be performed by switching to polar coordinates and expanding around the Fermi surface. The final result yields that the tunnelling density of states is modified by[64]

$$\nu(\omega) \sim |\omega|^{4\eta_\psi/z_b}. \quad (2.98)$$

This modification should, in principle, be observable in tunnelling experiments, although depending on the numerical value of η_ψ this may be cumbersome.

2.4 Summary and conclusions

In this chapter we have considered the Ising-nematic quantum critical point of two-dimensional metals. The theory of this is analogous to the theory

of a Fermi surface interacting with a $U(1)$ gauge field which is relevant for several different systems such as spin-liquids and half-filled Landau levels. In Section 2.1 we discussed how the standard Hertz-Millis approach to quantum criticality is not sufficient in this problem and how certain three-loop diagrams (see Figure 2.6) lead to, not only the breakdown of the $1/N$ -expansion, where N is the number of fermion flavours, but also to anomalous dimensions which modify the result for the self-energy given in Equations (2.6) and (2.15). As an alternative approach we developed in Section 2.2 a strategy for calculating the anomalous dimensions using the FRG. We were able to write down flow equations which contain, apart from many other diagrams, after iteration, the diagrams in Figure 2.6. For the flow equations of vertices containing fermionic legs (the fermionic self-energy and the mixed fermion-boson vertex) we truncated the flow equations at the level of the three-legged vertex, whilst for vertices containing only bosonic external legs we used truncated skeleton equations to close the hierarchy of equations. We finally found it most convenient to use a sharp cutoff in the bosonic sector only. By neglecting vertex corrections we were, in Section 2.2.5, able to recover the known [54, 55, 65, 72, 73, 92, 95] result for the one-loop fermionic and bosonic self-energies. In agreement with previous work we also found the existence of a non-Fermi liquid state at the quantum critical point. By reproducing the one-loop result we moreover obtained the one-loop values for the (flowing) quasi-particle residue Z_Λ and momentum-renormalization factor Y_Λ . These, together with the one-loop result for the polarization, were used to renormalize all propagators in subsequent calculations. Doing so we were able to include vertex corrections and derive expressions for the anomalous dimensions η and $\tilde{\eta}$ related to the frequency- and momentum dependence of the fermionic self-energy respectively. These are given in Equations (2.93). Without further approximations these expressions are in principle exact (within our truncation scheme and with the caveat that we have used one-loop results for the renormalization factors Z_Λ and Y_Λ such that these would have to be modified to get truly exact results) and do not rely on the smallness of any parameter. To compute the anomalous dimensions we however assumed small frequencies and momenta and expanded in $N(z_b - 2)$, where z_b is the bosonic dynamic exponent. A similar approximation had been used by Mross et al. [55] in a previous work. The resulting expressions for the anomalous dimensions could then be computed analytically and the result is given in Equations (2.94). Whilst these expressions are divergent in the ultraviolet we argued that this is only due to the approximations made in the calculation. Because the divergence was only logarithmic we were moreover able to choose a sensible value for the ultraviolet cutoff. Thus, extrapolating to $N = 2$ and $z_b = 3$ (as is relevant for the Ising-nematic quantum critical point), we were finally able to obtain results for the anomalous dimensions. While it is not surprising that these are somewhat different than previous results [54, 55], due to the approximations involved in the various approaches, it is reassuring that we

also obtain a finite value for the anomalous dimensions. Unlike previous works we moreover explicitly calculated the anomalous dimension related to the frequency dependence of the fermionic self-energy. This was possible due to the fact that our flow equations also contain, after iterations, diagrams with more loops than three. However it is not clear whether all diagrams which contribute to η are included in our flow. This could be the reason why we, unlike previous works[54, 55], find a small renormalization of the fermionic dynamic exponent.

We finally mentioned briefly that it should be possible to observe the calculated anomalous dimensions in tunnelling experiments.

There are many ways that the work presented in this chapter could be extended. Indeed the main advantage of our method is that it does not rely on the presence of a small parameter. Therefore it is, in principle, possible to calculate the anomalous dimensions for general N and z_b . Such a calculation should be done starting from Equations (2.93) without any further approximations and would have to be done numerically. Doing this would also have the added benefit that all integrals would be ultraviolet convergent such that the anomalous dimensions would not depend on an ultraviolet cutoff. In a similar fashion it should be possible to obtain the vertices for general frequencies and momenta. Let us however point out that it is already clear from our results, that it is important to keep both bosonic and fermionic degrees of freedom. This can be seen from the fact that the three-boson vertex (2.75) is highly singular. An other route to get more reliable results (at least for the anomalous dimension of the frequency dependence of the fermionic self-energy) would be to identify which diagrams contribute at higher loops than three. Such an identification has however not been done and seems very non-trivial. Finally let us point out that our solutions to the flow equations showed that the renormalization of the three-boson vertex is essential in order to obtain finite anomalous dimensions. This is the reason these are not present in Hertz-Millis theory. The renormalization of the three-boson vertex is crucial to obtain the diagrams in Figure 2.6 which have previously[54] been identified as the important diagrams to obtain finite anomalous dimensions. It is therefore not surprising that our results point in the same direction, but let us note that the effective non-compactness of the Fermi surface (see Section 2.1.2) plays an important role in the vanishing of other contributions. It would be interesting to consider also a system with a compact Fermi surface such as the one considered in Reference [57].

Chapter 3

Non-analytic corrections in Fermi liquid theory

3.1 Introduction

As discussed in Section 1.3, the main assumption of Fermi liquid theory leads to a one-to-one correspondence between the eigenstates of the non-interacting and the interacting Fermi gas. This correspondence in particular manifests itself in the fact that it is permissible to use the same quantum labels, such as mass, Landé g-factor, etc., in the interacting case as in the non-interacting case, except that the quantum labels are renormalized in the former. In this case it is natural to expect the familiar Sommerfeld expansion from the free Fermi gas[100]

$$\gamma(T, H = 0) = \gamma(0, 0) + \mathcal{O}(T^2), \quad (3.1a)$$

$$\chi(T, H = 0) = \chi(0, 0) + \mathcal{O}(T^2), \quad (3.1b)$$

$$\chi(T = 0, H) = \chi(0, 0) + \mathcal{O}(H^2), \quad (3.1c)$$

where $\gamma = C/T$ is the heat capacity divided by temperature, χ is the spin-susceptibility and H is an external magnetic field, to be valid within Fermi liquid theory, but with renormalized values for the thermodynamic quantities. Similar analytic expansions should exist for other quantities. Analytic expansions such as Equations (3.1a)-(3.1c) are however not explicitly contained in Fermi liquid theory. Indeed the free energy in the usual Landau Fermi liquid theory is given by (see Section 1.3)¹

$$F = F_0 + \sum_{\mathbf{k}} (E_{\mathbf{k}} - \mu) \delta n_{\mathbf{k}} + \frac{1}{2} \sum_{\mathbf{k}, \mathbf{k}'} f(\mathbf{k}, \mathbf{k}') \delta n_{\mathbf{k}} \delta n_{\mathbf{k}'} + \mathcal{O}(\delta n_{\mathbf{k}}^3), \quad (3.2)$$

¹Spin is neglected for simplicity here.

where we recall $E_{\mathbf{k}}$ is the energy of a quasi-particle, $\delta n_{\mathbf{k}}$ is the difference between the interacting and non-interacting distribution functions and $f(\mathbf{k}, \mathbf{k}')$ is a Landau function which describes the interaction between quasi-particles. Now since at low temperatures $T \ll \mu$, $\delta n_{\mathbf{k}} \sim T/E_F$ (if we were working at zero temperature but with a finite magnetic field the temperature should be replaced by the Zeeman energy $g\mu_B H$, where μ_B is the Bohr magneton and g the electron Landé g-factor) it follows that the free energy within Landau Fermi liquid theory can at most be quadratic in temperature (or magnetic field if this is the relevant energy scale). Thus there is no way to predict the next-to-leading order term in Equations (3.1a)-(3.1c) within Landau Fermi liquid theory itself. To go beyond the leading, constant, terms it is necessary to consider a microscopic model and employ perturbation theory or some other method. Doing this it has in recent years become more and more evident that the Sommerfeld expansion is not sufficient beyond the leading order[101, 102, 104, 103, 105, 106, 107, 108, 109, 110, 111, 112, 113, 114, 115, 116]. Experimentally, a quadratic term in the heat capacity has been observed in, for example, liquid ^3He monolayers[117] whilst, at least, a quasi-linear behaviour is seen in the susceptibility in the iron-pnictides[118] and in heterostructures based on Si and other materials[119, 120, 121, 122]. Whilst there is agreement about the form of the quadratic term in the former, there is still debate about the latter where, for example, different experiments obtain different signs of the prefactor of the linear term, see for example References [118, 119]. The significance of this will be discussed later.

In this chapter we will go beyond the Sommerfeld expansion and consider non-analytic corrections. We begin by reviewing existing work on this topic and discuss the origin of non-analyticities. In Section 3.2 we then show that non-analytic terms also appear in quasi-particle properties such as the quasi-particle residue, momentum-renormalization factor, and electron Landé g-factor. We will also discuss how these non-analyticities can be observed in experiments.

The work presented in this chapter was done together with Philipp Lange, Peter Kopietz, and Dmitrii Maslov and most of it has been published in [123].

3.1.1 How to break the Sommerfeld expansion

We wish to consider next-to-leading order corrections in different parameters that do not take the form of the analytic Sommerfeld expansions given in Equations (3.1a)-(3.1c). To do this it is useful to consider the origin of these analytic expansions and when they are no longer valid. For this purpose note that any thermodynamic observable \mathcal{O} can be written in the following form[100]

$$\mathcal{O} = \int dE f(E) n_F(E). \quad (3.3)$$

Here $f(E)$ is some function of the energy and $n_F(E) = 1/(e^{\beta(E-\mu)} + 1)$, with β being the inverse temperature and μ denoting the chemical potential, is the Fermi function. The existence of an analytic expansion of the observable, such as the Sommerfeld expansion, is then directly related to the analyticity of the function $f(E)$ around $E = 0$. In order to get a non-analytic expansion one should therefore look for cases where $f(E)$ is not analytic.

From a microscopic point of view the equivalent of (3.3) is the second order self-energy, which for a constant momentum-independent interaction constant U is given by

$$\Sigma(K) = -U^2 \int_Q \Pi_0(Q) G_0(K-Q), \quad (3.4)$$

where we have suppressed the spin dependence, $G_0(K)$ denotes the free Green's function as defined in Equation (1.7), and we recall that we use the label² $K = (i\omega, \mathbf{k})$ to represent the $(D+1)$ -momentum and notation $\int_K = 1/(\beta V) \sum_\omega \sum_{\mathbf{k}}$, where V is the volume. Also, in this chapter, $Q = (i\bar{\omega}, \mathbf{q})$ will denote a bosonic $(D+1)$ -momentum. Finally $\Pi_0(Q)$ is the free particle-hole polarization bubble in a vanishing magnetic field³

$$\Pi_0(Q) = \int_K G_0(K) G_0(K-Q). \quad (3.5)$$

Both Equations (3.4) and (3.5) are shown graphically in Figure 3.1.

Comparing Equations (3.3) and (3.4) it is now natural to consider the polarization bubble (3.5) in more detail. The polarization defined in Equation (3.5) can be calculated exactly by performing the K -integration. The result for small momenta and frequencies is in two dimensions[105]

$$\Pi_0(Q) \approx -\nu \left[1 - \frac{|\omega|}{\sqrt{\omega^2 + (v_F q)^2}} \right], \quad (3.6)$$

where ν is the density of states per spin projection on the Fermi surface ($\nu = m/(2\pi)$ in two dimensions) and v_F is the Fermi velocity. For small frequencies $|\omega| \ll v_F q$, the dynamic part of the bubble then goes as⁴

$$\Pi_0(Q) \sim \frac{|\omega|}{v_F q}. \quad (3.7)$$

²In this chapter we will be working both at finite and zero temperature. At finite temperatures the frequency should simply be replaced by the corresponding Matsubara frequency.

³If we introduce a spin-label as well, there are different ways of defining the polarization bubble which are however all equivalent as long as one does not restrict the momentum integrations by introducing a cutoff. We shall discuss this point later.

⁴This form of the polarization also leads to Landau damping which played a crucial role in Chapter 2.

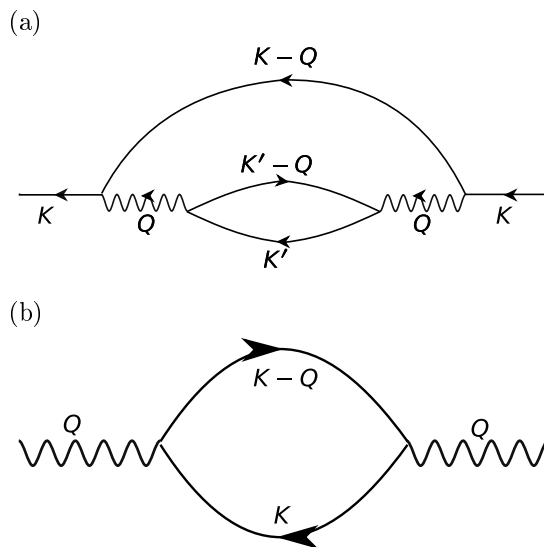


Figure 3.1: Diagram (a) represents the fermionic self-energy to second-order in the interaction (3.4), while (b) is the polarization bubble (3.5). Solid lines represent fermionic propagators whilst the wavy line represents the interaction.

As now the imaginary part of the Green's function only provides a δ -function contribution [see Equation (1.48)], it follows that the imaginary part of the self-energy on the mass shell (i.e. $\omega = \xi_{\mathbf{k}}$) picks up a non-analyticity

$$\text{Im}\Sigma(\omega) \sim -\frac{U^2 m}{v_F^2} \int_0^\omega d\Omega \Omega \int_{|\Omega|/v_F}^\Lambda \frac{dq}{q} \sim \frac{U^2 m}{v_F} \omega^2 \ln \frac{W}{|\omega|}, \quad (3.8)$$

where the infrared cutoff in the momentum integration comes from the condition $|\omega| \ll v_F q$, Λ is an ultraviolet cutoff related to some relevant internal momentum scale of the problem, $W \sim \Lambda v_F$, and the ultraviolet cutoff in the frequencies comes from the Pauli principle. Performing a Kramers-Kronig transformation this yields a $\omega|\omega|$ type of non-analyticity in the real part of the self-energy. By power counting this will thus lead to a linear in temperature non-analytic term in, for example, the heat capacity coefficient $\gamma = C/T$.

Now that we know that the non-analyticity came from the specific form of the polarization bubble given in Equation (3.7), the next question is what physical processes this corresponds to. To answer this question, note that if the fermions interact by polarizing the surrounding medium, the effective interaction is proportional to the polarization bubble. If we moreover Fourier transform Equation (3.7), we see that the effective interaction leading to the non-analyticity discussed above is dynamic and decays slowly as $|\omega|/r$ in two dimensions. With this in mind we would expect an other region of momentum space to contribute in a similar way. Indeed the Kohn anomaly at $q = 2k_F$ leads to dynamic Friedel oscillations that decay as $\omega \cos(2k_F r) / \sqrt{r}$ [114]. This also leads to non-analyticities. In other dimensions the decay would be different

but, as long as the effective interaction is long ranged, the conclusion would be the same. To see that this is the case one can perform a scaling argument which is due to Maslov and Chubukov[114]. Assume that the interaction has a range specified by some length L . By the uncertainty principle $L \sim v_F/\epsilon$ where ϵ is the relevant energy scale. If this energy scale is small the range of interactions via polarizing the medium can be large. Now, the contribution from the long-range interactions to the free energy per unit volume is given, in $D > 1$ dimensions, by

$$f_{\text{sing}} \sim \frac{U^2 \epsilon}{L^D}. \quad (3.9)$$

At finite temperatures where the relevant energy scale is temperature we then find that

$$\gamma(T) = -\frac{\partial^2 f_{\text{sing}}}{\partial T^2} \propto T^{D-1}, \quad (3.10)$$

while at zero temperature but at a finite magnetic field H , where the relevant energy scale is the Zeeman energy $g\mu_B|H|$,

$$\chi(H) = -\frac{\partial^2 f_{\text{sing}}}{\partial H^2} \propto |H|^{D-1}. \quad (3.11)$$

In three dimensions such scaling analysis breaks down and logarithmic corrections appear which can only be found in an explicit calculation[114]. We will review a renormalization group argument for the above scaling results in Section 3.1.3.

3.1.2 The susceptibility

To further study the origin of non-analyticities and to motivate the interest in the field, it is worth considering the non-analytic contributions to the spin susceptibility in more detail. The susceptibility follows from the free energy which to second order in the interaction, at finite temperatures and in D dimensions, is given by (see e.g. Reference [108])

$$f = f_0 - \frac{U^2}{2} T \sum_{\omega_n} \int \frac{d^D q}{(2\pi)^D} \Pi_0^{\uparrow\uparrow}(Q) \Pi_0^{\downarrow\downarrow}(Q), \quad (3.12)$$

where ω_n denotes a Matsubara frequency and we have added a spin-label to the polarization bubble to anticipate that spin will matter when turning on a finite magnetic field. Equation (3.12) is shown diagrammatically in Figure 3.2. Here the small momentum (and magnetic field) part of the bubble is given exactly by the expression in Equation (3.6).

As was discussed above, in general non-analytic corrections appear due to long range effective interactions coming from two regions in momentum space, namely $q = 0$ and $q = 2k_F$. It turns out however that non-analyticities in

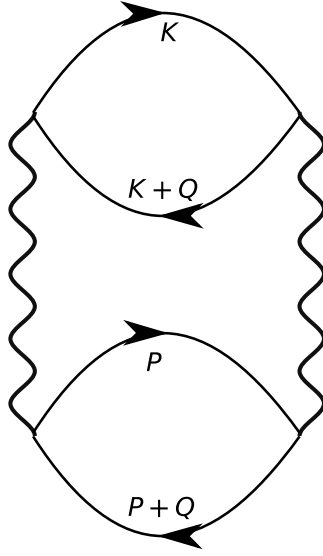


Figure 3.2: Diagrammatic representation of the free energy (3.12).

the susceptibility only come from $q = 2k_F$ contributions. To see this, note that the susceptibility is a response to an infinitesimal magnetic field. In a magnetic field the Fermi surface now splits which manifests itself in (3.6) through a splitting of the Fermi velocity v_F into v_F^\uparrow and v_F^\downarrow . Such a splitting however only leads to extra analytic terms of order H^2 and thus the small momentum part of the polarization bubble cannot contribute to sub-leading non-analytic terms in the susceptibility. For the $2k_F$ part, on the other hand, the non-analyticities arise due to $\Pi^{\uparrow\uparrow}(Q)$ and $\Pi^{\downarrow\downarrow}(Q)$ being non-analytic at the same point[108]. In a finite magnetic field, this is no longer the case as the Fermi momentum splits into k_F^\uparrow and k_F^\downarrow and so the magnetic field regularizes the non-analyticity in the free energy. However, taking a derivative removes this regularization and so the susceptibility becomes non-analytic.

With the above in mind we are interested in the $2k_F$ part of Equation (3.12) in order to study non-analyticities in the susceptibility. This thus means that we need the same-spin polarization bubbles around $q = 2k_F$. These turn out to be very complicated (the opposite-spin bubble for general momenta and frequencies will be given later) and so, such a computation would prove cumbersome. Fortunately it turns out[103, 104] that the $2k_F$ terms contributing to the non-analyticities in the polarization bubbles in Figure 3.2 come from fermions with momenta close to $\mathbf{q}/2$. Then the $2k_F$ part of the free energy (3.12) can be rewritten as the product of two opposite-spin bubbles $\Pi^{\uparrow\downarrow}(Q)$, where the momentum-transfer \mathbf{q} is now small:

$$f = f_0 - \frac{U^2}{2} T \sum_{\omega_n} \int \frac{d^D q}{(2\pi)^D} [\Pi^{\uparrow\downarrow}(Q)]^2, \quad (3.13)$$

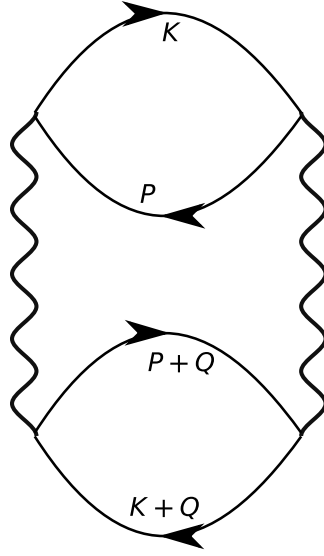


Figure 3.3: Diagrammatic representation of the free energy (3.13)

where the opposite-spin particle-hole bubble in a weak magnetic field is given, at small momenta, by [105, 114]

$$\Pi_0^{\uparrow\downarrow}(Q) \approx -\nu \left[1 - \frac{|\omega_n|}{\sqrt{(\omega_n - 2ih)^2 + v_F^2 q^2}} \right] \quad (3.14)$$

and $h = g\mu_B H$ is the Zeemann energy associated with the magnetic field H . A diagrammatic representation of Equation (3.13) is shown in Figure 3.3. We will show later that this scattering channel is not sufficient if one wants to calculate the non-analytic contribution to various quasi-particle properties.

With this behind us we can now evaluate the free energy. First of all we see that the expression (3.13) is divergent in the ultraviolet such that we need to introduce an ultraviolet cutoff. The calculation has been done previously by Maslov and Chubukov [114] who first performed the momentum integration and then the frequency sum. After performing the momentum integration and subtracting analytic terms (which diverge in the ultraviolet) they got logarithmic terms which they identified as causing the non-analyticities in the susceptibility similarly to our earlier discussion of the heat capacity. We will here reproduce their result but change the order of integration. Thereby we will explicitly see that the ultraviolet cutoff drops out of the leading non-analytic contribution to the susceptibility.

The Matsubara sum is performed using

$$T \sum_{\omega_n} F(i\omega_n) = \frac{1}{2\pi i} \int_{\mathcal{C}} dz F(z) \frac{1}{2} \coth\left(\frac{\beta z}{2}\right), \quad (3.15)$$

where $F(i\omega_n)$ is any function of the Matsubara frequencies and the contour \mathcal{C}

is chosen to circle all Matsubara frequencies in the positive direction. In our case the function F is the opposite-spin particle-hole bubble, given in Equation (3.14), squared. The contour integration hence yields

$$\begin{aligned}
T \sum_{\omega_n} \left[\Pi_0^{\uparrow\downarrow}(Q) \right]^2 &= T\nu^2 - \frac{\nu^2}{4v_F q} \left[(v_F q + 2h)^2 \coth \left(\frac{\beta(v_F q + 2h)}{2} \right) \right. \\
&\quad \left. + (v_F q - 2h)^2 \coth \left(\frac{\beta(v_F q - 2h)}{2} \right) \right] \\
&\quad + \frac{\nu^2}{\pi} \int_0^{v_F q} \frac{d\omega}{\sqrt{(v_F q)^2 - \omega^2}} \left[(\omega + 2h) \coth \left(\frac{\beta(\omega + 2h)}{2} \right) \right. \\
&\quad \left. + (\omega - 2h) \coth \left(\frac{\beta(\omega - 2h)}{2} \right) \right]. \tag{3.16}
\end{aligned}$$

Here the first and second terms come from respectively the square of the static (constant) and square of the dynamic part of Equation (3.14), whilst the last term is a branch cut contribution from the mixed static and dynamic part.

If we now focus only on zero temperature we may use that $\coth(\beta x) \rightarrow \text{sgn}(x)$ as $\beta \rightarrow \infty$ to perform the remaining momentum and frequency integrations. We find in two dimensions (introducing an ultraviolet cutoff Λ_0 in the momentum integration)

$$f = f_0 + \frac{u^2 v_F \Lambda_0^3}{4\pi} \left[\frac{1}{6} + \frac{x^2}{2} - \frac{|x|^3}{6} - \frac{2}{3\pi} (1 - x^2)^{3/2} - \frac{x}{\pi} \arcsin x - \frac{x^2}{\pi} \sqrt{1 - x^2} \right], \tag{3.17}$$

where $x = 2h/(v_F \Lambda_0)$ and we have introduced the dimensionless interaction $u = \nu U$. From Equation (3.17) we see that the branch cut terms do not contribute to the non-analytic $|x|^3$ part and that the ultraviolet cutoff drops out of the non-analytic part which thus takes on a universal low-energy form. Moreover differentiating twice with respect to the magnetic field we see that

$$\chi(h) = \chi(0) + \chi_1 |h| + \mathcal{O}(h^2), \tag{3.18}$$

with $\chi_1 = 2\nu u^2/E_F$. This is in agreement with the results found in reference [114] and the scaling analysis in the previous section.

It should be mentioned here that the fact that the prefactor χ_1 is positive (similar behaviour is found for the temperature and momentum dependence of χ , and for the heat capacity[105, 106, 107, 108, 124]) is still under debate and that there are conflicting results as to whether it holds to higher orders[114]. If it does hold it would have a significant impact on the phase diagram of electrons in a magnetic field[114]. Indeed it would imply that the susceptibility increases with energy. As, however, one would expect it to drop off at some energy larger than the Fermi energy this would mean that χ has a maximum

at a certain energy. Now, a maximum of the susceptibility at a finite magnetic field would imply that the free energy has a minimum at a finite magnetisation. Increasing the susceptibility would then mean that this minimum becomes degenerate with a non-magnetic state which implies a first order phase transition into a ferromagnetic state. On the other hand, a maximum of the susceptibility at a finite momentum would imply more exotic states such as a spiral state. In either case the Hertz-Millis theory of quantum phase transitions (see Section 2.1.1) would break down as it assumes a second order transition. Let us however again stress that the sign of the prefactors are still under debate and, although there exist arguments that they should remain positive[116], an explicit calculation is still missing.

3.1.3 Renormalization group

Before moving on to the main part of this chapter on non-analyticities in quasi-particle properties, let us briefly consider an alternative way, based on the renormalization group (RG), of viewing the non-analyticities discussed in the previous sections due to Belitz and Kirkpatrick[116]. To do this, recall that in dimensions $D > 1$ Fermi liquid theory can be described as an RG fixed point[1, 38, 103]. The fixed point has associated two relevant (in the RG sense⁵) couplings, namely the temperature and magnetic field. As such one might postulate that the free energy has a singular part which leads to the non-analyticities discussed above, and that this singular part satisfies certain scaling relations. In particular the assumption is that this singular part can be written in terms of a fermionic and bosonic (arising from particle-hole fluctuations) part

$$f_{\text{sing}}(T, H) = f_{\text{sing}}^F(T, H) + f_{\text{sing}}^B(T, H), \quad (3.19)$$

which in dimensions $1 < D < 3$ satisfy the following scaling relations

$$f_{\text{sing}}^F(bT, bH) = b^2 f_{\text{sing}}^F(T, H), \quad (3.20a)$$

$$f_{\text{sing}}^B(bT, bH) = b^{D+1} f_{\text{sing}}^B(T, H). \quad (3.20b)$$

Differentiating twice with respect to the relevant control parameter and setting the other to zero, one thus obtains the scaling behaviour discussed in the previous sections.

As an alternative route to obtain the same results one can postulate the existence of a given irrelevant coupling r . In that case the scaling ansatz should be modified to

$$f_{\text{sing}}(bT, bH, b^y r) = b^2 f_{\text{sing}}(T, H, r), \quad (3.21)$$

⁵For an overview of the renormalization group we refer to the literature[1, 3, 6].

where r has the scaling dimension $y = -(D - 1)/2$. Hence, for $1 < D < 3$, $-1 < y < 0$ and r is less irrelevant than any other irrelevant couplings. Since now $f_{\text{sing}}(1, 0, z)$ and $f_{\text{sing}}(0, 1, z)$ are analytic in z one finds

$$\chi(T = 0, H) = \chi(0, 0) + \chi_1 H^{D-1}, \quad (3.22a)$$

$$\gamma(T, H = 0) = \gamma(0, 0) + \gamma_1 T^{D-1}, \quad (3.22b)$$

where the prefactors χ_1 and γ_1 are proportional to r . This thus again agrees with our earlier scaling analysis.

The advantage of the RG analysis is twofold. First of all it provides a simple scaling reason for the existence of the non-analytic terms. Moreover, while the scaling analysis itself does not provide insights into the sign of the prefactors to the non-analytic terms that we discussed in Section 3.1.2, it does provide hints as to how one could proceed. Indeed if one would like to go beyond second order, using for instance the FRG (see Section 1.2), it is possible to identify r with an irreducible three-point vertex. This would provide a justification for truncating the FRG flow equations at the level of the three-point vertex. However, as we will see in the main part of this chapter, various quasi-particle properties also acquire non-analytic magnetic field dependencies. This means, that, in order to calculate the non-analytic terms in the thermodynamic parameters beyond leading order in a consistent way, it would be important to allow the quasi-particle residue and momentum-renormalization factor to flow. This in itself would complicate the solutions of the FRG flow equations. Moreover, we shall also see that the non-analytic terms in the quasi-particle properties receive contributions from all momenta in the range $q \in [0, 2k_F]$. Hence this should also be implemented in the FRG. A way of doing this would be to include all relevant scattering channels (see Section 3.2.6 below) in the FRG. To extract the non-analytic behaviour from such a calculation (either numerically or analytically) is rather non-trivial however and has not yet been done.

3.2 Non-analytic magnetic field dependence of quasi-particle properties

Let us now turn to the main part of this chapter. As was discussed above, electron-electron interactions in Fermi liquids may lead to sub-leading non-analytic corrections to thermodynamic quantities such as the susceptibility and heat capacity. It is therefore natural to ask if these non-analyticities also occur in other quantities. In fact for a different system of gapless magnons in Heisenberg antiferromagnets, it has been found[125] that the leading correction in $1/S$, where S is the spin, to the self-energy is non-analytic in the presence of a weak external magnetic field in dimensions $D \leq 3$. Inspired by this result we will therefore now focus on quasi-particle properties of a generic Fermi liquid.

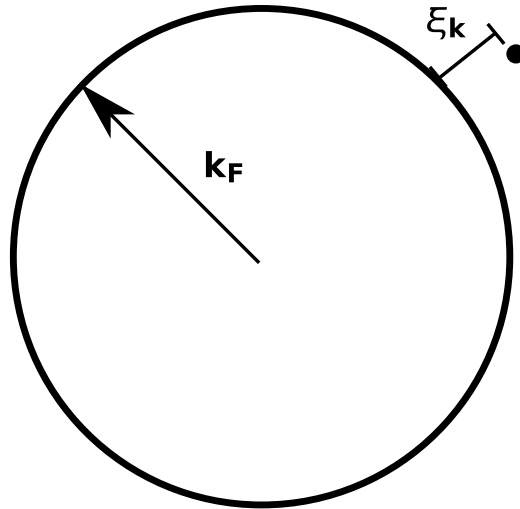


Figure 3.4: *An example of a circular Fermi surface considered in this chapter. The black dot represents a quasi-particle with dispersion $\xi_{\mathbf{k}}$.*

Doing so we will show, using second order perturbation theory, that sub-leading non-analyticities also occur in the magnetic field dependence of the quasi-particle residue Z , momentum-renormalization factor Y , and Landé g -factor (see below). We will furthermore show that the non-analyticities are universal in the sense that they do not depend on an ultraviolet cutoff, and that they may be calculated from a low-energy theory. In doing this we will be applying a higher-dimensional analogue of the g -ology model[126] used to describe the low-energy physics of lattice models in one dimension. This procedure has previously been used by Belitz, Kirkpatrick, and Vojta[103].

3.2.1 Model

We will be working in two dimensions and consider a generic Fermi liquid in a magnetic field entering through the Zeeman energy, at zero temperature. Later in the chapter we will also discuss finite temperatures. For simplicity we moreover only consider a circular Fermi surface as shown in Figure 3.4. As the non-analyticities are expected to arise because of electron-electron interactions it is sufficient to consider a continuum model, ignoring the lattice. If we also simply consider a momentum-independent Hubbard-like interaction U only allowing for scattering between different spins, our action is given by

$$\begin{aligned}
 S[\bar{c}, c] = & - \int_K \sum_{\sigma} [G_0^{\sigma}(K)]^{-1} \bar{c}_{K\sigma} c_{K\sigma} \\
 & + \frac{U}{2} \int_K \int_{K'} \int_Q \sum_{\sigma_1 \neq \sigma_2} \bar{c}_{K+Q, \sigma_1} \bar{c}_{K'-Q, \sigma_2} c_{K'\sigma_2} c_{K\sigma_1}, \quad (3.23)
 \end{aligned}$$

where $c_{K\sigma}$ is a fermionic Grassmann-field, σ denotes the spin, and the free, magnetic field dependent Green's function is given by

$$G_0^\sigma(K) = \frac{1}{i\omega - \frac{\mathbf{k}^2}{2m} + \mu + \sigma h}. \quad (3.24)$$

Here m is the electron mass, μ is the chemical potential, and we recall that $h = g\mu_B H$ is the Zeeman energy related to the magnetic field H . Note that, because we are only considering a circular Fermi surface, this only depends on momentum as

$$G_0^\sigma(i\omega, \mathbf{k}) = G_0^\sigma(i\omega, k). \quad (3.25)$$

Soon we will want to include self-energy corrections and write the Green's function in a Fermi liquid form as discussed in Section 1.3. In a finite magnetic field the Fermi surface however splits into two such that it is important to work with the true Fermi surface when expanding the self-energy. The true Fermi surface in a magnetic field is defined by solving

$$\frac{(k_F^\sigma)^2}{2m} + \Sigma^\sigma(0, k_F^\sigma) = \mu + \sigma h, \quad (3.26)$$

where at zero temperature $\mu = E_F$. Neglecting self-energy corrections the magnetic field dependent Fermi momentum corresponding to a certain spin projection thus becomes

$$k_F^\sigma = k_F \sqrt{1 + \frac{\sigma h}{E_F}}, \quad (3.27)$$

with k_F and E_F denoting the Fermi momentum and Fermi energy at a vanishing magnetic field respectively, and where $\Sigma^\sigma(K)$ is the self-energy associated with an electron of spin σ . This way of defining the Fermi surface is of course equivalent to defining it through Equation (1.42) in a vanishing magnetic field. Now, defining the dispersion relative to the true Fermi surfaces as

$$\xi_k^\sigma = \frac{k^2 - (k_F^\sigma)^2}{2m} = \xi_k - \sigma h, \quad (3.28)$$

with

$$\xi_k = \frac{k^2 - k_F^2}{2m} \quad (3.29)$$

denoting the dispersion relative to the zero-field Fermi surface, we may expand the self-energy of an electron with spin σ around its true Fermi surface as

$$\Sigma^\sigma(K) = \Sigma^\sigma(0, k_F^\sigma) + (1 - Z^{-1}) i\omega - (1 - Y^{-1}) \xi_k^\sigma + \dots \quad (3.30)$$

The Green's function corresponding to an electron with spin σ then takes on the Fermi liquid form

$$G^\sigma(K) = \frac{1}{Z^{-1}i\omega - Y^{-1}\xi_k^\sigma}. \quad (3.31)$$

This and Equation (3.30) will be our starting point for calculating the quasi-particle properties.

3.2.2 Extracting quasi-particle properties

To extract the quasi-particle properties such as the quasi-particle residue and the momentum-renormalization factor, it follows from Equation (3.30) that we need the derivative of the self-energy with respect to frequency and momentum respectively, at the true Fermi surface. Once we have calculated Z and Y we can readily find expressions for the Landé g-factor. To see how this works let us substitute the dispersion relative to the true Fermi surface (3.28) into Equation (3.31). Using (3.27) and multiplying through by Z we thus arrive at

$$G^\sigma(K) = \frac{Z}{i\omega - \frac{k^2 - \bar{k}_F^2}{2m_*} + \sigma g_* h}, \quad (3.32)$$

where we have defined the average Fermi momentum via

$$\frac{\bar{k}_F^2}{2m} = \mu - \frac{\Sigma^\uparrow(0, k_F^\uparrow) + \Sigma^\downarrow(0, k_F^\downarrow)}{2}, \quad (3.33)$$

and the renormalized mass and Landé g-factor by

$$\frac{m_*}{m} = \frac{Y}{Z}, \quad (3.34a)$$

$$g_* = \frac{Z}{Y} X, \quad (3.34b)$$

with

$$X = 1 - \frac{\Sigma^\uparrow(0, k_F^\uparrow) - \Sigma^\downarrow(0, k_F^\downarrow)}{2h}, \quad (3.35)$$

denoting a new renormalization factor relating to the self-energy at the true Fermi surface. To obtain the Landé g-factor we hence not only need the derivatives of the self-energy at the true Fermi surface but also the value of the self-energy itself on the true Fermi surface. For all quantities the starting point however is the self-energy and we will therefore discuss this quantity now.

3.2.3 The second order self-energy

The frequency- and momentum dependence of the self-energy at second order in the interaction is given by

$$\Sigma^\sigma(K) = -U^2 \int_Q \Pi_0^{\uparrow\downarrow}(\sigma Q) G_0^{-\sigma}(K - Q), \quad (3.36)$$

where

$$\Pi_0^{\sigma\sigma'}(Q) = \int_K G_0^\sigma(K) G_0^{\sigma'}(K - Q) \quad (3.37)$$

is the particle-hole polarization bubble which was defined in a vanishing magnetic field in Equation (3.5) and which was given for opposite spins, in a weak magnetic field, for small frequencies and momenta in (3.14). By simply relabelling and changing the order of integration we now see that the self-energy can also be written in the two following ways

$$\Sigma^\sigma(K) = -U^2 \int_Q \Pi_0^{-\sigma, -\sigma}(Q) G_0^\sigma(K - Q) \quad (3.38a)$$

$$= -U^2 \int_Q \Phi_0^{\uparrow\downarrow}(Q) G_0^{-\sigma}(-K + Q). \quad (3.38b)$$

Here the particle-particle polarization bubble is given by

$$\Phi_0^{\sigma\sigma'}(Q) = \int_K G_0^\sigma(K) G_0^{\sigma'}(-K + Q). \quad (3.39)$$

The three different ways of writing the self-energy given in Equations (3.36) and (3.38) are shown diagrammatically in Figure 3.5. Let us here stress that as long as we do not impose a cutoff on the momentum label Q , these three ways of writing the self-energy are completely equivalent. If we however introduce a cutoff in Q , the three diagrams will contribute to different scattering channels. We shall discuss this in more details later. For now let us include all momenta in the integration. In that case it makes no physical difference which representation of the self-energy we use and we can simply choose the one that is more convenient.

3.2.4 The opposite-spin particle-hole bubble

Which representation is more convenient is not obvious though and so, given that the anti-parallel spin particle-hole bubble $\Pi_0^{\uparrow\downarrow}(Q)$ turned out to be more convenient for the calculation of the free energy, we pick (3.36) as our starting point. We thus need an expression for $\Pi_0^{\uparrow\downarrow}(Q)$ for arbitrary frequencies and momenta in a magnetic field. This is in general given by the Lindhard function[127] which for small frequencies, momenta, and for a weak external magnetic field was quoted in Equation (3.14). For arbitrary frequencies and momenta but with a vanishing magnetic field, it has likewise been calculated[128]. In a finite magnetic field however the result changes. At zero

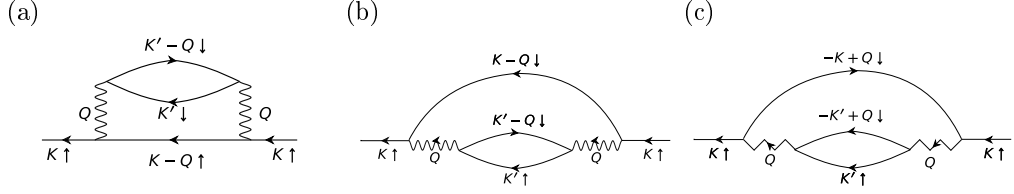


Figure 3.5: The three equivalent ways of drawing the self-energy corresponding to (3.38a) (a), (3.36) (b), and (3.38b) (c). If the momentum Q carried by the interaction is not restricted, these expressions are all identical. If however we introduce a cutoff they correspond to different scattering processes (see Section 3.2.6). To distinguish between the three processes we introduce different lines for the three scattering channels: A wavy line without an arrow corresponds to forward scattering (scattering with small momentum transfer), a wavy line with an arrow corresponds to exchange scattering (large-angle scattering), whilst a zig-zag line with an arrow corresponds to Cooper scattering (scattering of states $2k_F$ apart).

temperature the frequency integral in Equation (3.37) can be performed using the method of residues with the result

$$\Pi_0^{\uparrow\downarrow}(Q) = \int \frac{d^2k}{(2\pi)^2} \frac{\Theta(-\xi_{\mathbf{k}}^{\uparrow}) - \Theta(-\xi_{\mathbf{k}-\mathbf{q}}^{\downarrow})}{\xi_{\mathbf{k}}^{\uparrow} - \xi_{\mathbf{k}-\mathbf{q}}^{\downarrow} - i\bar{\omega}}. \quad (3.40)$$

Splitting the integrand into two parts and shifting $\mathbf{k} \rightarrow \mathbf{k} + \mathbf{q}$ in the second term the integral may be written as

$$\Pi_0^{\uparrow\downarrow}(Q) = \int \frac{d^2k}{(2\pi)^2} \left[\frac{\Theta(k_F^{\uparrow} - |\mathbf{k}|)}{\xi_{\mathbf{k}}^{\uparrow} - \xi_{\mathbf{k}-\mathbf{q}}^{\downarrow} - i\bar{\omega}} + (\bar{\omega} \rightarrow -\bar{\omega}, \mathbf{q} \rightarrow -\mathbf{q}, \sigma \rightarrow -\sigma) \right], \quad (3.41)$$

where $\sigma \rightarrow -\sigma$ denotes a flip of all spins. Since now

$$\xi_{\mathbf{k}}^{\uparrow} - \xi_{\mathbf{k}-\mathbf{q}}^{\downarrow} = \xi_{\mathbf{k}} - \xi_{\mathbf{k}-\mathbf{q}} + 2h = v_k q \cos \varphi - \frac{q^2}{2m} + 2h, \quad (3.42)$$

with $v_k = k/m$ we see that, switching to polar coordinates, the angular integral is of the general form

$$I = \int_0^{2\pi} \frac{d\varphi}{2\pi} \frac{1}{a + ib + \cos \varphi}, \quad (3.43)$$

which, with $z = a + ib$ for a and b real, may be evaluated by transforming the integral into a contour integral over the unit circle \mathcal{C} and using the residue theorem such that

$$I = \frac{1}{2\pi i} \int_{\mathcal{C}} \frac{dx}{x} \frac{1}{z + \frac{1}{2}(x + x^{-1})} = \frac{\text{sgn}(1 - |z - \sqrt{z^2 - 1}|)}{\sqrt{z^2 - 1}}, \quad (3.44)$$

where we have chosen the principal branch of the complex square root which is defined such that its real part is always positive:

$$\sqrt{A + iB} = \sqrt{\frac{R+A}{2}} + i \operatorname{sgn} B \sqrt{\frac{R-A}{2}}, \quad (3.45)$$

with $R = \sqrt{A^2 + B^2}$. We thus obtain

$$\begin{aligned} \int_0^{2\pi} \frac{d\varphi}{2\pi} \frac{1}{a + ib + \cos \varphi} &= \frac{\operatorname{sgn} a}{\sqrt{(a + ib)^2 - 1}} \\ &= \frac{1}{\operatorname{sgn} a \sqrt{\frac{R+A}{2}} + i \operatorname{sgn} b \sqrt{\frac{R-A}{2}}}, \end{aligned} \quad (3.46)$$

where we have used that

$$\operatorname{sgn}(1 - |z - \sqrt{z^2 - 1}|) = \operatorname{sgn} a, \quad (3.47)$$

which can be verified numerically. Also $A = a^2 - b^2 - 1$, $B = 2ab$ while we still set $R = \sqrt{A^2 + B^2}$.

Performing the angular integral in (3.41), using (3.46) and assuming that $m^\uparrow = m^\downarrow$, which is clearly satisfied for a linearised dispersion and not expected to differ much in general, the final radial integral then yields

$$\Pi_0^{\uparrow\downarrow}(Q) = -\nu P(i\bar{\omega}, q; h), \quad (3.48)$$

with

$$\begin{aligned} P(i\bar{\omega}, q; h) &= 1 - i \operatorname{sgn} \bar{\omega} \frac{k_F}{q} \left[\sqrt{1 - \left(\frac{q}{2k_F}\right)^2 + \left(\frac{\bar{\omega} - 2ih}{v_F q}\right)^2} - \frac{i\bar{\omega}}{2E_F} \right. \\ &\quad \left. - \sqrt{1 - \left(\frac{q}{2k_F}\right)^2 + \left(\frac{\bar{\omega} - 2ih}{v_F q}\right)^2 + \frac{i\bar{\omega}}{2E_F}} \right]. \end{aligned} \quad (3.49)$$

The polarization given here has the following asymptotic behaviour for large momenta

$$P(i\bar{\omega}, q; h) \sim 2 \left(\frac{k_F}{q}\right)^2, \quad (3.50)$$

whilst its asymptotic form for large frequencies is

$$P(i\bar{\omega}, q; h) \sim \frac{2h}{i\bar{\omega}} - \frac{2h^2}{\bar{\omega}^2} + \frac{(v_F q)^2}{2\bar{\omega}^2} \left[1 - \left(\frac{q}{2k_F}\right)^2 \right]. \quad (3.51)$$

These asymptotes guarantee that the self-energy (3.36) converges in the ultraviolet. Note also that for small momenta, frequencies, and magnetic fields (3.48) of course reduces to its low-energy approximation (3.14).

3.2.5 Numerical results

With the results from the previous sections we are ready to calculate the leading non-analytic corrections. In this section these will be calculated taking the full frequency- and momentum dependence of the Green's functions and polarization bubbles into account. For the latter we will use the opposite-spin particle-hole bubble given in Equations (3.48) and (3.49). As discussed in the previous section it would be equivalent to use the form of the polarization in other channels. As however the opposite-spin particle-hole bubble turned out to be the useful quantity to use for the susceptibility calculation we use it here as well. Because we, in this section, take the full frequency- and momentum dependence into account the non-analytic terms can only be obtained numerically. Thus all results for the prefactors of the leading non-analyticities quoted in this section are the result of numeric evaluations.

As discussed in Section 3.2.2, in order to extract the renormalized mass and Landé g-factor, we need the self-energy and its derivatives with respect to frequency and momentum on the true (magnetic field dependent) Fermi surface. The relevant self-energy is to second order in the interaction given by Equation (3.36). As the momentum dependence of the polarization only appears as $|\mathbf{q}| = q$, the only angular dependence is in the Green's function and of the same form as in the previous section. Hence, using polar coordinates, it is possible to perform the angular integration analytically. Using Equation (3.46) we find

$$\begin{aligned} \Sigma^\sigma(K) = & -\nu U^2 \int \frac{d\bar{\omega}}{2\pi} \int_0^\infty \frac{dq q}{2\pi} P(i\bar{\omega}, q; \sigma h) \\ & \times \frac{\text{sgn}\left(\xi_k + \frac{q^2}{2m} + \sigma h\right)}{\sqrt{\left(i\omega - i\bar{\omega} - \xi_k - \frac{q^2}{2m} - \sigma h\right)^2 - \left(\frac{kq}{m}\right)^2}}, \end{aligned} \quad (3.52)$$

where we have used that $\xi_{\mathbf{k}} = \xi_k$. The renormalization factor X , which we recall gives information about the renormalized Landé g-factor, is then obtained by simply setting $k = k_F^\sigma$ and $\omega = 0$ in the above. Then, using (3.35)

$$\begin{aligned} X = & 1 + \frac{\nu U^2}{2h} \int \frac{d\bar{\omega}}{2\pi} \int_0^\infty \frac{dq q}{2\pi} \left[P(i\bar{\omega}, q; h) \right. \\ & \left. \times \frac{\text{sgn}\left(\frac{q^2}{2m} + 2h\right)}{\sqrt{\left(i\bar{\omega} + \frac{q^2}{2m} + 2h\right)^2 - \left(v_F^\uparrow q\right)^2}} + (h \rightarrow -h) \right], \end{aligned} \quad (3.53)$$

with $v_F^\sigma = k_F^\sigma/m$.

Calculating the quasi-particle residue and momentum-renormalization factors

we have to be more careful as we here need the derivatives of the self-energy with respect to frequency and momentum respectively. Problems appear because the angular integral (3.46) is discontinuous at $b = 0$, for $|a| < 1$. To calculate Z and Y we now need the derivatives with respect to a and ib but due to the discontinuity the derivatives do not commute with the integral. This becomes more apparent by using the following identity of sign-functions,

$$\operatorname{sgn} b = 2\Theta(b) - 1, \quad (3.54)$$

to rewrite the integral. Taking a derivative then yields a function which depends on both a step-function and δ -function with the same argument. This is ill-defined when the argument vanishes. To resolve this issue it is possible to use the so-called Morris-Lemma[1, 29] which states that, for any function $f(\Theta(x))$ of the step-function

$$\delta(x)f(\Theta(x)) = \delta(x) \int_0^1 dt f(t). \quad (3.55)$$

Using the Morris-Lemma it then follows that[97]

$$\begin{aligned} \frac{\partial}{\partial(ib)} \int_0^{2\pi} \frac{d\varphi}{2\pi} \frac{1}{a + ib + \cos \varphi} &= \frac{\partial}{\partial a} \int_0^{2\pi} \frac{d\varphi}{2\pi} \frac{1}{a + ib + \cos \varphi} \\ &\quad - 2\delta(b) \frac{\Theta(1 - a^2)}{\sqrt{1 - a^2}}. \end{aligned} \quad (3.56)$$

The extra δ -contribution will play a crucial role when calculating the prefactors of the leading non-analytic contributions.

Taking into account the δ -contribution we then find by performing the angular integral and differentiating with respect to ξ_k at $k = k_F^\sigma$ and $\omega = 0$ that

$$\begin{aligned} \frac{1}{Y} &= 1 + \nu U^2 \int \frac{d\bar{\omega}}{2\pi} \int_0^\infty \frac{dq q}{2\pi} P(i\bar{\omega}, q; \sigma h) \\ &\quad \times \frac{\left(i\bar{\omega} - \frac{q^2}{2m} + 2\sigma h\right) \operatorname{sgn}\left(\frac{q^2}{2m} + 2\sigma h\right)}{\left[\left(i\bar{\omega} + \frac{q^2}{2m} + 2\sigma h\right)^2 - (v_F^\sigma q)^2\right]^{3/2}}, \end{aligned} \quad (3.57)$$

whilst differentiating with respect to $i\omega$ and setting $k = k_F^\sigma$ as well as $\omega = 0$ yields

$$\begin{aligned}
 \frac{1}{Z} = & 1 + \nu U^2 \int \frac{d\bar{\omega}}{2\pi} \int_0^\infty \frac{dq q}{2\pi} P(i\bar{\omega}, q; \sigma h) \left[\frac{\left(i\bar{\omega} + \frac{q^2}{2m} + 2\sigma h\right) \operatorname{sgn}\left(\frac{q^2}{2m} + 2\sigma h\right)}{\left[\left(i\bar{\omega} + \frac{q^2}{2m} + 2\sigma h\right)^2 - (v_F^\sigma q)^2\right]^{3/2}} \right. \\
 & \left. + 2\delta(\bar{\omega}) \frac{\Theta\left[(v_F^\sigma q)^2 - \left(\frac{q^2}{2m} + 2\sigma h\right)^2\right]}{\sqrt{(v_F^\sigma q)^2 - \left(\frac{q^2}{2m} + 2\sigma h\right)^2}} \right]. \tag{3.58}
 \end{aligned}$$

We have now expressed the renormalization factors X , Y , and Z in terms of two-dimensional integrals. Taking the full frequency- and momentum dependence of the integrands into account, these are however too complicated to be done analytically. We therefore simply compute the remaining integrals numerically. Plotting the resulting expressions with respect to h (see Figure 3.6) we see that, at small magnetic fields, all renormalization factors acquire a non-analytic term proportional to $|h|$. By reading of the slopes of the resulting plots we conclude that

$$X(h) = X(0) + X_1|h| + \mathcal{O}(h^2), \tag{3.59a}$$

$$Y(h) = Y(0) + Y_1|h| + \mathcal{O}(h^2), \tag{3.59b}$$

$$Z(h) = Z(0) + Z_1|h| + \mathcal{O}(h^2), \tag{3.59c}$$

with

$$X_1 \approx Y_1 \approx Z_1 \approx 0.50 \frac{u^2}{E_F} + \mathcal{O}(u^3), \tag{3.60}$$

where we recall that $u = \nu U$, with $\nu = m/(2\pi)$ denoting the two-dimensional density of states per spin projection, and we have, for the calculation of X_1 first differentiated with respect to the magnetic field, in order to make the integrand fall off faster (we will describe this in more details below). We estimate that the numerical error in these results is of the order of one percent.

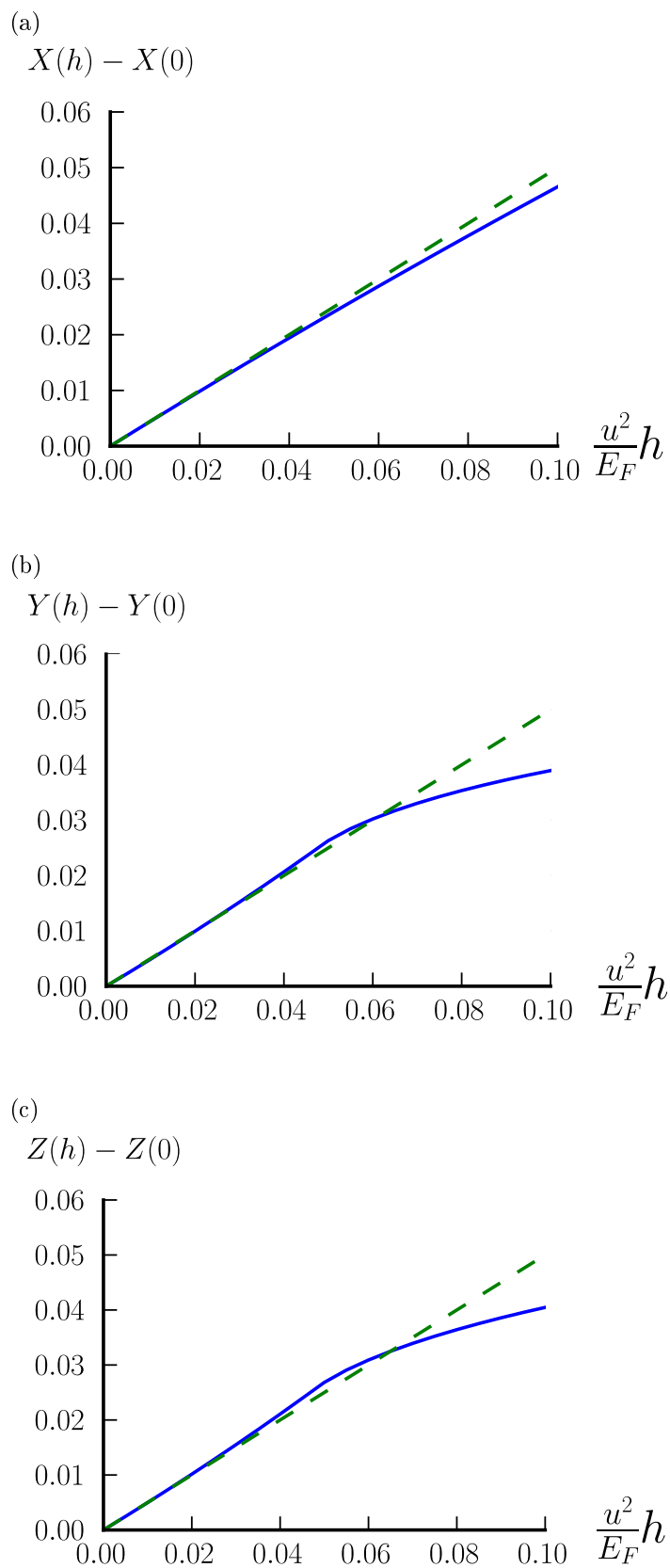


Figure 3.6: We here show numerical results for the renormalization factors X , Y , and Z as a function of magnetic field h (solid lines). The dashed lines are straight lines with slope $1/2$.

The fact that we find $Y_1 \approx Z_1$ indicates that, at this order in the interaction, the renormalized mass (3.34a) does not acquire a non-analytic correction proportional to $|H|$. We will later establish this analytically as well but let us point out that there is no reason to expect this to remain true at higher orders in the interaction. Indeed it is known[105] that the renormalized mass does acquire a temperature dependence proportional to the temperature (see also later). As such, from scaling, it would be expected to also find a term linear in $|H|$, although it should be noted that a proper calculation is yet to be done.

Finally let us note that by repeating the numeric evaluation of the integrals, but using the low-energy approximation of the opposite-spin particle-hole bubble (3.14), we see that the non-analytic correction to X comes solely from the low-energy part of the opposite-spin particle-hole bubble. Thus only small momenta in the integral contribute to X_1 and it would be enough to use (3.14) instead of the full polarization bubble (3.48). As using the opposite-spin particle-hole bubble at low energies corresponds to exchange scattering near the Fermi surface (see Section 3.2.6 and Figure 3.7 below), we therefore conclude that the leading non-analyticity in X comes only from exchange scattering processes. This situation exactly corresponds to the calculation of the leading non-analyticity in the susceptibility as discussed in Section 3.1.2. On the other hand we found that we really need the full polarization bubble to extract the prefactors Y_1 and Z_1 . This indicates that not only small momenta, but momenta in the whole range $q \in [0, 2k_F]$, contribute to the integrals involved in calculating these prefactors, and that they do not only come from exchange scattering processes. Indeed we will show later that also Cooper-scattering is important to recover Y_1 and Z_1 .

3.2.6 Phase-space decomposition

In the previous section we saw that all renormalization factors X , Y , and Z acquire non-analytic terms proportional to $|H|$. The prefactors were extracted numerically taking the full frequency- and momentum dependence into account. In this section we will employ a low-energy model to confirm the results in the previous section. In doing so we will show that the non-analytic terms arise due to low-energy scattering of electrons near the Fermi surface, in different channels.

To motivate our low-energy theory let us point out that relabelling momenta in the interaction part of the action (3.23) allows us to rewrite it as (where we for the moment allow the interaction to depend on momenta)[38, 103]

$$S_{\text{int}}[\bar{c}, c] = \frac{1}{2} \int_K \int_{K'} \int_Q \sum_{\sigma_1, \sigma_2} U(\mathbf{q}) (\bar{c}_{K+Q, \sigma_1} c_{K\sigma_1}) (\bar{c}_{K'\sigma_2} c_{K'+Q, \sigma_2}) \quad (3.61a)$$

$$= -\frac{1}{2} \int_K \int_{K'} \int_Q \sum_{\sigma_1, \sigma_2} U(\mathbf{k} - \mathbf{k}') (\bar{c}_{K+Q, \sigma_2} c_{K\sigma_1}) (\bar{c}_{K'\sigma_1} c_{K'+Q, \sigma_2}) \quad (3.61b)$$

$$= \frac{1}{2} \int_K \int_{K'} \int_Q \sum_{\sigma_1, \sigma_2} U(\mathbf{k} + \mathbf{k}') (\bar{c}_{-K+\frac{Q}{2}, \sigma_2} \bar{c}_{K+\frac{Q}{2}, \sigma_1}) (c_{-K'+\frac{Q}{2}, \sigma_1} c_{K'+\frac{Q}{2}, \sigma_2}). \quad (3.61c)$$

As such there is nothing special about rewriting the interaction in this way and it is completely analogous to writing the self-energy in the three equivalent ways given in Equations (3.36) and (3.38). If we however reduce the available phase-space and restrict the \mathbf{q} integration by imposing an ultraviolet cutoff $|\mathbf{q}| \leq \Lambda_0 \ll k_F$, limiting the integration to take place in a thin shell around the Fermi surface, the three interaction channels in (3.61) (and corresponding self-energies) are no longer equivalent but describe three different scattering processes. It can moreover be shown[103] that, in two dimensions, the three scattering channels in (3.61) are the only ones which contribute to the low-energy properties of scattering between electrons near a Fermi surface. The three distinct scattering processes are thus:

- Forward scattering which describes scattering with small momentum transfer. This process is shown pictorially in Figure 3.7(a),
- exchange scattering which describes large-angle scattering. This is represented in Figure 3.7(b),
- Cooper scattering which describes scattering of states $2k_F$ apart as depicted in Figure 3.7(c).

If we now assume that all relevant scattering processes take place near the Fermi surface and that the prefactors X_1 , Y_1 , and Z_1 all receive contributions only from low-energy processes (this will be justified a posteriori), we may introduce an ultraviolet cutoff in the interaction part of the action and arrive at an effective low-energy model with interaction part given by

$$S_{\text{int}}[\bar{c}, c] \approx \frac{1}{2} \int_Q \Theta(\Lambda_0 - |\mathbf{q}|) \sum_{\sigma_1 \neq \sigma_2} \left[U_f \bar{D}_Q^{\sigma_1 \sigma_1} D_Q^{\sigma_2 \sigma_2} - U_x \bar{D}_Q^{\sigma_1 \sigma_2} D_Q^{\sigma_1 \sigma_2} + U_c \bar{C}_Q^{\sigma_1 \sigma_2} C_Q^{\sigma_1 \sigma_2} \right], \quad (3.62)$$

where we have introduced the composite fermion fields

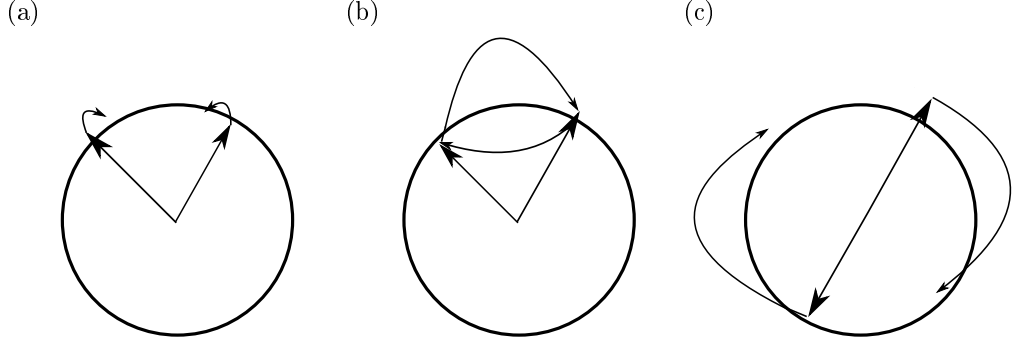


Figure 3.7: These are, in two dimensions, the three possible low-energy scattering processes of electrons close to a Fermi surface. (a) represents forward scattering, (b) represents exchange scattering, while (c) represents Cooper scattering. The straight arrows represent the states before scattering whilst the curved arrows represent the momentum transfer in each scattering process.

$$D_Q^{\sigma_1\sigma_2} = \int_K \bar{c}_{K\sigma_1} c_{K+Q,\sigma_2}, \quad (3.63a)$$

$$C_Q^{\sigma_1\sigma_2} = \int_K c_{-K,\sigma_1} c_{K+Q,\sigma_2}, \quad (3.63b)$$

and where $U_f = U(0)$, $U_c = U(2k_F)$, while U_x is some Fermi surface average of $U(\mathbf{k} - \mathbf{k}')$. To recover our original model (3.23) we should finally set $U_f = U_x = U_c = U$ but in order to more easily distinguish between the different scattering channels, we will not do this till the end.

Within our low-energy we may now treat each channel separately when calculating the self-energy. In order to cover the whole of phase space, we then in the end, need to sum all contributions. Hence the self-energy may now be written as

$$\Sigma^\sigma(K) \approx \Sigma_f^\sigma(K) + \Sigma_x^\sigma(K) + \Sigma_c^\sigma(K). \quad (3.64)$$

Here the self-energies on the right-hand side are in principle still given in Equations (3.38a), (3.36), and (3.38b), and depicted in Figures 3.5(a), 3.5(b), and 3.5(c) respectively, but now all integrals over \mathbf{q} are restricted to a thin shell around the Fermi surface such that we should introduce an ultraviolet cutoff as discussed above. Then

$$\Sigma_f^\sigma(K) = -U_f^2 \int_Q \Theta(\Lambda_0 - |\mathbf{q}|) \Pi_0^{-\sigma, -\sigma}(Q) G_0^\sigma(K - Q), \quad (3.65a)$$

$$\Sigma_x^\sigma(K) = -U_x^2 \int_Q \Theta(\Lambda_0 - |\mathbf{q}|) \Pi_0^{\uparrow\downarrow}(\sigma Q) G_0^{-\sigma}(K - Q), \quad (3.65b)$$

$$\Sigma_c^\sigma(K) = -U_c^2 \int_Q \Theta(\Lambda_0 - |\mathbf{q}|) \Phi_0^{\uparrow\downarrow}(Q) G_0^{-\sigma}(-K + Q). \quad (3.65c)$$

Here the polarization bubbles are still given by the expressions (3.37) and (3.39), but due to the ultraviolet cutoff, we may now approximate all bubbles by their low-energy form and neglect any terms of order q^2 in the propagators. In the exchange channel the renormalization factors (3.53), (3.57), and (3.58) then reduce to

$$X = 1 + \frac{\nu U_x^2}{2h} \int \frac{d\bar{\omega}}{2\pi} \int_0^{\Lambda_0} \frac{dq q}{2\pi} \left[P(i\bar{\omega}, q; h) \times \frac{\text{sgn} h}{\sqrt{(i\bar{\omega} + 2h)^2 - (v_F^\uparrow q)^2}} - (h \rightarrow -h) \right], \quad (3.66a)$$

$$\frac{1}{Y} = 1 + \nu U_x^2 \int \frac{d\bar{\omega}}{2\pi} \int_0^{\Lambda_0} \frac{dq q}{2\pi} P(i\bar{\omega}, q; h) \times \frac{(i\bar{\omega} + 2\sigma h) \text{sgn}(\sigma h)}{[(i\bar{\omega} + 2\sigma h)^2 - (v_F^\sigma q)^2]^{3/2}}, \quad (3.66b)$$

$$\frac{1}{Z} = 1 + \nu U_x^2 \int \frac{d\bar{\omega}}{2\pi} \int_0^{\Lambda_0} \frac{dq q}{2\pi} P(i\bar{\omega}, q; h) \times \left[\frac{(i\bar{\omega} + 2\sigma h) \text{sgn}(2\sigma h)}{[(i\bar{\omega} + 2\sigma h)^2 - (v_F^\sigma q)^2]^{3/2}} + 2\delta(\bar{\omega}) \frac{\Theta[(v_F^\sigma q)^2 - 4h^2]}{\sqrt{(v_F^\sigma q)^2 - 4h^2}} \right]. \quad (3.66c)$$

In the other channels we arrive at similar expressions except that the interaction and polarization bubbles have to be replaced by their relevant counterparts. Moreover, because the propagator in the Cooper channel depends on the momenta in the combination $Q - K$ instead of $K - Q$, the derivative with respect to frequency in the calculation of Z will pick up a sign. We will discuss the forward and Cooper channels in more details below. For now we just point out that these expressions are now tractable analytically in all channels.

3.2.7 Scaling analysis

Our low-energy model is a two-dimensional analogue of the g-ology model[126] (see also Reference [1]) used to describe the low-energy physics of lattice models. In the g-ology model the essential low-energy physics is, like above, taken

into account by only considering scattering processes close to the Fermi surface (which in one dimension is a set of points). Like in our model, it depends on an ultraviolet cutoff, but all low-energy properties of the system turn out to be cutoff-independent. This gives us hope that the ultraviolet cutoff introduced in our low-energy model will likewise cancel in the prefactors X_1 , Y_1 , and Z_1 , if these are fully determined by low-energy scattering processes. Indeed we recall that this is exactly what happens for the free energy, and hence the susceptibility. Here we found that the free energy, given in Equation (3.17), depends explicitly on the ultraviolet cutoff Λ_0 such that the analytic terms were ultraviolet divergent. However, in the leading non-analytic term (proportional to $|H|^3$ for the free energy) this cutoff was seen to cancel exactly. To see that one might expect something similar to happen for the prefactors X_1 , Y_1 , and Z_1 it is useful to do a brief scaling analysis of the low-energy expressions (3.66). Thus, defining the dimensionless variables $\tilde{q} = q/\Lambda_0$, $\tilde{\omega} = \bar{\omega}/(v_F\Lambda_0)$, and $\tilde{h} = h/(v_F\Lambda_0)$, we see that in the exchange channel

$$X = 1 + \frac{\nu U_x^2 \Lambda_0}{2\tilde{h}v_F} \int \frac{d\tilde{\omega}}{2\pi} \int_0^1 \frac{d\tilde{q}\tilde{q}}{2\pi} \left[P(i\tilde{\omega}, \tilde{q}; \tilde{h}) \times \frac{\text{sgn}\tilde{h}}{\sqrt{(i\tilde{\omega} + 2\tilde{h})^2 - \tilde{q}^2}} - (\tilde{h} \rightarrow -\tilde{h}) \right], \quad (3.67a)$$

$$\frac{1}{Y} = 1 + \frac{\nu U_x^2 \Lambda_0}{v_F} \int \frac{d\tilde{\omega}}{2\pi} \int_0^1 \frac{d\tilde{q}\tilde{q}}{2\pi} P(i\tilde{\omega}, \tilde{q}; \tilde{h}) \times \frac{(i\tilde{\omega} + 2\sigma\tilde{h})\text{sgn}(\sigma\tilde{h})}{\left[(i\tilde{\omega} + 2\sigma\tilde{h})^2 - \tilde{q}^2 \right]^{3/2}}, \quad (3.67b)$$

$$\frac{1}{Z} = 1 + \frac{\nu U_x^2 \Lambda_0}{v_F} \int \frac{d\tilde{\omega}}{2\pi} \int_0^1 \frac{d\tilde{q}\tilde{q}}{2\pi} P(i\tilde{\omega}, \tilde{q}; \tilde{h}) \times \left[\frac{(i\tilde{\omega} + 2\sigma\tilde{h})\text{sgn}(\sigma\tilde{h})}{\left[(i\tilde{\omega} + 2\sigma\tilde{h})^2 - \tilde{q}^2 \right]^{3/2}} + 2\delta(\tilde{\omega}) \frac{\Theta[\tilde{q}^2 - 4\tilde{h}^2]}{\sqrt{\tilde{q}^2 - 4\tilde{h}^2}} \right], \quad (3.67c)$$

where we have also neglected the spin dependence of the Fermi velocity as this only leads to terms analytic in the magnetic field. The scaling behaviour in the other channels is exactly the same and so from this scaling analysis it thus follows that, provided that all integrals converge, any terms proportional to $|h|$ cannot depend on the ultraviolet cutoff Λ_0 as the cutoff will be exactly cancelled out by the factor of Λ_0 in front of the integral when switching to dimensionful units. We will reach the same conclusion when we explicitly perform the integrals and extract the prefactors.

3.2.8 Analytic results

Having written down an effective low-energy theory in the previous section we are now ready to calculate the prefactors X_1 , Y_1 , and Z_1 . We will consider each scattering channel separately starting with the exchange channel as this was the important channel for the susceptibility and also the channel we used for the numeric calculation of the prefactors.

Exchange scattering channel

In the exchange channel the relevant polarization bubble is the opposite-spin particle-hole bubble which at low-energies and in a weak external magnetic field is given in Equation (3.14). To calculate X_1 it now turns out to be more convenient to consider the quantity

$$\Delta = h(1 - X), \quad (3.68)$$

which for small momenta is given by

$$\begin{aligned} \Delta = & -\sigma\nu U_x^2 \int \frac{d\bar{\omega}}{2\pi} \int_0^{\Lambda_0} \frac{dq}{2\pi} \left[1 - \frac{|\bar{\omega}|}{\sqrt{(\bar{\omega} - 2i\sigma h)^2 + (v_F q)^2}} \right] \\ & \times \frac{\text{sgn}(\sigma h)}{\sqrt{(i\bar{\omega} + 2\sigma h)^2 - (v_F q)^2}}. \end{aligned} \quad (3.69)$$

Now, using that

$$\text{sgn}(\sigma h) \sqrt{(i\bar{\omega} + 2\sigma h)^2 - (v_F q)^2} = i \text{sgn} \bar{\omega} \sqrt{(\bar{\omega} - i\sigma h)^2 + (v_F q)^2}, \quad (3.70)$$

together with the fact that the integrand in (3.69) is symmetric under the simultaneous shift of $\bar{\omega} \rightarrow -\bar{\omega}$ and complex conjugation, we may write

$$\Delta = -\sigma\nu U_x^2 \int_0^\infty d\bar{\omega} 2\text{Re} \int_0^{v_F^2 \Lambda_0^2} \frac{dx}{2(2\pi)^2 v_F^2} \frac{i\bar{\omega}}{(\bar{\omega} - 2i\sigma h)^2 + x}, \quad (3.71)$$

where we have also defined $x = v_F^2 q^2$. To ensure convergence in the ultraviolet we now take the derivative of this with respect to the magnetic field. Then performing the integration over x yields

$$\frac{\partial \Delta}{\partial h} = \frac{4\nu U_x^2}{(2\pi)^2 v_F^2} \int_0^\infty d\bar{\omega} \text{Re} \frac{\bar{\omega}}{\bar{\omega} - 2i\sigma h} = \frac{4\nu U_x^2}{(2\pi)^2 v_F^2} \int_0^\infty d\bar{\omega} \frac{\bar{\omega}^2}{\bar{\omega}^2 + 4h^2}. \quad (3.72)$$

The remaining frequency integral is still ultraviolet divergent but can be regularized by subtracting the magnetic field independent part of the integrand⁶. We thus obtain

⁶I am grateful to D. L. Maslov for pointing out how to perform the regularization.

$$\frac{\partial \Delta}{\partial h} = -\frac{\nu U_x^2}{\pi v_F^2} |h|. \quad (3.73)$$

Since also it is easy to show that if

$$\frac{\partial \Delta}{\partial h} = \Delta_0 + \Delta_1 |h| + \dots, \quad (3.74)$$

then

$$X_1 = -\frac{\Delta_1}{2}, \quad (3.75)$$

we conclude that the exchange channel contribution to the prefactor X_1 is

$$X_{1,x} = \frac{\nu U_x^2}{2\pi v_F^2} = \frac{u_x^2}{2E_F}. \quad (3.76)$$

Note that this is independent of the ultraviolet cutoff Λ_0 .

Let us now calculate Y_1 in the exchange channel. At low momenta we have, using (3.66b) and (3.70),

$$\begin{aligned} 1 - \frac{1}{Y} &= -\nu U_x^2 \int \frac{d\bar{\omega}}{2\pi} \int_0^{\Lambda_0} \frac{dq q}{2\pi} \left[1 - \frac{|\bar{\omega}|}{\sqrt{(\bar{\omega} - 2i\sigma h)^2 + (v_F q)^2}} \right] \\ &\times \frac{|\bar{\omega}| - 2i\sigma h \operatorname{sgn} \bar{\omega}}{[(\bar{\omega} - 2i\sigma h)^2 + (v_F q)^2]^{3/2}}. \end{aligned} \quad (3.77)$$

Again, noticing that the integrand is symmetric under $\bar{\omega} \rightarrow -\bar{\omega}$ and complex conjugation, the momentum integral is a standard integral such that we arrive at

$$1 - \frac{1}{Y} = \frac{\nu U_x^2}{(2\pi)^2 v_F^2} \int_0^\infty d\bar{\omega} \operatorname{Re} \frac{\bar{\omega}}{2\bar{\omega} + 4i\sigma h} = \frac{\nu U_x^2}{(2\pi)^2 v_F^2} \int_0^\infty d\bar{\omega} \frac{\bar{\omega}^2}{\bar{\omega}^2 + 4h^2}, \quad (3.78)$$

which can be regularized subtracting the magnetic field independent terms, in the same way as in the calculation of X_1 . We hence find

$$Y_{1,x} = \frac{u_x^2}{4E_f}, \quad (3.79)$$

for the prefactor of Y in the exchange channel.

Finally, the quasi-particle residue Z only differs from the momentum-renormalization factor Y in the δ -contribution in (3.66c). As however we see that, after performing the frequency integral, this term only depends on the

magnetic field through h^2 , we conclude that it can only give rise to analytic terms in the expansion of Z . Thus, in the exchange channel

$$Z_{1,x} = Y_{1,x} = \frac{u_x^2}{4E_F}. \quad (3.80)$$

Forward scattering channel

We now consider the forward scattering channel. In this case we need the same-spin particle-hole bubble which can be obtained from the opposite-spin particle-hole bubble (3.14) by simply setting $h = 0$. Therefore it is given by

$$\Pi_0^{\sigma\sigma}(Q) \approx -\nu \left[1 - \frac{|\bar{\omega}|}{\sqrt{\bar{\omega}^2 + (v_F q)^2}} \right], \quad (3.81)$$

which we again stress, is independent of the magnetic field. As moreover the magnetic field dependence of the propagator drops out after performing the momentum integral for all renormalization factors, we see that, in the forward scattering channel,

$$X_{1,f} = Y_{1,f} = Z_{1,f} = 0. \quad (3.82)$$

Cooper scattering channel

The Cooper (or particle-particle) channel is different from the other channels in that the polarization bubble $\Phi_0^{\uparrow\downarrow}(Q)$ takes on a very different form. At low energies and in a vanishing magnetic field the bubble is given by [105]

$$\Phi_0(Q) \approx \nu \ln \frac{2\Omega_0}{|\bar{\omega}| + \sqrt{\bar{\omega}^2 + (v_F q)^2}}, \quad (3.83)$$

where Ω_0 is an ultraviolet cutoff of the order of the Fermi energy, limiting the integration to a small momentum shell around the Fermi surface, and where we have suppressed the spin dependence of the bubble as spin does not enter in a vanishing magnetic field. In a finite magnetic field the calculation is slightly different. The opposite-spin Cooper bubble is then given by [see Equation (3.39)]

$$\Phi_0^{\uparrow\downarrow}(Q) = \int_K G_0^{\uparrow}(K) G_0^{\downarrow}(Q - K) = \int_K \frac{1}{i\omega - \xi_{\mathbf{k}}^{\uparrow}} \frac{1}{i\bar{\omega} - i\omega - \xi_{\mathbf{q}-\mathbf{k}}^{\downarrow}}, \quad (3.84)$$

where the spin dependent dispersion relative to the true (magnetic field dependent) Fermi surface was defined in Equation (3.28). The frequency integration may now be performed using the method of residues and yields

$$\Phi_0^{\uparrow\downarrow}(Q) = - \int \frac{d^2k}{(2\pi)^2} \frac{1}{i\bar{\omega} - \xi_{\mathbf{k}}^{\uparrow} - \xi_{\mathbf{q}-\mathbf{k}}^{\downarrow}} \left[\Theta(\xi_{\mathbf{k}}^{\uparrow}) - \Theta(-\xi_{\mathbf{q}-\mathbf{k}}^{\downarrow}) \right]. \quad (3.85)$$

Notice the sign in the argument of the second step function. It arises because the second propagator now depends on momenta and frequency through the combination $Q - K$ instead of $K - Q$, and makes a simple expansion in \mathbf{q} less useful.

Since now the dispersions appear in the combination (an other consequence of the different sign of the argument of the second propagator)

$$\xi_{\mathbf{k}}^{\uparrow} + \xi_{\mathbf{q}-\mathbf{k}}^{\downarrow} \approx \frac{k^2 - k_F^2}{m} + \frac{kq}{m} \cos \varphi, \quad (3.86)$$

where we have neglected terms of order \mathbf{q}^2 , we see that the magnetic field only enters via the step functions. Moreover, using polar coordinates, the angular integral is again of the form (3.46) such that we are left with an integral over the radial components. Splitting the integral into two parts and assuming that only momenta in a thin shell around the Fermi surface contribute we then get for the first part

$$\Phi_0^{\uparrow\downarrow,(1)} \approx \nu \int_{k_F^{\uparrow}}^{\sqrt{2m\Omega_0}} \frac{dkk}{\sqrt{\left[\frac{k^2 - k_F^2}{m} + i\bar{\omega}\right]^2 - (v_F q)^2}}. \quad (3.87)$$

This is a standard integral which yields

$$\Phi_0^{\uparrow\downarrow,(1)}(Q) \approx \frac{\nu}{2} \ln \frac{2\Omega_0}{i\bar{\omega} + 2h + \text{sgn}\bar{\omega} \sqrt{(i\bar{\omega} + 2h)^2 - (v_F q)^2}}, \quad (3.88)$$

where the factor of two in front of the magnetic field comes from the fact that, using Equation (3.27),

$$[k_F^{\uparrow}]^2 - k_F^2 = \frac{k_F^2 h}{E_F} = 2mh. \quad (3.89)$$

The second term in the integral is simply the complex conjugate of this and so we arrive at the following expression for the low-energy Cooper bubble in a finite external magnetic field

$$\Phi_0^{\uparrow\downarrow}(Q) \approx \nu \ln \left| \frac{2\Omega_0}{\bar{\omega} - 2ih + \text{sgn}\bar{\omega} \sqrt{(\bar{\omega} - 2ih)^2 + (v_F q)^2}} \right|. \quad (3.90)$$

This of course reduces to Equation (3.83) if we set $h = 0$.

With the expression for the polarization bubble we may now write down the second order self-energy at low energies. We find

$$\begin{aligned} \Sigma_c^\sigma(K) &= \nu U_c^2 \int \frac{d\bar{\omega}}{2\pi} \int_0^{\Lambda_0} \frac{dq q}{2\pi} \ln \left| \frac{2\Omega_0}{\bar{\omega} - 2ih + \text{sgn}\bar{\omega} \sqrt{(\bar{\omega} - 2ih)^2 + (v_F q)^2}} \right| \\ &\times \int_0^{2\pi} \frac{d\varphi}{2\pi} \frac{1}{i\bar{\omega} - i\omega - \xi_k - \sigma h + \frac{kq}{m} \cos \varphi}. \end{aligned} \quad (3.91)$$

Performing the angular integration using Equation (3.46), differentiating with respect to the external frequency and setting $\omega = \xi_k = 0$, the quasi-particle residue is then given by

$$\begin{aligned} \frac{1}{Z} &= 1 - \nu U_c^2 \int \frac{d\bar{\omega}}{2\pi} \int_0^{\Lambda_0} \frac{dq q}{2\pi} \ln \left| \frac{2\Omega_0}{\bar{\omega} - 2ih + \text{sgn}\bar{\omega} \sqrt{(\bar{\omega} - 2ih)^2 + (v_F q)^2}} \right| \\ &\times \left[\frac{i\bar{\omega} + 2h}{[(i\bar{\omega} + 2h)^2 - (v_F q)^2]^{3/2}} + 2\delta(\bar{\omega}) \frac{\Theta[(v_F q)^2 - 4h^2]}{\sqrt{(v_F q)^2 - 4h^2}} \right]. \end{aligned} \quad (3.92)$$

We first of all see that the static (cutoff dependent) part of the polarization does not contribute to the prefactor of the leading non-analytic term. Thus only considering the dynamic part (the part in the denominator of the argument of the logarithm) and splitting the integral into two we get a contribution with and without a δ -function. Considering first the latter contribution we make use of the fact that the integrand is symmetric under the simultaneous shift of $\bar{\omega} \rightarrow -\bar{\omega}$ and complex conjugation. The momentum integration can then be performed and we arrive at the following contribution to the leading non-analytic part of the quasi-particle residue

$$\frac{1}{Z^{(1)}} = \frac{\nu U_c^2}{4\pi^2 v_F^2} \int_0^\infty d\bar{\omega} \text{Re} \ln \frac{v_F \Lambda_0}{\bar{\omega} - 2ih} = \frac{\nu U_c^2}{8\pi^2 v_F^2} \int_0^\infty d\bar{\omega} \ln \frac{v_F^2 \Lambda_0^2}{\bar{\omega}^2 + 4h^2}. \quad (3.93)$$

The frequency integral is now again ultraviolet divergent but can be regularized, as before, by subtracting the magnetic field independent part. We thus find, after regularization, that the prefactor of the leading non-analytic term coming from the first contribution to the quasi-particle residue in the Cooper channel is given by

$$Z_{1,c}^{(1)} = -\frac{\nu U_c^2}{4\pi v_F^2} = -\frac{u_c^2}{4E_F}. \quad (3.94)$$

The fact that this is exactly minus the contribution from the exchange channel is not surprising. Indeed it can be seen by doing an integration by parts that one arrives at the same expression for $1/Z$ as in the exchange channel, apart from a sign and the δ -function contribution.

We now consider the second contribution. Since this term contains a δ -function, the frequency integration is trivial and we end up with the following momentum integral

$$\frac{1}{Z^{(2)}} = \frac{\nu U_c^2}{8\pi^2 v_F^2} \int_0^\infty dx \ln(x) \frac{\Theta(x - 4h^2)}{\sqrt{x - 4h^2}}, \quad (3.95)$$

with $x = v_F^2 q^2$. If we again regularize by subtracting the magnetic field independent part, the integration can be performed and we obtain

$$Z_{1,c}^{(2)} = \frac{\nu U_c^2}{2\pi v_F^2} = \frac{u_c^2}{2E_F}. \quad (3.96)$$

Adding up the two contributions to the Cooper channel result for Z_1 we hence find

$$Z_{1,c} = \frac{u_c^2}{4E_F}, \quad (3.97)$$

which we recall is the same as the contribution from the exchange scattering channel.

To calculate Y_1 in the Cooper channel let us first point out that, in the exchange channel, Y only differed from Z in the lack of a term proportional to a δ -function. The reason the contribution to Z coming from the term without a δ -function is the same as in Y can be traced back to the form of the self-energy (3.65b). Because the polarization bubble in this expression only depends on the loop momentum, the only external frequency- and momentum dependence of the self-energy comes from the propagator. This, in turn, depends only on the combination $K - Q$ which implies that the derivative with respect to $i\omega$ and ξ_k differ by a sign (since the dependence is of the form $i\omega - \xi_k$ at low momenta). This sign is however cancelled by the fact that Y is defined with an opposite sign to Z [see e.g. Equation (3.30)]. Turning now back to the Cooper channel we see, from Equation (3.65c), that the external frequency and momentum appear in the combination $Q - K$. Since also $\xi_{\mathbf{k}-\mathbf{q}} = \xi_{\mathbf{q}-\mathbf{k}}$, we see using the same arguments as above, that now the derivatives with respect to $i\omega$ and ξ_k come with the same sign. As Z and Y however still differ by a sign in their definition we come to the conclusion that Y is simply given by minus the term not containing the δ -function in Z (what we called $Z^{(1)}$ above). We thus infer that

$$Y_{1,c} = -Z_{1,c}^{(1)} = \frac{u_c^2}{4E_F}. \quad (3.98)$$

Notice that, also in the Cooper channel, Z and Y give identical contributions to the non-analytic term proportional to $|H|$. In this case however, unlike the situation in the exchange- and forward scattering channels, it is worth noting that the δ -function contribution to Z was crucial in order to obtain this result. This can be understood by noting that the Cooper polarization bubble differs from the other bubbles in already being logarithmic in the magnetic field.

Finally let us note that the calculation of X_1 in the Cooper channel is more involved, because the polarization bubble $\Phi_0^{\uparrow\downarrow}$ given in Equation (3.90) depends explicitly on an ultraviolet cutoff Ω_0 (which however drops out when calculating the prefactors of the leading non-analytic term in the magnetic field), which is set by the Fermi energy. Since in a magnetic field the Fermi surface is split, this introduces a magnetic field dependence of the Fermi energy (see Section 3.2.1). It is therefore likely that Ω_0 will also depend on the magnetic field which could influence the result. The trick we used in the exchange channel of differentiating first with respect to the magnetic field is therefore not useful. As however our numerics in Section 3.2.5, which took into account the full frequency- and momentum dependence implied that only the small momentum part of the polarization bubble in the exchange channel contributes to X_1 , we infer that

$$X_{1,c} = 0. \quad (3.99)$$

Adding up the various contributions to the prefactors we find that our low-energy theory predicts the following values for the prefactors

$$X_1 = X_{1,x} + X_{1,f} + X_{1,c} = \frac{u_x^2}{2E_F} + \mathcal{O}(u^3) = \frac{u^2}{2E_F} + \mathcal{O}(u^3), \quad (3.100a)$$

$$Y_1 = Y_{1,x} + Y_{1,f} + Y_{1,c} = \frac{u_x^2 + u_c^2}{4E_F} + \mathcal{O}(u^3) = \frac{u^2}{2E_F} + \mathcal{O}(u^3), \quad (3.100b)$$

$$Z_1 = Z_{1,x} + Z_{1,f} + Z_{1,c} = \frac{u_x^2 + u_c^2}{4E_F} + \mathcal{O}(u^3) = \frac{u^2}{2E_F} + \mathcal{O}(u^3), \quad (3.100c)$$

where we have, to recover our original theory, set $u_x = u_f = u_c = u$ in the final equalities. We thus see that we have recovered our numeric results (3.60) and that the prefactors do not depend on any ultraviolet cutoffs. This justifies a posteriori our assumption that we may extract the prefactors from a low-energy model taking different scattering channels into account. The fact that the prefactors are independent of any ultraviolet cutoffs or other material-specific properties implies that the prefactors are universal. We moreover see that we have established the identity $Y_1 = Z_1$ exactly (at least to second order in the interaction) such that it is indeed the case that the mass renormalization does not acquire a non-analytic term proportional to $|H|$ to second order in the interaction. The Landé g-factor on the other hand does acquire a non-analytic correction which can be found from the calculated prefactors using Equation (3.34b).

3.3 Non-analytic frequency and temperature dependence

So far in this chapter we have only considered non-analyticities in the magnetic field. However it is also possible to imagine these arising in expansions with respect to other control parameters. Indeed it is for instance known [105, 106, 107, 108, 124] that the susceptibility also exhibits a linear, non-analytic momentum and temperature dependence. Also as we have already seen in Section 3.1.1 (see also References [105] and [107]), the real part of the self-energy itself obtains a non-analytic dependence on frequency of the form $\omega|\omega|$ at zero temperature. At finite temperatures this translates into an ωT non-analyticity and is what is responsible for the non-analytic temperature dependence of various thermodynamic quantities. In fact, temperature is, also for the quasi-particle properties, a second control parameter one could consider. From a renormalization group perspective, both temperature and magnetic field are relevant couplings with the same scaling dimension. Therefore, from scaling, it would be expected that, also at finite temperatures, we should find non-analytic terms proportional to the temperature T^7 . In this section we will discuss the frequency and temperature non-analyticities in more detail.

3.3.1 Non-analytic frequency dependence of the self-energy

We begin with the frequency dependence of the self-energy. As mentioned above we already considered this in Section 3.1.1 where we showed how it leads to non-analytic terms in the heat capacity. In this section we will calculate the $\omega|\omega|$ type non-analyticities from our low-energy model. A similar calculation has been performed by Chubukov and Maslov [105] and by Chubukov et al [107].

We begin with our low-energy model developed in Section 3.2.6, but now set $\hbar = 0$ and work directly with the self-energy at a finite external frequency. We will still restrict all external momenta to lie on the Fermi surface such that $\xi_k = \xi_{k_F} = 0$. For calculating the prefactor of the $\omega|\omega|$ term in the real part of the self-energy we moreover find it convenient to first differentiate with respect to $i\omega$. In the exchange channel we then find, after performing the angular integral using (3.46),

⁷To see why a term proportional to T is denoted “non-analytic” note that a usual expansion in temperature is in powers of T^2 . This is clear for the heat capacity (which we recall has a leading non-analyticity linear in T) if one recalls that the typical quantity one considers is $\gamma = C/T$, which yields an analytic expansion in T^2 without non-analytic corrections.

$$\begin{aligned} \frac{\partial \Sigma_x(i\omega, \mathbf{k}_F)}{\partial(i\omega)} &= -\nu U_x^2 \int \frac{d\bar{\omega}}{2\pi} \int_0^{\Lambda_0} \frac{dq}{2\pi} \left[1 - \frac{|\bar{\omega}|}{\sqrt{\bar{\omega}^2 + (v_F q)^2}} \right] \\ &\times \left[\frac{i\bar{\omega} - i\omega}{[-(\bar{\omega} - \omega)^2 - (v_F q)^2]^{3/2}} + 2\delta(\bar{\omega} - \omega) \frac{1}{\sqrt{(v_F q)^2 + (\bar{\omega} - \omega)^2}} \right]. \end{aligned} \quad (3.101)$$

It is quick to see that the static part does not contribute to the $\omega|\omega|$ term (like it was the case for the $|h|$ non-analyticity in a finite magnetic field) and so we are left with two terms which we consider separately. The first term (without the δ -function) depends on momentum the same way as in the case where $\omega = 0$ and $h \neq 0$. The momentum integral can therefore be done like in Section 3.2.8. By symmetrising the resulting integrand with respect to $\bar{\omega}$ and regularizing by subtracting the static ($\omega = 0$) part we then arrive at

$$\frac{\partial \Sigma_x^{(1)}(i\omega, \mathbf{k}_F)}{\partial(i\omega)} = \frac{\nu U_x^2}{2\pi^2 v_F^2} \int_0^\infty d\bar{\omega} \left[\frac{4\bar{\omega}^2}{4\bar{\omega}^2 - \omega^2} - 1 \right] = \frac{-i u_x^2}{8 E_F} |\omega|. \quad (3.102)$$

The factor of i is solely there because we have differentiated with respect to $i\omega$ instead of ω such that this term really contributes to the real part of the self-energy. The prefactor of the $\omega|\omega|$ term is then half of the contribution calculated above times i . The half is again due to the fact that we have, for convenience, considered the frequency derivative of the self-energy instead of the self-energy itself. The second term (containing the δ -function) yields

$$\begin{aligned} \frac{\partial \Sigma_x^{(2)}(i\omega, \mathbf{k}_F)}{\partial(i\omega)} &= \frac{\nu U_x^2 |\omega|}{2\pi^2 v_F} \int_0^{\Lambda_0} \frac{dq}{\sqrt{\omega^2 + (v_F q)^2}} \\ &= \frac{u_x^2}{2\pi E_F} |\omega| \ln \frac{v_F \Lambda_0 + \sqrt{\omega^2 + (v_F \Lambda_0)^2}}{|\omega|}. \end{aligned} \quad (3.103)$$

Whilst this is obviously also non-analytic in the frequency, notice that the right-hand side is real. Therefore this contributes only to the imaginary part of the self-energy, which, as we indeed know from Section 3.1.1, has a logarithmic non-analyticity.

Since for vanishing magnetic fields the forward scattering channel is identical to the exchange scattering channel, the former yields the same contribution to the non-analytic frequency dependence of the self-energy as above. If we therefore set $u_f = u_x$, the forward scattering channel simply produces a factor of two. In the Cooper channel, on the other hand, we find using (3.83) that the singular (that is contributing to the non-analytic frequency dependence of the self-energy) part of the self-energy is

$$\begin{aligned} \frac{\partial \Sigma_c(i\omega, \mathbf{k}_F)}{\partial(i\omega)} &= \frac{\nu U_c^2}{2(2\pi)^2 v_F^2} \int d\bar{\omega} \int_0^{(v_F \Lambda_0)^2} dx \ln \frac{2\Omega_0}{|\bar{\omega}| + \sqrt{\bar{\omega}^2 + x}} \\ &\times \left[\frac{\omega - \bar{\omega}}{[(\bar{\omega} - \omega)^2 + x]^{3/2}} + 2\delta(\omega - \bar{\omega}) \frac{1}{\sqrt{x}} \right], \end{aligned} \quad (3.104)$$

with $x = v_F^2 q^2$. We now again divide the integral into two parts. For the first part, we may perform the momentum integration and obtain for the singular part

$$\frac{\partial \Sigma_c^{(1)}(i\omega, \mathbf{k}_F)}{\partial(i\omega)} = -\frac{\nu U_c^2}{(2\pi)^2 v_F^2} \int d\bar{\omega} \ln \frac{v_F \Lambda_0}{\bar{\omega} - \omega}. \quad (3.105)$$

Subtracting again the static part the integral becomes convergent. We thus find

$$\frac{\partial \Sigma_c^{(1)}(i\omega, \mathbf{k}_F)}{\partial(i\omega)} = -i \frac{u_c^2}{4E_F} |\omega|, \quad (3.106)$$

such that the contribution to the prefactor of the $\omega|\omega|$ term in the self-energy from this term is $u_c^2/(8E_F)$. For the second part of the integral, the frequency integration is trivial due to the δ -function. Likewise the momentum integral is then a standard integral which can be performed with the result

$$\begin{aligned} \frac{\partial \Sigma_c^{(2)}(i\omega, \mathbf{k}_F)}{\partial(i\omega)} &= \frac{u_c^2}{2\pi E_F} \left[v_F \Lambda_0 \ln \frac{|\omega| + \sqrt{\omega^2 + (v_F \Lambda_0)^2}}{v_F \Lambda_0} \right. \\ &\quad \left. - |\omega| \ln \frac{\omega}{v_F \Lambda_0 + \sqrt{\omega^2 + (v_F \Lambda_0)^2}} \right], \end{aligned} \quad (3.107)$$

which again only contributes to the imaginary part of the self-energy. We thus see that the contribution from the Cooper channel is exactly twice as big as the contribution from the exchange channel. This agrees with the result of Reference [105]. Let us however point out that non-perturbative effects coming from zero-sound modes may change this result significantly[107].

Before moving on it is interesting to note that it has been shown[105, 107, 129, 130], that the above non-analyticities in frequency arise only due to interactions at momenta $q = 0$ and $q = 2k_F$. This can be shown by considering a momentum-dependent interaction and expanding in angular harmonics. Doing thus one finds that all other contributions vanish, such that the interaction can be written fully, in terms of its values at $q = 0$ and $q = 2k_F$. This should be contrasted with our results in Section 3.2 where we found that all momenta in the range $q \in [0, 2k_F]$ contribute to the non-analyticities in quasi-particle

properties in a magnetic field. The non-analyticity in the quasi-particle residue can now be traced back to a non-analyticity proportional to $\omega|h|$ in the real part of the self-energy on resonance. This implies that for general magnetic fields and frequencies the leading non-analytic behaviour of the real part of the self-energy on resonance is of the form

$$\text{Re}\Sigma(\omega, \mathbf{k}_F) = \Sigma_1^{(\omega)} \omega |\omega| g\left(\frac{|h|}{|\omega|}\right), \quad (3.108)$$

where $g(x)$ is some scaling function with the following limits

$$\lim_{x \rightarrow 0} g(x) = 1, \quad (3.109a)$$

$$\lim_{x \rightarrow \infty} g(x) = \frac{\Sigma_1^{(h)}}{\Sigma_1^{(\omega)}} x, \quad (3.109b)$$

with $\Sigma_1^{(\omega)}$ and $\Sigma_1^{(h)}$ denoting the prefactors of the $\omega|\omega|$ and $\omega|h|$ non-analyticities respectively.

The scaling function must then take into account the fact that only certain momenta are picked out when $\omega \gg h$. It would be very interesting to calculate the scaling function but this has not yet been done. Let us however mention that, albeit there the same momenta contribute in the opposite limits, the singular parts of the real part of the self-energy at arbitrary frequencies and temperatures take on a similar scaling form as (3.108). In this case the scaling function has been calculated in Reference [105].

3.3.2 Non-analytic temperature dependence

The previous section was a slight detour in that we considered the self-energy itself rather than the quasi-particle properties that one can derive from it. We now return to considering quasi-particle properties and will calculate the leading non-analytic temperature dependence. As mentioned earlier one would expect from scaling that the leading non-analytic temperature contribution should be linear in the temperature, like it is the case for an external magnetic field. Indeed we will show that this is the case. Let us also point out that a linear temperature dependence of the heat capacity factor $\gamma = C/T$ has been observed in experiments in, for example, liquid ^3He monolayers[117]. Let us also mention that, unlike our findings for zero temperature at a finite external magnetic field, it has been shown[105], by calculating the ωT terms in the real part of the self-energy at resonance for $\omega \ll T$, that the renormalized mass does acquire a non-analytic linear in temperature dependence at second order. We will recover this result in this section.

Because it will turn out that the momentum-renormalization factor Y is the most important quantity experimentally we will focus on this. Let us

only mention that it is possible, in a similar way, to calculate the prefactor of the linear temperature term in the quasi-particle residue. Such a calculation yields⁸

$$Z_1^{(T)} = (1 + 2 \ln 2) \frac{u^2}{4E_F} + \mathcal{O}(u^3), \quad (3.110)$$

with $u = u_x = u_f = u_c$ as usual. To calculate the corresponding prefactor for Y we follow the procedure outlined in Reference [105]. First of all we begin by expressing the polarization bubble through its spectral representation (for a review see for example Reference [131]) which in the exchange channel takes the form

$$\Pi_0(i\bar{\omega}, \mathbf{q}) = \frac{1}{\pi} \int d\Omega \frac{\text{Im}\Pi_0(\Omega + i\eta, \mathbf{q})}{\Omega - i\bar{\omega}}, \quad (3.111)$$

where $\eta > 0$ is a positive infinitesimal, Ω is now a real frequency, and we have suppressed the spin-indices because we are working at vanishing magnetic field. To see that this representation is correct one should simply perform the integral on the right-hand side using the method of residues. Equation (3.111) can now be substituted into Equation (3.65b) whereby the Matsubara summation over $i\bar{\omega}$ can be performed. Furthermore performing an analytic continuation of frequencies in the propagator to the real axis viz. $i\omega \rightarrow \omega + i\eta$ and using Equation (1.48), the imaginary part of the self-energy yields

$$\begin{aligned} \text{Im}\Sigma_x(\omega + i\eta, \mathbf{k}) &= \frac{U_x^2}{2} \int \frac{d^2q}{(2\pi)^2} \Theta(\Lambda_0 - |\mathbf{q}|) \int d\Omega \text{Im}\Pi_0(\Omega + i\eta, \mathbf{q}) \\ &\times \delta(\xi_{\mathbf{k}-\mathbf{q}} - \omega + \Omega) \left[\coth\left(\frac{\Omega}{2T}\right) - \tanh\left(\frac{\omega - \Omega}{2T}\right) \right]. \end{aligned} \quad (3.112)$$

Using polar coordinates, the angular integral is now straightforward due to the δ -function whilst the radial integration can be performed in a standard way. Applying a Kramers-Kronig transform we hence arrive at the following expression for the singular[105] contribution to the real part of the self-energy

$$\begin{aligned} \text{Re}\Sigma_x(\omega + i\eta, \mathbf{k}) &= \frac{\nu U_x^2}{(2\pi)^3 v_F^2} \mathcal{P} \int \frac{d\omega'}{\omega' - \omega} \int d\Omega \Omega \ln \left| \frac{v_F \Lambda_0}{2\Omega + \omega' - \xi_k} \right| \\ &\times \left[\coth\left(\frac{\Omega}{2T}\right) - \tanh\left(\frac{\omega' + \Omega}{2T}\right) \right], \end{aligned} \quad (3.113)$$

where we recall that \mathcal{P} denotes the principal part. By now differentiating with respect to ξ_k and setting $\omega = \xi_k = 0$, the remaining frequency integrals can be done by symmetrising the integrand with respect to ω' . Doing thus we find

⁸D. L. Maslov, private communication.

$$Y_{1,x}^{(T)} = \frac{u_x^2}{8E_F}, \quad (3.114)$$

for the contribution from the exchange channel to the prefactor $Y_1^{(T)}$ of the linear in temperature term in an expansion of Y .

As it was the case in the previous section we are here working at a vanishing magnetic field and, therefore, the forward scattering channel yields for $u_x = u_f$ an identical contribution to $Y_1^{(T)}$. We are consequently left with only the Cooper channel. Here we find, after performing the angular integration, that

$$\begin{aligned} \text{Im}\Sigma_c(\omega + i\eta, \mathbf{k}) &= -\frac{\nu U_c^2}{(2\pi)^2} \int_0^{\Lambda_0} dq q \int d\Omega \frac{\ln \left[\frac{2\Omega_0}{|\Omega| + \sqrt{\Omega^2 + (v_F q)^2}} \right]}{\sqrt{(v_{\mathbf{k}} q)^2 - (\xi_k - \omega + \Omega)^2}} \\ &\times \left[\coth \left(\frac{\Omega}{2T} \right) - \tanh \left(\frac{\omega - \Omega}{2T} \right) \right]. \end{aligned} \quad (3.115)$$

We may then again obtain the real part of the self-energy by using a Kramers-Kronig transform. Differentiating the resulting expression with respect to ξ_k and setting $\omega = \xi_k = 0$ we obtain, with $x = v_F^2 q^2$,

$$\begin{aligned} \left. \frac{\partial \Sigma_c(i\eta, \mathbf{k})}{\partial \xi_k} \right|_{\xi_k=0} &= \frac{\nu U_c^2}{(2\pi)^3 v_F^2} \int_0^{(v_F \Lambda_0)^2} dx \int d\Omega \ln \frac{2\Omega_0}{|\Omega| + \sqrt{\Omega^2 + x}} \\ &\times \mathcal{P} \int \frac{d\omega'}{\omega'} \frac{\omega' - \Omega}{[x - (\omega' - \Omega)^2]^{3/2}} \\ &\times \left[\coth \left(\frac{\Omega}{2T} \right) - \tanh \left(\frac{\omega' - \Omega}{2T} \right) \right]. \end{aligned} \quad (3.116)$$

Because the integrand is odd under the simultaneous shift of $\omega' \rightarrow -\omega'$ and $\Omega \rightarrow -\Omega$ the integral vanishes exactly. The reason we obtain a finite contribution in this channel in a finite magnetic field or with a finite frequency is that these parameters break the symmetry.

Adding together all terms we finally obtain for $h = \omega = 0$ at finite temperatures

$$Y(T) = Y(0) + Y_1^{(T)} T + \mathcal{O}(T^2), \quad (3.117)$$

with

$$Y_1^{(T)} = \frac{u_x^2 + u_f^2}{8E_F} + \mathcal{O}(u^3) = \frac{u^2}{4E_F} + \mathcal{O}(u^3), \quad (3.118)$$

where, as usual, we have set $u_x = u_f = u_c = u$ in the final equality to recover our original model.

We may now use this result together with Equation (3.110) in order to obtain the leading non-analytic temperature behaviour of the renormalized mass. This follows from Equation (3.34a) which yields for the prefactor of the linear in temperature term of the renormalized mass

$$\frac{m_{*,1}^{(T)}}{m} = -\frac{\ln 2}{2} \frac{u^2}{E_F} + \mathcal{O}(u^3), \quad (3.119)$$

in agreement with Reference [105].

3.4 Implications for experiments

As we have already mentioned, the linear in temperature non-analyticity in the heat capacity factor $\gamma = C/T$ has been observed in, for example, liquid ^3He monolayers[117]. Likewise the susceptibility has been shown experimentally to have a linear dependence on both temperature and magnetic field in various heterostructures in two dimensions[119, 120, 121, 122] and even in the normal phase of the iron-based superconductors[118]. Whilst the behaviour of the heat capacity seems to be settled, even the sign of the prefactor of the non-analytic terms of the susceptibility is still under debate with different experiments giving different outcomes[118, 119, 120, 121, 122]. In this section we will discuss how the non-analyticities of quasi-particle properties derived in this chapter can be seen in experiments. While the possibly most direct way of seeing the non-analyticities would be to measure the quasi-particle residue in photoemission experiments, we will focus on the momentum renormalization factor Y as this turns out to appear in various interesting quantities.

3.4.1 Tunnelling experiments

Let us first point out that the momentum renormalization factor Y appears in the expression for the tunnelling density of states, accessible in tunnelling experiments. Indeed within Fermi liquid theory the propagator is given in Equation (3.31). The spectral function can then be readily calculated using (1.48) whereby we arrive at

$$A(\omega, \mathbf{k}) = -\frac{1}{\pi} \text{Im}G(\omega + i\eta, \mathbf{k}) = Z\delta\left(\omega - \frac{Z}{Y}\xi_k\right). \quad (3.120)$$

Notice that this depends on the magnetic field [or temperature as seen from Equations (3.110) and (3.118)] through the renormalization factors Z and Y . The renormalized tunnelling density of states thus also depends on the magnetic field and is given by (setting $\omega = 0$ in the spectral function as we are only interested in the magnetic field dependence)

$$\nu_*(h) = \int \frac{d^2k}{(2\pi)^2} A(0, \mathbf{k}) = Z \int \frac{d^2k}{(2\pi)^2} \delta\left(\frac{Z}{Y}\xi_k\right). \quad (3.121)$$

This integral can most easily be obtained by substituting the integral over momenta with an integral over the dispersion. Assuming all energies lie close to the Fermi energy we then find

$$\nu_*(h) = \nu Y. \quad (3.122)$$

We therefore expect the tunnelling density of states close to the Fermi surface to have the following non-analytic magnetic field dependence

$$\frac{\nu_*(h) - \nu_*(0)}{\nu} = Y_1 |h| + \mathcal{O}(h^2), \quad (3.123)$$

where Y_1 is given in Equation (3.100b). Let us point out that the non-analytic dependence of the tunnelling density of states on the magnetic field is different from the case where $h = 0$ but we have a finite external frequency. In this case it has been shown[107] that the tunnelling density of states remains analytic in the frequency.

3.4.2 Magnetoconductivity

A different experimentally observable quantity which exhibits a non-analytic dependence on the magnetic field (or temperature) is the conductivity. Whilst this has been known for some time[132, 133, 134, 135] the non-analyticities observed so far arise from a different physical mechanism. We will discuss this point later but let us first show how non-analyticities in the quasi-particle properties can lead to non-analyticities in the conductivity.

To get a finite value for the conductivity we first add elastic impurity scattering. For simplicity we will consider weak, δ -correlated (white-noise) impurities such that the impurity potential $u(\mathbf{x})$ satisfies[8]

$$\langle u(\mathbf{x}) \rangle = 0, \quad (3.124a)$$

$$\langle u(\mathbf{x})u(\mathbf{x}') \rangle = \frac{1}{2\pi\nu\tau} \delta(\mathbf{x} - \mathbf{x}'), \quad (3.124b)$$

where $\langle \dots \rangle$ denotes disorder averaging and τ is the bare elastic lifetime. Recall also that ν is the density of states per spin projection which at the Fermi surface is $\nu = m/(2\pi)$. As is shown in Appendix A [see Equation (A.6)] the disorder averaged propagator, in the absence of interactions, may then be written as

$$G_0(K) = \frac{1}{i\omega - \xi_{\mathbf{k}}^\sigma - \Sigma_{\text{imp}}(i\omega)}, \quad (3.125)$$

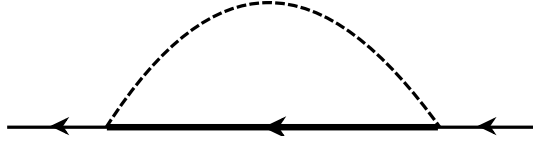


Figure 3.8: This diagram is to lowest order the self-energy arising from impurity scattering. The thick solid line represents the renormalized fermionic propagator, while the dashed line is the correlator related to the disorder.

such that the full effect of the impurities is encoded in the impurity self-energy. In the presence of interactions we simply assume a Fermi liquid form of the propagator and find

$$G^\sigma(K) = \frac{Z}{i\omega - \frac{Y}{Z}\xi_k^\sigma - Z\Sigma_{\text{imp}}(i\omega)}. \quad (3.126)$$

To lowest order the impurity self-energy is given, within the Fermi liquid picture, by the diagram shown in Figure 3.8. Using the methods described in Appendix A we may evaluate this as

$$\Sigma_{\text{imp}}(i\omega) = \frac{Z}{2\pi\nu\tau} \int \frac{d^2k}{(2\pi)^2} \frac{1}{i\omega - \frac{Z}{Y}\xi_k}. \quad (3.127)$$

We now change the integration to be over the dispersion, assume all energies lie close to the Fermi energy, and perform the analytic continuation $i\omega \rightarrow \omega + i\text{sgn}(\omega)\eta$, where $\eta > 0$ is as usual an infinitesimal and the factor of $\text{sgn}\omega$ is necessary to take into account the fact that for $\omega > 0$ we wish to regularize the integral such that we pick up a pole in the upper half of the complex plane while for $\omega < 0$ we regularize such that we pick up a pole in the lower half of the complex plane. Doing thus we may write

$$\Sigma_{\text{imp}}(i\omega) = \frac{Z}{2\pi\tau} \int \frac{d\xi_k}{\omega - \frac{Z}{Y}\xi_k + i\text{sgn}(\omega)\eta}. \quad (3.128)$$

Splitting the integrand into its real and imaginary parts, and using Equation (1.48), we see that the real part vanishes such that

$$\Sigma_{\text{imp}}(i\omega) = -i\frac{Z\text{sgn}\omega}{2\tau} \int d\xi_k \delta\left(\omega - \frac{Z}{Y}\xi_k\right) = -i\text{sgn}\omega\frac{Y}{2\tau}. \quad (3.129)$$

The disorder averaged propagator can therefore be written as

$$G^\sigma(K) = \frac{Z}{i\omega - \frac{m}{m_*}\xi_k^\sigma + \frac{i\text{sgn}\omega}{2\tau_*}}, \quad (3.130)$$

with

$$\frac{1}{\tau_*} = -2Z\text{Im}\Sigma_{\text{imp}}(i\eta) = \frac{ZY}{\tau}, \quad (3.131)$$

denoting the (inverse) renormalized elastic lifetime and where we recall that m_* is the renormalized mass as given in Equation (3.34a). To see that this yields a non-analytic contribution to the conductivity coming from the quasi-particle properties we now simply use the Drude formula, replacing the mass and lifetime by their renormalized counterparts. Thus the conductivity yields

$$\sigma(h) = \frac{ne^2\tau_*}{m_*} = \frac{\sigma_0}{Y^2}, \quad (3.132)$$

where

$$\sigma_0 = \frac{ne^2\tau}{m}, \quad (3.133)$$

with $n = k_F^2/(2\pi)$ is just the Drude expression for the conductivity in the absence of interactions[100]. We hence see that expanding Equation (3.132) in the magnetic field leads to the following non-analytic behaviour of the conductivity at second order in the interaction

$$\frac{\sigma(h)_2 - \sigma(0)_2}{\sigma_0} = -2Y_1|h| + \mathcal{O}(h^2, u^3) = -\frac{u_x^2 + u_c^2}{2E_F}|h| + \mathcal{O}(h^2, u^3). \quad (3.134)$$

However, the validity of the Drude formula with renormalized quantities in the presence of interaction is not obvious[4]. Let us therefore discuss an alternative route to the result (3.134). In fact Equation (3.132) can also be derived by including vertex corrections in the Kubo formula for the conductivity. For a Fermi liquid in D dimensions one then arrives at the following expression for the conductivity

$$\sigma = \frac{e^2 v_F^2}{2\pi D} \sum_{\sigma} \left[1 + \frac{\partial \Sigma(0, \mathbf{k})}{\partial \xi_k^{\sigma}} \Big|_{\xi_k^{\sigma}=0} \right]^2 \int \frac{d^D k}{(2\pi)^D} G^{\sigma}(i\eta, \mathbf{k}) G^{\sigma}(-i\eta, \mathbf{k}), \quad (3.135)$$

which is shown diagrammatically in Figure 3.9. As, for a vanishing magnetic field, this was first derived by Langer[136, 137] we shall call this the Langer formula. Let us note that the Langer formula contains vertex corrections due to interactions in the Kubo formula. Furthermore we see, by comparing with Equation (3.30), that the expression in the square brackets exactly gives the factor of $1/Y^2$ that is present in (3.132).

The Langer formula has been often used in a vanishing magnetic field[136, 137, 138, 139, 140, 141]. In a magnetic field the situation is more unclear. However, the important point in this context is that it shows, that the conductivity can be expressed via the momentum-derivative of the self-energy. This fact is guaranteed by a Ward identity which relates the vertex corrections to the momentum-derivative of the self-energy[136, 137, 142]. We expect it to hold

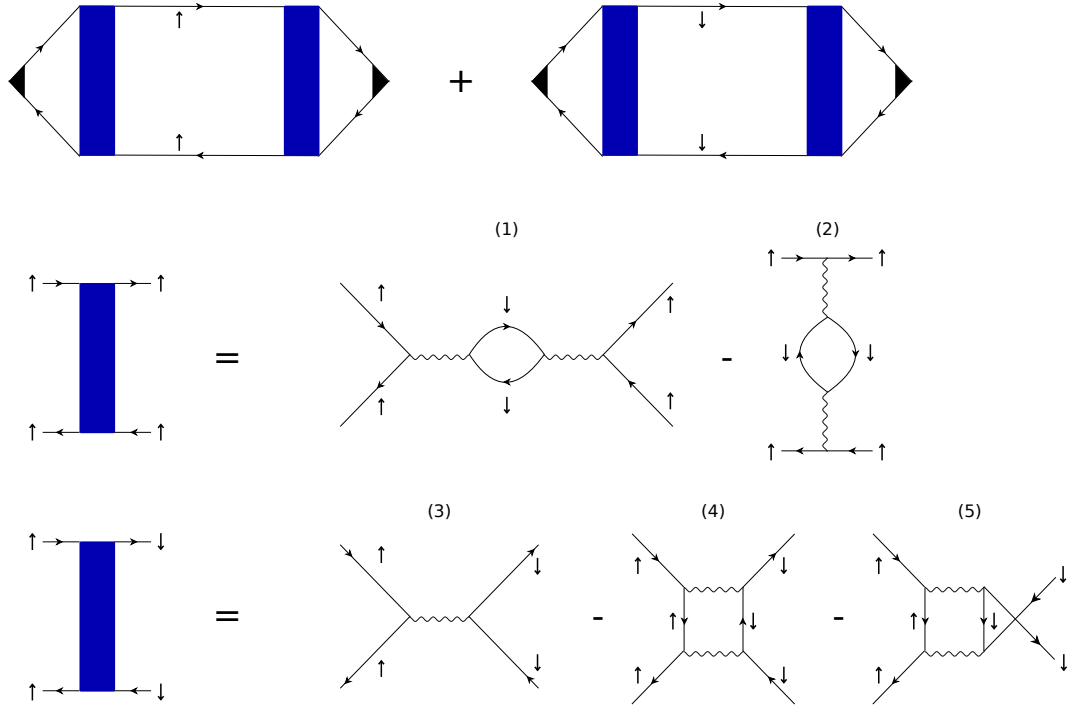


Figure 3.9: *Top line: Diagrammatic representation of the Kubo formula for the conductivity with vertex corrections as given in (3.135). The black triangles are the bare current vertices, whilst the blue boxes denote vertex corrections. These are, to second order in the interaction, shown in the two bottom lines. If we insert the diagrams labelled (4) and (5) we generate the Aslamazov-Larkin contributions to the conductivity. The diagrams (2), (4), and (5) generate, after introducing an ultraviolet cutoff $\Lambda_0 \ll k_F$, the corrections coming from the diagrams in Figure 3.5.*

in a magnetic field as well. As this is an important point we will briefly review how to arrive at this conclusion. The derivation will mainly follow the derivation found in Reference [142] (see also References [136] and [137]). To begin let us recall that the Kubo formula relates the real part of the conductivity tensor (we consider only a diagonal conductivity but for the sake of generality we keep the tensor structure in the following. This should also help distinguish between the current-current correlation function which contains indices and the $(D + 1)$ -momentum K which does not) to the imaginary part of the (retarded) current-current correlation function $K_{\mu\nu}(\omega, \mathbf{k})$ as follows⁹

$$\text{Re}\sigma_{\mu\nu}(\omega, \mathbf{k}) = -\frac{e^2}{\omega} \text{Im}K_{\mu\nu}(\omega, \mathbf{k}). \quad (3.136)$$

To arrive at the DC conductivity we then take the limits¹⁰

⁹Taking the real part only corresponds to taking the so-called paramagnetic part of the current-current correlation function. See also Reference [141].

¹⁰The order of the limits is important which can be traced back to the fact that, according

$$\text{Re}\sigma_{\mu\nu} = -e^2 \lim_{\omega \rightarrow 0} \lim_{k \rightarrow 0} \frac{1}{\omega} \text{Im}K_{\mu\nu}(\omega, \mathbf{k}). \quad (3.137)$$

We are thus interested in the zero-momentum limit of the current-current correlation function which for finite momenta is given by

$$K_{\mu\nu}(\omega, \mathbf{k}) = -\frac{i}{V} \int \frac{d^{D+1}k}{(2\pi)^{D+1}} v_{\mathbf{k}\mu} G\left(K' + \frac{K}{2}\right) G\left(K' - \frac{K}{2}\right) \Lambda_\nu(K, K'), \quad (3.138)$$

where V is the volume of the system and $\Lambda_\nu(K, K')$ is the dressed vertex function (blue box in Figure 3.9) which yields the vertex corrections. The latter is given by the solution to the following integral equation

$$\begin{aligned} \Lambda_\mu(K', K) &= v_{\mathbf{k}'\mu} - i \int \frac{d^{D+1}k''}{(2\pi)^{D+1}} \Gamma_0(K', K'') \\ &\quad \times G\left(K'' + \frac{K}{2}\right) G\left(K'' - \frac{K}{2}\right) \Lambda_\mu(K'', K), \end{aligned} \quad (3.139)$$

where $\Gamma_0(K', K'')$ denotes the bare vertex. The arguments of the vertices simply denote outgoing and ingoing momenta. Because we are interested in the current-current correlation function in the limit of vanishing momenta we also want the vertex corrections in this limit. Denoting the vertex function in this limit by $\Lambda_\mu(K')$ we see that

$$\Lambda_\mu(K') = v_{\mathbf{k}'\mu} - i \int \frac{d^{D+1}k''}{(2\pi)^{D+1}} \Gamma_0(K', K'') [G(K'')]^2 \Lambda_\mu(K''). \quad (3.140)$$

As however also a straightforward derivative of the self-energy yields

$$\frac{\partial \Sigma(\omega, \mathbf{k})}{\partial k_\mu} = -i \int \frac{d^{D+1}k'}{(2\pi)^{D+1}} \Gamma_0(K, K') [G(K')]^2 \left(v_{\mathbf{k}'\mu} + \frac{\partial \Sigma(\omega', \mathbf{k}')}{\partial k'_\mu} \right), \quad (3.141)$$

we see, by comparing (3.140) and (3.141), that

$$\Lambda_\mu(K') = v_{\mathbf{k}'\mu} + \frac{\partial \Sigma(\omega', \mathbf{k}')}{\partial k'_\mu}. \quad (3.142)$$

As promised this is the Ward identity relating the vertex corrections to the momentum-derivative of the self-energy. To get it into the form used in (3.135), all that remains is to change the derivative to be with respect to the dispersion.

to Equation (3.138), the current-current correlation function depends on the combination $G(K' + \frac{K}{2})G(K' - \frac{K}{2})$. For this combination the order in which the limits are taken matters as the two limits differ by a δ -function[142].

Given the fact that the conductivity is proportional to $1/Y^2$ we could also consider the case of vanishing magnetic field and finite temperatures. It then follows from Equations (3.117) and (3.118) that the conductivity also becomes proportional to the temperature at low temperatures. In particular at second order in the interaction

$$\frac{\sigma(T)_2 - \sigma(0)_2}{\sigma_0} = -\frac{u_x^2 + u_f^2}{4E_F}T + \mathcal{O}(T^2, u^3). \quad (3.143)$$

A linear temperature dependence of the conductivity is also seen in the Cuprates. However, let us point out that, whilst in the Cuprates and other materials, the constant of proportionality is independent of the type of disorder[143], this is not the case here where we would find a different result if we had considered a different type of disorder. This implies that the origin of the linear term is different.

The fact that the conductivity becomes linear in the magnetic field (or temperature) has been predicted by other authors before[132, 133, 134, 135]. In particular it is worth considering the result for the conductivity of a two-dimensional metal in the ballistic high-field regime (that is $1/\tau \ll T \ll h \ll E_F$), derived by Zala, Narozhny, and Aleiner[132] (ZNA). They showed that the magnetic field dependent conductivity can be written as

$$\frac{\sigma(h)_{\text{ZNA}} - \sigma(0)_{\text{ZNA}}}{\sigma_0} = \frac{|h|}{E_F} \frac{2F_0^\sigma}{1 + F_0^\sigma} g(F_0^\sigma). \quad (3.144)$$

Here F_0^σ is a dimensionless Landau parameter (see Section 1.3) which contains information about the strength of the spin-exchange interaction and is included to take into account effects of scattering processes which do not take place close to the Fermi surface, and

$$g(z) = \frac{1}{2z} \ln(1+z) + \frac{1}{2(1+2z)} + \frac{z(z+1) \ln 2}{(1+2z)^2}, \quad (3.145)$$

is a scaling function that goes to unity as the argument vanishes. For small arguments it has the following expansion

$$g(z) = 1 - \left(\frac{5}{4} - \ln 2 \right) z + \mathcal{O}(z^2). \quad (3.146)$$

It is clear that the ZNA result agrees with our result (3.134) in predicting the existence of a non-analytic term proportional to $|h|$ in the conductivity. However, because $F_0^\sigma = -u$ at leading order in the interaction we see that to leading order the ZNA result is linear in the interaction. This should be contrasted with our result which is proportional to the square of the interaction. The latter is obviously due to the fact that we have only considered processes which are quadratic in the interaction. To reconcile this difference let us show how to recover the leading term in the ZNA formula from a disorder averaged

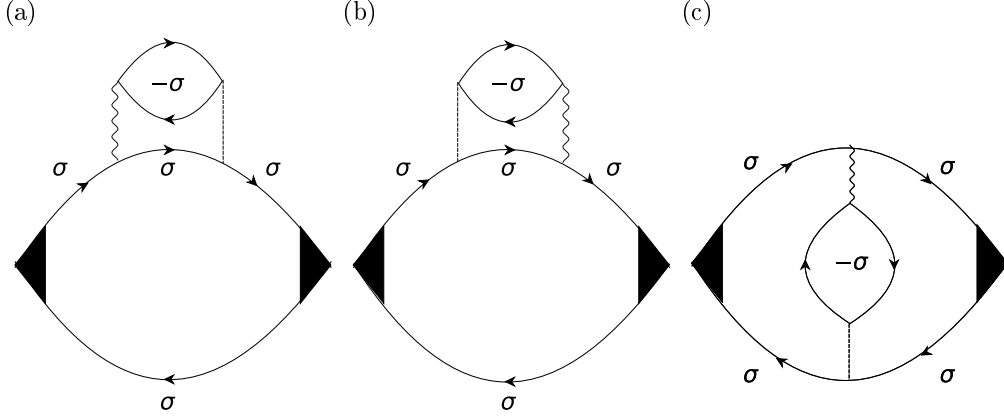


Figure 3.10: These diagrams are the three first-order contributions to the disorder averaged Kubo formula. Diagrams (a) and (b) give identical contributions to the leading non-analyticity of the conductivity. The diagram (c) which is given by (3.154) is not included in the Langer formula (3.135).

Kubo formula. To first order in the interaction the diagrams which contribute are shown in Figure 3.10. In this figure the first two diagrams [3.10(a) and 3.10(b)] give identical contributions. Summing them up then yields

$$\Sigma_1^\sigma(i\omega, \mathbf{k}) = \frac{U}{\pi\nu\tau} \int \frac{d^2q}{(2\pi)^2} \Pi_0^{-\sigma, -\sigma}(0, \mathbf{q}) G_0^\sigma(i\omega, \mathbf{k} - \mathbf{q}). \quad (3.147)$$

Here the interaction U corresponds to the interaction in our original model (3.23). If we wish to use the Langer formula we need an expression for the renormalized elastic lifetime. This means that the interesting quantity is the imaginary part of the self-energy at $i\omega = i\eta$. Because for vanishing frequency the equal-spin particle-hole polarization bubble, $\Pi_0^{\sigma, \sigma}(0, \mathbf{q}) = -\nu P^\sigma(q)$ with

$$P^\sigma(q) = 1 - \frac{2k_F^\sigma}{q} \Theta(q - 2k_F^\sigma) \sqrt{\left(\frac{q}{2k_F^\sigma}\right)^2 - 1}, \quad (3.148)$$

is real we may use Equation (1.48) and obtain

$$\begin{aligned} \text{Im}\Sigma_1^\sigma(i\eta, \mathbf{k}) &= -\frac{u}{\pi\nu\tau} \int \frac{d^2q}{(2\pi)^2} P^{-\sigma}(q) \text{Im} \frac{1}{-\xi_{\mathbf{k}_F^{\sigma-\mathbf{q}}} + 2\sigma h + i\eta} \\ &= \frac{u}{\nu\tau} \int_0^\infty \frac{dq q}{(2\pi)^2} P^{-\sigma}(q) \int_0^{2\pi} d\varphi \delta\left(2\sigma h - \frac{q^2}{2m} + v_F^\sigma q \cos\varphi\right). \end{aligned} \quad (3.149)$$

If we now consider only spin up we see that after performing the angular integration, for $h > 0$,

$$\begin{aligned} \text{Im}\Sigma_1^\uparrow(i\eta, \mathbf{k}) &= \frac{2u}{(2\pi)^2\nu\tau} \int_0^\infty dq q \left[1 - \Theta(q - 2k_F^\downarrow) \sqrt{\frac{q - 2k_F^\downarrow}{k_F^\downarrow}} \right] \\ &\times \frac{1}{\sqrt{(v_F^\uparrow q)^2 - \left[2h - \frac{q^2}{2m}\right]^2}}. \end{aligned} \quad (3.150)$$

The non-analytic magnetic field dependence of the self-energy now comes from momenta in the polarization bubble (3.148) around $2k_F^\sigma$. We may therefore approximate $P^{-\sigma}(q)$ for $|\mathbf{p}| = |\mathbf{q} - 2\mathbf{k}_F| \ll 2k_F^\sigma$. In this case we find, after subtracting the field-independent part, that

$$\begin{aligned} \text{Im}\Sigma_1^\uparrow(i\eta, k_F^\uparrow) - \text{Im}\Sigma_1^\uparrow(i\eta, k_F^\uparrow)|_{h=0} &= -\frac{2u}{(2\pi)^2\nu\tau v_F} \int_{-2h/v_F}^{2h/v_F} dp \sqrt{\frac{2h + v_F p}{2h - v_F p}} \\ &= -\frac{uh}{E_F\tau}. \end{aligned} \quad (3.151)$$

The (inverse) renormalized elastic lifetime for the spin-up case is then given by

$$\frac{1}{\tau_{*\uparrow}} = \frac{1}{\tau} - 2\text{Im}\Sigma_1^\uparrow(i\eta, k_F^\uparrow) = \frac{1}{\tau} \left[1 + \frac{2uh}{E_F} \right], \quad (3.152)$$

which is valid for $h > 0$. For $h < 0$ there is no renormalization of the lifetime. If we had considered the spin-down case we would have got the same result, except that we would have only got a finite contribution for $h < 0$ and no renormalization for $h > 0$. In total, the two diagrams 3.10(a) and 3.10(b) thus contribute the following to the conductivity at leading order in the interaction:

$$\sigma(h)_{a+b} = \frac{ne^2}{m} \frac{\tau_{*\uparrow} + \tau_{*\downarrow}}{2} = \sigma_0 \left[1 - u \frac{|h|}{E_F} + \mathcal{O}(u^2, h^2) \right]. \quad (3.153)$$

We note that this is half of what we find if we expand the ZNA result to leading order in the interaction. The other half comes from the diagram 3.10(c). This diagram is given by

$$\begin{aligned} \sigma(h)_c &= -\frac{e^2}{2\pi m^2} \frac{u}{\pi\nu\tau} \sum_\sigma \int \frac{d^2k}{(2\pi)^2} \int \frac{d^2k'}{(2\pi)^2} \frac{\mathbf{k} \cdot \mathbf{k}'}{2} P^{-\sigma}(\mathbf{k} - \mathbf{k}') \\ &\times G_0^\sigma(i\eta, \mathbf{k}) G_0^\sigma(-i\eta, \mathbf{k}) G_0^\sigma(i\eta, \mathbf{k}') G_0^\sigma(-i\eta, \mathbf{k}'), \end{aligned} \quad (3.154)$$

where the propagators are all disorder averaged such that they take on the form given in Equation (3.130). To calculate this integral it is simplest to notice

that the propagators all come in pairs of retarded and advanced propagators. These may be evaluated separately¹¹

$$\begin{aligned}
G_0^\sigma(i\eta, \mathbf{k})G_0^\sigma(-i\eta, \mathbf{k}) &= \frac{1}{i\eta - \xi_k^\sigma - \Sigma_{\text{imp}}(i\eta)} \frac{1}{-i\eta - \xi_k^\sigma - \Sigma_{\text{imp}}(-i\eta)} \\
&= \frac{1}{i\eta - \xi_k^\sigma + \frac{i}{2\tau}} \frac{1}{-i\eta - \xi_k^\sigma - \frac{i}{2\tau}} \\
&= -2\tau \text{Im} \frac{1}{-\xi_k^\sigma + \frac{i}{2\tau}} \\
&\approx 2\pi\tau \delta(\xi_k^\sigma),
\end{aligned} \tag{3.155}$$

where we have used that, in the absence of interactions, $\tau_* = \tau$ and $m_* = m$. Moreover we have, at the last equality, used that $\tau \gg 1$ for weak disorder. Applying this identity in Equation (3.154) all integrals become straightforward and we find, for $h > 0$,

$$\sigma(h)_c = -\frac{e^2}{2\pi m^2} \frac{u\tau m}{\pi\nu} \frac{[k_F^\dagger]^2}{2} \approx -\frac{e^2 u\tau}{2\pi m} k_F^2 \left[1 + \frac{h}{2E_F}\right]^2, \tag{3.156}$$

where we have expanded k_F^\dagger as given in Equation (3.27) for small magnetic fields in the last equality. Using $n = k_F^2/(2\pi)$ we thus see that this diagram yields a contribution to the non-analytic term proportional to $|h|$ which is identical to the contribution coming from the first two diagrams in Figure 3.10. Hence these diagrams exactly reproduce the ZNA result for the conductivity. It should be stressed however that the second contribution (3.156) [corresponding to Figure 3.10(c)] is not contained in the Langer formula. To see this, note that the diagram 3.10(c) does not transfer any energy and is fully due to interference effects, albeit with renormalized impurity lines. Indeed, the factor of Y in the Langer formula is at leading order in the interaction solely given by the momentum derivative of the self-energy given in Equation (3.147). But this self-energy vanishes in the extreme ballistic limit $1/\tau \rightarrow 0$ in contrast to the conductivity (3.156). Therefore the latter cannot be contained in the Langer formula. With this in mind our use of the Langer formula is not sufficient in order to calculate all contributions to the leading non-analytic behaviour of the conductivity at first order in the interaction. It is therefore also not certain if our second order result takes into account all relevant contributions. On the other hand a relevant question is now whether our contribution to the conductivity is implicitly included in the ZNA formula. This does not seem to be the case because ZNA have only considered exchange scattering and have included interaction effects by renormalizing the interaction lines within RPA. The relevant diagrams used by ZNA are shown in Figure 3.11 and whilst their result is obtained by a proper disorder calculation it is evident from Equation (3.134) that, in our case, also Cooper scattering is important.

¹¹This identity holds for any product of advanced and retarded Green's functions. For free non-interacting fermions without disorder the last equality becomes exact[4].

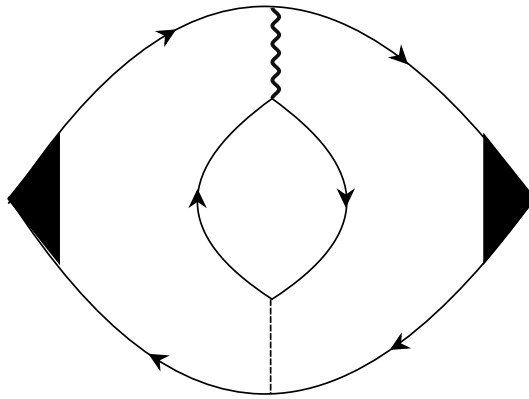


Figure 3.11: *This is the diagram taken into account by ZNA and Gornyi and Mirlin[132, 134, 135]. The thick wavy line denotes the interaction which has been dressed within the RPA.*

Similarly let us note that the magnetoconductivity of two-dimensional electrons in a transverse magnetic field has also been calculated by Gornyi and Mirlin[134, 135]. They considered the same scattering processes as ZNA but also included long-range disorder. Because they also do not take into account the Cooper channel, we expect that our result is also not contained in theirs. Moreover they find that the corrections coming from interactions are exponentially suppressed by the disorder. This is not the case in our result for the conductivity.

It would be interesting to perform a proper disorder calculation of the conductivity taking into account all scattering processes to second order. Such a calculation has however not yet been performed.

Let us also note that other non-analytic contributions to the conductivity, and other transport and thermodynamic parameters, may appear. In particular let us mention that, at third order in the interaction, the conductivity picks up a non-analyticity proportional to $|h|^{1/3}$ [144, 145, 146]. The same authors find a similar correction at second order in the interaction but with two impurity lines. These corrections come from orbital effects that we have neglected. Indeed, in a magnetic field the paths of the quasi-particles will curve such that they pick up an Aharonov-Bohm phase. This effect, which is neglected if the magnetic field is only implemented through a Zeeman term, leads to these non-analyticities. Naturally, at low magnetic fields, the non-analyticities proportional to $|h|^{1/3}$ are dominant over the non-analyticities discussed in this work. However, because they only appear at third order in the interaction there exists a regime of parameters where the contributions discussed in this work are dominant. Indeed this is the case for $u^{3/2} \ll |h|/E_F \ll 1$. Likewise our contribution is dominant over the $|h|^{1/3}$ contribution appearing at sec-

ond order in the interaction for weak disorder because the latter comes from diagrams with two impurity lines.

3.5 Summary and conclusions

In this chapter we have used second order perturbation theory to investigate the sub-leading properties of a two-dimensional Fermi liquid in the presence of a weak external magnetic field. In Section 3.1 we discussed how non-analyticities appear in various thermodynamic properties, such as the susceptibility and heat capacity, beyond leading order. These non-analyticities appear as a linear term breaking the usual Sommerfeld expansion, and are due to non-analyticities in the polarization bubbles. We then went on to consider the magnetic-field dependence of quasi-particle properties, such as the quasi-particle residue Z , the momentum-renormalization factor Y , and a renormalization factor X related to the self-energy on the (magnetic field dependent) Fermi surface. The two former were used to extract the renormalized mass whilst the latter was shown to give information about the Landé g-factor. We found, by evaluating the relevant diagrams numerically, that all renormalization factors acquire a non-analytic term proportional to the absolute value of the magnetic field and that the prefactors of this term are all identical. The result for the prefactors is given in Equation (3.60). The fact that Y and Z gives rise to the same non-analyticity was used to conclude that the renormalized mass does not acquire a non-analyticity in the magnetic field, at least to second order in the interaction. From our numerics we moreover found that, unlike the non-analytic contribution to the susceptibility[114], not only the low-energy part of the opposite-spin particle-hole bubble gives rise to non-analyticities in Y and Z . Instead momenta in the entire range $q \in [0, 2k_F]$ were found to contribute. For the renormalization factor X on the other hand, the situation was similar to the susceptibility, in that only the low-energy part of the opposite-spin particle-hole bubble was found to contribute to the leading non-analyticity. To confirm the numeric findings and to classify the contributions to the non-analytic terms we then, in Section 3.2.6, performed a phase-space decomposition previously used by Belitz, Kirkpatrick, and Vojta[103] (see also Reference [38]). This phase-space decomposition, which is a two-dimensional analogue of a well-known[126] procedure in one dimension called g-ology, allowed us to express all quantities in terms of low-energy self-energies with the caveat that we had to include all possible scattering processes. These were exchange scattering (which corresponds to large-angle scattering), forward scattering (corresponding to scattering with small momentum transfer), and Cooper scattering (corresponding to scattering of states $2k_F$ apart). The fact that we were able to use the low-energy expressions for the polarization bubbles enabled us to perform all calculations analytically. We thus confirmed our numeric results. Furthermore, whilst the quasi-particle properties in such an approach are dependent on an ultraviolet cutoff, we

found that the cutoff cancels in the prefactors of the leading non-analyticities such that these are universal low-energy properties of the system. As expected from our numerics we also found that both exchange and Cooper scattering contribute to the leading non-analytic behaviour of Y and Z .

In Section 3.3 we then considered the case of a vanishing magnetic field, but with a finite frequency or temperature. We calculated both the leading non-analytic contribution proportional to $\omega|\omega|$ of the real part of the self-energy and the leading non-analyticity proportional to the temperature T in Y . Because it is known[105, 107, 129, 130] that the former only comes from momentum-transfers $q = 0$ and $q = 2k_F$, whilst our results, with a finite magnetic field, come from the entire regime $q \in [0, 2k_F]$, we inferred that, for finite frequencies and magnetic fields, the leading non-analytic contribution to the self-energy must satisfy a scaling form given in Equation (3.108).

Finally we considered how the non-analytic behaviour can be detected in experiments. Whilst the quasi-particle residue should be measurable in photoemission experiments, we also pointed out that the momentum-renormalization factor Y appears in the tunnelling density of states and in the conductivity, meaning that both should show a non-analytic behaviour proportional to the absolute value of the magnetic field. Likewise both should become proportional to the temperature at finite temperatures. Even though both these results for the conductivity were known before[132, 133, 134, 135], we found that Cooper scattering also contributes to the non-analytic dependence on the magnetic field. Such processes have been neglected in previous works. On the other hand our approach, based on the Langer formula (3.135), may not be sufficient because interference effects also play a role.

There are numerous ways to extend the work presented in this chapter. First of all, as was discussed in Section 3.1.2, the sign of the prefactor of the term proportional to the absolute value of the magnetic field, temperature, and momentum in the susceptibility is still under debate. While second order perturbation theory implies a positive prefactor, some higher order calculations suggest that this may change[114]. Experimentally the case is also not settled. As the sign of this prefactor has important consequences for the phase diagram of the system, it would therefore be very interesting to perform a calculation taking higher orders in the interaction into account. The model developed in Section 3.2.6 should be a good starting point for such a calculation, which could be done using the FRG. With the insight from the usual renormalization group (see Section 3.1.3), it should further be possible to extract the non-analyticities by truncating at the level of the three-legged vertices.

An other extension of this work stems from our remarks that the non-analytic contribution to the real part of the self-energy at finite external magnetic fields and frequencies must be given by some scaling function. For the case of finite frequencies and temperatures such a scaling function likewise exists and has

been calculated[105]. In this case however, the scaling function must have the property that it picks out certain momentum transfers in the limit where $\omega \gg \hbar$. It would be very interesting to calculate this scaling function. Such a calculation should be done along the lines of Reference [114], where a momentum dependent interaction is introduced and expanded in angular harmonics. Thereby it is possible to see which momentum transfers contribute.

Finally it remains to be done to calculate the conductivity within a proper disorder calculation, while at the same time taking into account all relevant scattering processes. Such a calculation would be important because the result of Zala, Narozhny, and Aleiner[132] [see Equation (3.144)] relate the measurable conductivity to the Landau function F_0^σ and hence provides a way to measure this.

Appendix A

Disorder averaging

For completeness we will, in this appendix, briefly review the basics of diagrammatic disorder averaging, which was used in Section 3.4.2. The methods presented in this appendix were developed starting from the 50's and 60's (see e.g. References [147] and [148]) and up through the 80's [149, 150]. More recent reviews and alternative approaches can also be found in, for example, References [4, 8, 151]. For details and derivations we will refer to the literature.

We assume that the impurities are described by a random potential which depends only on position and that the scattering amplitude is small. In this case we may write the full Hamiltonian as

$$H = H_0 + u(\mathbf{x}), \quad (\text{A.1})$$

where H_0 denotes the disorder-free part of the Hamiltonian and $u(\mathbf{x})$ is the disorder potential. The latter is allowed to be random and is specified only through a probability distribution. It satisfies

$$\langle u(\mathbf{x}) \rangle = 0 \quad (\text{A.2a})$$

$$\langle u(\mathbf{x})u(\mathbf{x}') \rangle = K(\mathbf{x} - \mathbf{x}'), \quad (\text{A.2b})$$

where, as in the main text, $\langle \dots \rangle$ denotes averaging with respect to the disorder and $K(\mathbf{x} - \mathbf{x}')$ is a function which specifies the correlation between impurities. For a Gaussian distribution of impurities (A.2) reduces to the δ -correlated case given in equations (3.124). For simplicity we shall take this case as the starting point. To begin we moreover first discuss how to average Green's functions. From equation (1.1) this satisfies

$$[\omega - H_0 - u(\mathbf{x})] G(\mathbf{x}, \mathbf{x}') = \delta(\mathbf{x} - \mathbf{x}'), \quad (\text{A.3})$$

where we note that we suppress the frequency-dependence of the Green's function in real space. Equation (A.3) can now be solved by writing it as an integral equation as follows

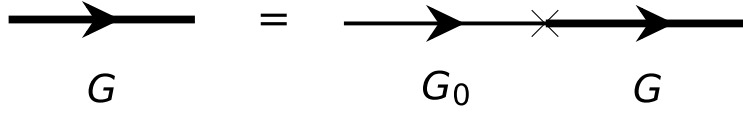


Figure A.1: Diagrammatic representation of the integral equation (A.4) for the disorder-averaged Green's function. Thin lines denote the disorder-free Green's function whilst thick line denote the full disorder-averaged Green's function. The cross represents an impurity.

$$G(\mathbf{x}, \mathbf{x}') = G_0(\mathbf{x}, \mathbf{x}') + \int d^D x'' G_0(\mathbf{x}, \mathbf{x}'') u(\mathbf{x}'') G(\mathbf{x}'', \mathbf{x}). \quad (\text{A.4})$$

In this $G_0(\mathbf{x}, \mathbf{x}')$ denotes the (retarded) Green's function in the absence of disorder, which in momentum-space is given by the form

$$G_0(\omega, \mathbf{k}) = \frac{1}{\omega - \xi_{\mathbf{k}} + i\eta}, \quad (\text{A.5})$$

with $i\eta$ replaced by $-i\eta$ for the advanced Green's function. This should not be confused with the interaction-free Green's function discussed in the main text. Indeed in this appendix we do not consider interactions at all. The full Green's function may be represented diagrammatically as shown in Figure A.1.

Note that the Green's function takes on the same form as the Dyson equation discussed in Section 1.1.1. The effect of disorder can therefore simply be included by adding a self-energy term coming from the disorder. The full disorder-averaged Green's function then takes on the form

$$G_0(\omega, \mathbf{k}) = \frac{1}{[G_0(\omega, \mathbf{k})]^{-1} - \Sigma_{\text{imp}}(\omega, \mathbf{k})}, \quad (\text{A.6})$$

which is equivalent to Equation (3.125) of the main text. Calculating the disorder-averaged Green's function thus amounts to calculating the impurity self-energy. Diagrammatically this can be done by connecting every cross in the expansion of the Green's function by impurity lines which are assumed to connect crosses at same spacial coordinates. To lowest order such a procedure then yields exactly the diagram shown in Figure 3.8. Each impurity line (the dashed line in Figure 3.8) then contributes a term which depends on the function $K(\mathbf{x} - \mathbf{x}')$ in (A.2b). For the case of δ -correlated disorder considered in the main text the contribution is simply a factor of $(2\pi\nu\tau)^{-1}$. Hence it is possible to recover the expression for the impurity self-energy used in Section 3.4.2 of the main text.

Let us finally note that beyond leading order it turns out[148] that, for weak disorder ($1/\tau \ll \omega$), the diagrams in which no impurity lines cross are the most important ones. A notable exception are the so-called maximally crossed diagrams which, in dimensions $D \leq 2$, give rise to singularities[152, 153]. These

diagrams contain quantum interference corrections to the diagrams without crossing.

Appendix B

Deutsche Zusammenfassung

In dieser Arbeit beschäftigen wir uns mit theoretischen Modellen die wechselwirkende Fermionen in der Nähe einer Fermi Fläche beschreiben. Die Landau'sche Fermi-Flüssigkeitstheorie[5, 30, 31] ist seit mehr als 50 Jahren die kanonische Methode solche Systeme mit schwacher Wechselwirkung zu beschreiben. Die Methode beschreibt wechselwirkende Fermionen in der Nähe von einer Fermi Fläche durch nichtwechselwirkende Quasiteilchen, mit den gleichen Eigenschaften wie die ursprünglichen Fermionen, aber mit renormierte Parametern wie Masse, Geschwindigkeit, etc. Mit dieser Methode ist es möglich viele Vielteilchensysteme qualitativ und quantitativ zu beschreiben, wie zum Beispiel das Verhalten von Elektronen in Metallen oder die Massenrenormierung in flüssigen ^3He [32, 33, 34]. Diese Arbeit diskutiert den ersten Fall. Fermi-Flüssigkeitstheorie ist gültig wenn die Quasiteilchen wohldefiniert sind, und damit die Bedingung

$$\frac{1}{\tau_{\mathbf{k}}} \ll |\xi_{\mathbf{k}}|, \quad (\text{B.1})$$

wobei $\tau_{\mathbf{k}}$ die Lebensdauer und $\xi_{\mathbf{k}} = E - E_F$, mit der Quasiteilchenenergie E und der Fermienergie E_F , die Dispersion der Quasiteilchen ist, erfüllen. Von einem mikroskopischen Standpunkt aus ist die Bedingung (B.1) erfüllt, wenn sich der Imaginärteil der Selbstenergie in der Nähe der Fermi Fläche wie

$$\text{Im}\Sigma(\omega, \mathbf{k}_{\mathbf{F}}) \sim \omega^{1+a}, \quad (\text{B.2})$$

mit $a > 1$ verhält. Bei $\mathbf{k}_{\mathbf{F}}$ handelt es sich um den Fermi-impuls, also die Lösung der Gleichung für die Fermi Fläche

$$\xi_{\mathbf{k}_{\mathbf{F}}} + \Sigma(0, \mathbf{k}_{\mathbf{F}}) = 0. \quad (\text{B.3})$$

Trotz der großen Erfolge der Fermi-Flüssigkeitstheorie, zeigen mehr und mehr Experimente auf die Existenz von Phasen in welchen die Fermi-Flüssigkeitstheorie zusammenbricht[40, 41]. In dieser Arbeit diskutieren wir zwei verschiedene Systeme. Eines lässt sich mit der Fermi-Flüssigkeitstheorie beschreiben, in dem anderen bricht sie zusammen.

B.1 Ising-nematischer quantenkritischer Punkt in zweidimensionalen Metallen

Wir diskutieren zuerst das System in dem die Fermi-Flüssigkeitstheorie zusammenbricht. Aus den Arbeiten [73, 78, 79] ist bekannt, dass die Kopplung der Fermionen in der Nähe einer Fermi Fläche an ein gedämpftes, lückenloses bosonisches Feld, über das die Fermionen wechselwirken, zum Zusammenbruch der Fermi-Flüssigkeitstheorie führt. Bei diesem bosonischen Feld könnte es sich zum Beispiel um ein $U(1)$ Eichfeld handeln. Wir betrachten allerdings ein System in dem das Feld einen nematischen Ordnungsparameter beschreibt, und damit den Phasenübergang zwischen einer ungeordneten Phase und einer Phase mit nematischer Ordnung kontrolliert. Bei einem nematischen Phasenübergang ist die Rotationssymmetrie des Gitter gebrochen, die Translationssymmetrie aber erhalten. Nematische Phasen wurden in vielen Materialien gefunden[42, 43, 44, 45, 46, 47, 48] und haben auch in theoretischen Arbeiten viel Beachtung erhalten[49, 50, 51, 52, 53, 54, 55, 56, 57, 58, 59, 60, 61]. In unserem Beispiel betrachten wir einen ‘‘Pomeranchuk’’[80] Quantenphasenübergang von einem zweidimensionalen Metall zu einer nematischen Phase. Es ist bekannt, dass an dem quantenkritischen Punkt die Fermi-Flüssigkeitstheorie zusammenbricht.

Das Verhalten wechselwirkender Fermionen am quantenkritischen Punkt wird üblicherweise mit der Hertz-Millis Theorie[82, 83, 85] beschrieben. In dieser Theorie wird mittels einer Hubbard-Stratonovich Transformation ein bosonisches Feld eingeführt. Der bosonische Anteil der Wirkung wird dann mit Landau Theorie behandelt und, aufgrund von Skalierungsargumenten, ab quadratischer Ordnung trunkiert. Nun können die fermionischen Felder ausintegriert werden und man erhält damit eine rein bosonische Wirkung, gegeben durch

$$S[\phi] = \frac{1}{2} \int \frac{d^2k}{(2\pi)^2} \frac{d\omega}{2\pi} \phi(-\omega, -\mathbf{k}) \left(b_0 \frac{|\omega|}{|\mathbf{k}|} + c_0 k^2 \right) \phi(\omega, \mathbf{k}) + g \int d^2k d\omega \phi(\omega, \mathbf{k})^4, \quad (\text{B.4})$$

mit $b_0 = c_0 = 1/(4\pi)$ und dem bosonischen Feld ϕ . Wegen der Landau Dämpfung $|\omega|/|\mathbf{k}|$ ist die Kopplungskonstante g irrelevant, und die vorhergegangene Trunkierung gerechtfertigt. Weitere Skalierungsargumente zeigen, dass die Selbstenergie

$$\Sigma(\omega, \mathbf{k}) \sim -i \text{sgn}(\omega) |\omega|^{2/3} \quad (\text{B.5})$$

erfüllt und damit nicht das in der Fermi-Flüssigkeitstheorie verlangte Verhalten zeigt. Die Quasiteilchen sind demnach nicht wohldefiniert und die Fermi-Flüssigkeitstheorie bricht zusammen. Da dieser Beitrag zu Selbstenergie singulärer ist als die ungestörte Frequenzabhängigkeit können wir den Propagator in folgender Form schreiben

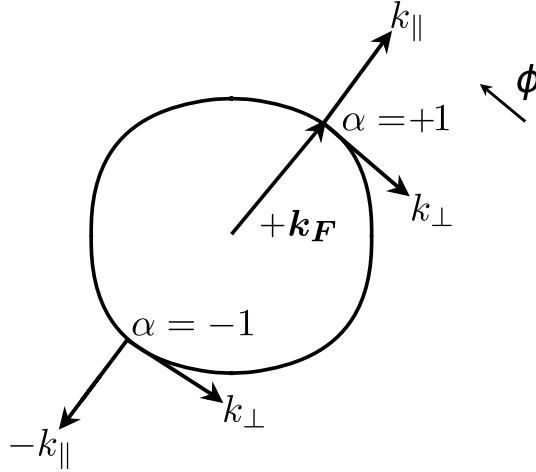


Abbildung B.1: Dies ist die benutzte Konstruktion. Die Fermionen und Bosonen sind nur an zwei Bereichen der Fermi Fläche ($\alpha = \pm 1$) stark gekoppelt.

$$G(\omega + i\eta, \mathbf{k}) \propto \frac{1}{A|\omega|^{2/3} - \xi_{\mathbf{k}}}, \quad (\text{B.6})$$

wobei A ein komplexer Parameter und $\eta > 0$ infinitesimal klein ist. Für lange Zeit galt dieses Ergebnis als exakt[63, 72, 73]. Um das Hertz-Millis Ergebnis zu erhalten, wurde eine mikroskopische Berechnung im Rahmen einer $1/N$ Entwicklung durchgeführt. Die Idee hinter dieser Entwicklung ist, dass es N verschiedene Typen an Fermionen gibt ($N = 2$ im physikalischen Fall). Ist N groß ist eine Entwicklung in $1/N$ gerechtfertigt. Da die Fermionen an der Fermi Fläche ebenfalls lückenlos sind, ist das Ausintegrieren der Fermionen in der Hertz-Millis Theorie problematisch. Aus diesem Grund ist es besser mit einer gemischten fermionischen und bosonischen Wirkung zu arbeiten. Das Problem ist daher sehr kompliziert, lässt sich aber vereinfachen wenn man bemerkt, dass aufgrund der Landau'schen Dämpfung, die Fermionen und Bosonen nur an zwei Bereichen der Fermi Fläche stark gekoppelt sind[63, 72, 73, 54]. Siehe Abbildung B.1. Deswegen entwickelt man die fermionische Dispersion um einen dieser Bereiche

$$\xi_{\mathbf{k}}^{\alpha} = \xi_{\mathbf{k}_F^{\alpha} + \mathbf{k}} - \xi_{\mathbf{k}_F^{\alpha}} \approx \alpha k_{\parallel} + k_{\perp}^2. \quad (\text{B.7})$$

σ steht für den Fermiontyp, k_{\parallel} ist die Impulskomponente parallel zum Fermi-Impuls, und k_{\perp} ist die Impulskomponente orthogonal zum Fermi-Impuls.

Im Ising-nematischen quantenkritischen Punkt findet man bei niedrigster (Ein-Schleifen) Ordnung[92]

$$\Sigma(\omega, \mathbf{k}) \sim -i \frac{1}{N} \text{sgn}(\omega) |\omega|^{2/3}. \quad (\text{B.8})$$

Das relevante Diagramm ist in Abbildung B.2(a) zu sehen. Um auf dieses

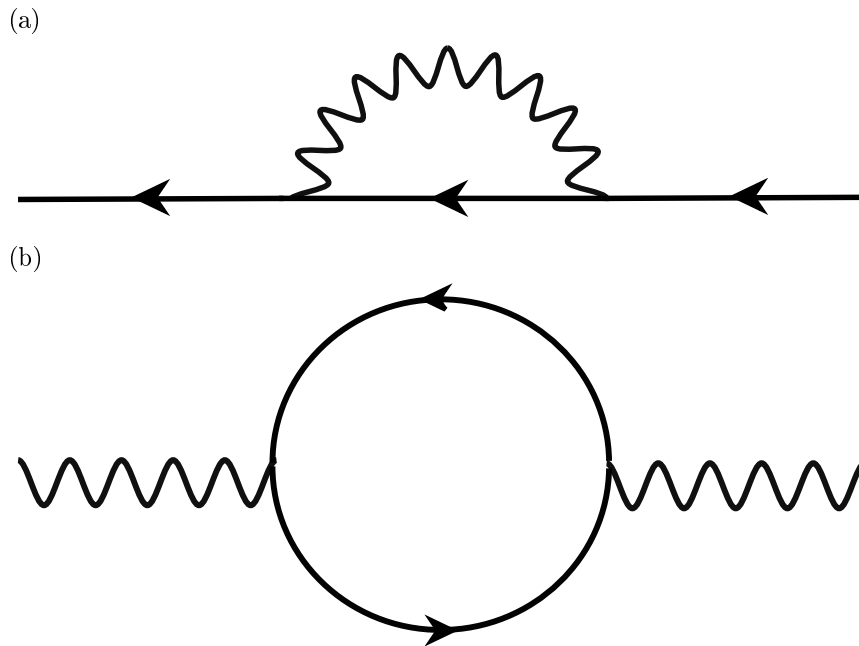


Abbildung B.2: (a) Fermionische Selbstenergie zur Ein-Schleifen Ordnung und (b) Ein-Schleifen bosonischen Selbstenergie. Die durchgezogene Linien repräsentiert fermionische Propagatoren und die Wellenlinien bosonische Propagatoren. Unrenormalisierte Vertices sind durch Schnittpunkte zweier Linien angegeben.

Ergebnis für die Selbstenergie zu kommen, wird der fermionische Propagator durch die bosonische Selbstenergie renormiert. Die bosonische Selbstenergie ist in Abbildung B.2(b) gezeigt und ist durch

$$\Pi(\omega, \mathbf{k}) = \frac{N}{4\pi} \frac{|\omega|}{|k_{\perp}|} \quad (\text{B.9})$$

gegeben. Wir erhalten also wieder die Landau'sche Dämpfung und bemerken wieder, dass diese von der Ordnung N ist.

Berücksichtigt man Diagramme bis zur Zwei-Schleifen Ordnung findet man die selbe Frequenzabhängigkeit der fermionischen Selbstenergie[72, 73, 79, 95], allerdings mit dem Vorfaktor

$$\left(\frac{\ln N}{N}\right)^2 \ll 1, \quad (\text{B.10})$$

für große N . Daher ist man davon ausgegangen, dass die $1/N$ Entwicklung kontrolliert und das Hertz-Millis Ergebnis exakt ist.

In den letzten Jahren hat sich aber herausgestellt, dass diese Schlussfolgerung nicht vollständig ist. Insbesondere hat Lee[77], mit einem System aus einer Fermi Fläche mit einem Bereich der an ein $U(1)$ Eichfeld gekoppelt ist,

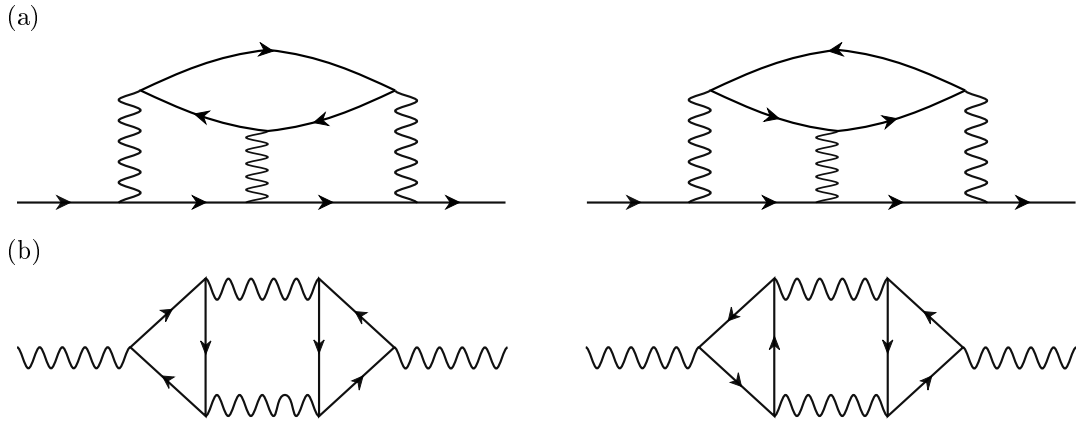


Abbildung B.3: Dies sind die Drei-Schleifen Diagramme die von Metlitski und Sachdev berücksichtigt wurden. (a) sind die Beiträge zu der fermionischen Selbstenergie und (b) sind die sogenannten Aslamazov-Larkin Beiträge zur bosonischen Selbstenergie.

gezeigt, dass die sogenannten “planaren” Diagramme die Ordnung in der $1/N$ -Entwicklung modifizieren. Damit bleibt die Theorie auch für große N stark gekoppelt. Dieses Problem wurde später von Metlitski und Sachdev[54, 65] in einem vollständigen Zwei-Bereich Modell erneut aufgegriffen. Sie haben anormale Dimensionen ab Drei-Schleifen Ordnung gefunden. Die entsprechenden Diagramme sind in Abbildung B.3 gezeigt. Die Existenz anormaler Dimensionen bedeutet, dass der fermionische Propagator aus Gleichung (B.6) durch

$$G(\omega + i\eta, \mathbf{k}) \propto \frac{1}{(A|\omega|^{2/z_b} - \xi_{\mathbf{k}})^{1-\eta_\psi/2}} \quad (\text{B.11})$$

ersetzt werden soll. η_ψ entspricht der anormalen Dimension und z_b ist der bosonische dynamische Exponent (im Ising-nematischen quantenkritischen Punkt ist $z_b = 3$). Aus diesem Grund ist das Hertz-Millis Resultat nicht korrekt. Was sie ebenfalls gefunden haben ist, dass die zwei Aslamazov-Larkin Diagramme für die bosonische Selbstenergie [siehe Abbildung B.3(b)] zusammen der Ordnung $N^{3/2}$ sind. Da die Ein-Schleifen bosonische Selbstenergie nur der Ordnung N ist, impliziert dies, dass die $1/N$ -Entwicklung nicht unter Kontrolle ist. Alle bisherigen Versuche einer kontrollierten Entwicklung (Kombination aus ϵ - und $1/N$ Entwicklung[71] und Kombination aus einer Entwicklung in $(z_b - 2)$ und $1/N$ [55]) führen zu stark voneinander abweichenden Ergebnissen für die anormale Dimension. Daher haben wir das Problem mit der funktionalen Renormierungsgruppe (FRG) betrachtet[84].

Die FRG (siehe zum Beispiel [1]) ist eine moderne Umsetzung der Wilson-Renormierungsgruppe. Dabei wird ein Cutoff Λ eingeführt, der die betrachtete Theorie regularisiert. Zunächst beschreibt man die Theorie mit endlichem Cutoff. Die Ergebnisse des ursprünglichen Problems erhält man dann für $\Lambda \rightarrow 0$. Mit dem eingeführten Cutoff ist es möglich formal exakte Flussgleichungen

für die erzeugenden Funktionale der Einteilchen-Irreduziblen-Vertices, $\Gamma[\bar{\phi}, \phi]$, für das betrachtete System herzuleiten[25]. Wenn man beide Seiten der Flussgleichung nach Potenzen der Felder entwickelt, erhält man eine unendliche Hierarchie von gekoppelten Integro-Differentialgleichungen für die Einteilchen-Irreduziblen-Vertices. Im Allgemeinen kann diese unendliche Hierarchie nicht gelöst werden. Trotzdem kann man durch die Anwendung von Trunkierungs- und Näherungsmethoden physikalische Erkenntnisse über das betrachtete System erhalten.

Um das Verhalten am Ising-nematischen quantenkritischen Punkt in zwei-dimensionalen Metallen zu beschreiben haben wir die FRG Flussgleichungen so trunziert, dass wir die selben Diagramme berücksichtigen wie Metlitski und Sachdev, Abbildung B.3. Dies erreichen wir, indem wir nur die fermionische und bosonische Selbstenergie und die Vertices die die Wechselwirkung zwischen zwei Fermionen und einem Boson, und zwischen drei Bosonen beschreiben mitnehmen. Die bosonische Selbstenergie und der Vertex der die Wechselwirkung zwischen drei Bosonen beschreibt behandeln wir außerdem mit trunzierten Skelettgleichungen. Letztendlich führen wir nur einen (scharfen) Cutoff in den bosonischen Propagator ein, so dass die Propagatoren durch

$$G^\alpha(K) = \frac{1}{i\omega - \xi_{\mathbf{k}}^\alpha - \Sigma^\alpha(K)}, \quad (\text{B.12a})$$

$$F(\bar{K}) = \frac{\Theta(|\bar{k}_\perp| - \Lambda)}{r_0 + c_0|\bar{k}_\perp|^{z_b-1} + \Theta(|\bar{k}_\perp| - \Lambda)\Pi(\bar{K})} \quad (\text{B.12b})$$

gegeben sind. Die sogenannten “single-scale Propagatoren” sind damit durch

$$\dot{G}^\alpha(K) = -[G^\alpha(K)]^2 \partial_\Lambda [G_{0,\Lambda}^\alpha(K)]^{-1} = 0, \quad (\text{B.13a})$$

$$\dot{F}(\bar{K}) = -[F(\bar{K})]^2 \partial_\Lambda [F_{0,\Lambda}(\bar{K})]^{-1} = -\frac{\delta(|\bar{k}_\perp| - \Lambda)}{r_0 + c_0\Lambda^{z_b-1} + \Pi(\bar{K})} \quad (\text{B.13b})$$

gegeben. Mit diesen Näherungen erhalten wir ein geschlossenes Gleichungssystem, gezeigt diagrammatisch in Abbildung B.4.

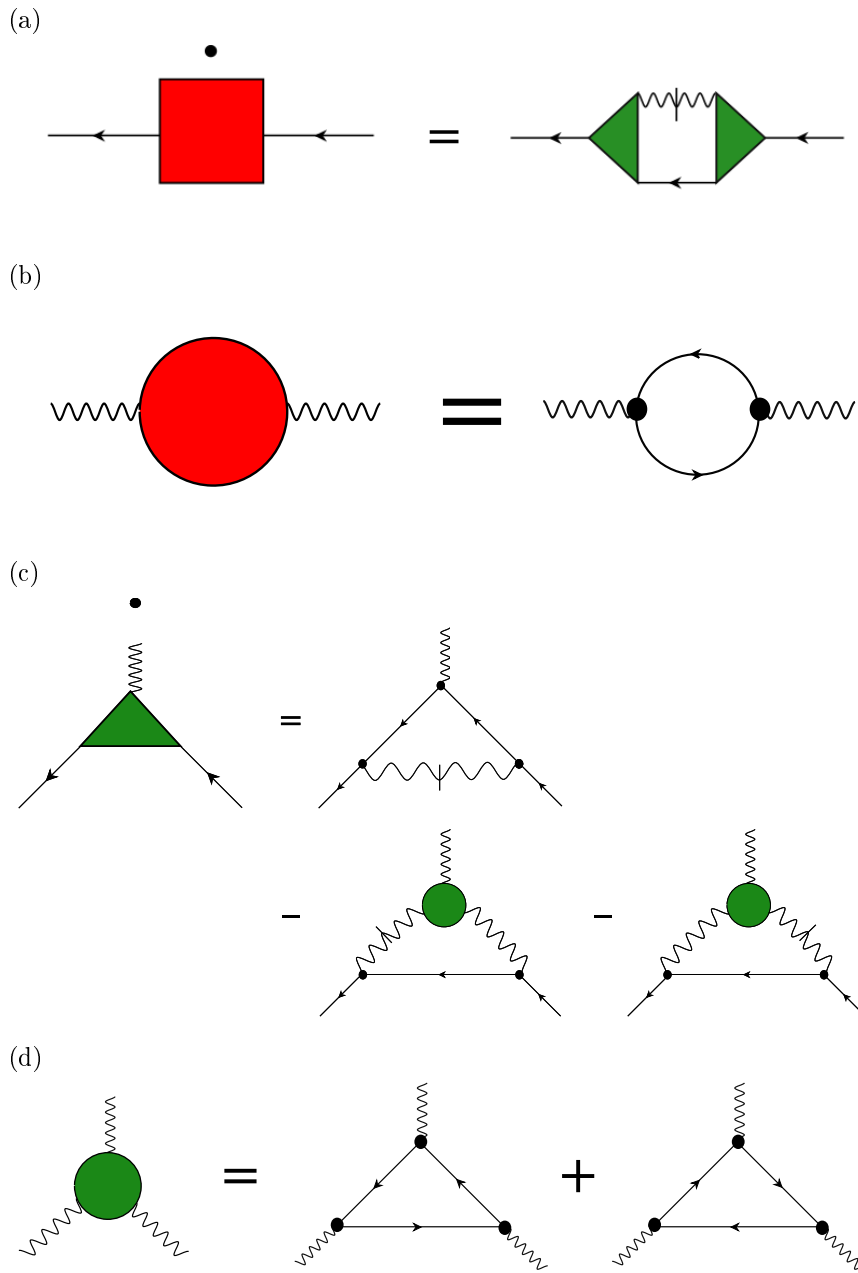


Abbildung B.4: Eine diagrammatische Darstellung der trunkierten Flussgleichungen unseres Problems. (a) ist die trunkierte Flussgleichung für die fermionische Selbstenergie, (b) ist die trunkierte Skelettgleichung für die bosonische Selbstenergie, (c) ist die trunkierte Flussgleichung für den Vertex der die Wechselwirkung zwischen zwei Fermionen und einem Boson beschreibt, und (d) ist die trunkierte Skelettgleichung für den Vertex der die Wechselwirkung zwischen drei Bosonen beschreibt. Ein rotes Viereck steht für die fermionische Selbstenergie, ein roter Kreis für die bosonische Selbstenergie, ein grünes Dreieck für den zwei-Fermionen-ein-Boson Vertex, und der grüne Kreis für den drei-Boson Vertex. Ein Punkt über dem Vertex steht für die Ableitung des selbigen nach dem Fluss-parameter Λ . Die durchgezogene Linie repräsentiert den fermionischen Propagator und die gewellte Linie den bosonischen Propagator. Sind die Propagatoren durchgestrichen beziehen wir uns auf einen "single-scale" Propagator. Da wir nur einen Cutoff im bosonischen Sektor eingeführt haben gibt es keine fermionischen single-scale Propagatoren. Bei den schwarzen Punkten handelt es sich um unrenormalisierte Vertices.

Im Prinzip ist dieses Gleichungssystem jetzt exakt lösbar, aber praktisch müssen wir weitere Näherungen einführen. Zuerst nähern wir die Propagatoren durch ihre Ein-Schleifen Resultate an. Diese erhalten wir, wenn wir in unserem Gleichungssystem Vertexkorrekturen vernachlässigen und stimmen mit den Propagatoren aus der Hertz-Millis Theorie überein. Anschließend berücksichtigen wir auch Vertexkorrekturen. Um zu einem sinnvollen Ergebnis zu kommen, machen wir noch einen niederenergetischen Ansatz und entwickeln in $N(z_b - 2)$. Diese Approximationen sind allerdings nicht zwingend notwendig, um das Gleichungssystem zu lösen. Letztendlich finden wir für die anormale Dimension den Ausdruck

$$\eta_\psi = \frac{(z_b - 2)^2}{2} \tilde{C}(\lambda_0) + \mathcal{O}((z_b - 2)^3), \quad (\text{B.14})$$

wobei es sich bei $\tilde{C}(\lambda_0)$ um eine ultraviolett divergente ‘‘Cutoff-Funktion’’ handelt, die in Abbildung B.5 gezeigt wird. Die Cutoff-Funktion ist lediglich logarithmisch divergent, und wir setzen den Cutoff $\lambda_0 = 1$ um zu einem Ergebnis zu kommen. Eine Extrapolation zu $z_b = 3$ liefert $\eta_\psi \approx 0.3$. Dieses Resultat sollte mit den Ergebnissen $\eta_\psi \approx 0.068$ von Metlitski und Sachdev[54] und $\eta_\psi \approx 0.6$ von Mross et al[55] verglichen werden. Es gibt keinen Grund aus dem wir quantitative Übereinstimmung finden sollten, da wir verschiedene Näherungen verwendet haben. Qualitativ stimmen die Resultate überein– wir finden einen endlichen Wert für die anormale Dimension. Darüber hinaus finden wir mit der FRG die anormale Dimension direkt, da diese erst ab Vier-Schleifen Ordnung auftritt und wir in unseren Flussgleichungen auch Diagramme höherer Ordnungen als drei betrachten. Die Werte der anormalen Dimension können in Tunnelexperimenten über die Zustandsdichte experimentell bestimmt werden. Schlussendlich finden wir eine kleine renormierung des fermionischen dynamischen Exponenten der durch

$$z = \frac{z_b}{2} + \frac{(z_b - 2)^2}{4} \left[C(\lambda_0) - \tilde{C}(\lambda_0) \right] + \mathcal{O}((z_b - 2)^3), \quad (\text{B.15})$$

gegeben ist, wobei $C(\lambda_0)$ eine zweite (auch ultraviolett divergenten) Cutoff-Funktion ist. Eigentlich würde man erwarten, dass der fermionische Exponent nicht renormiert wird. Metlitski und Sachdev haben das bis zur Drei-Schleifen Ordnung gezeigt. Es kann sein, dass unsere Trunkierung nicht alle relevante Diagramme höherer Ordnung berücksichtigt.

Dieser Teil ist in Kollaboration mit Lorenz Bartosch, Aldo Isidori, und Peter Kopietz entstanden und in [84] publiziert.

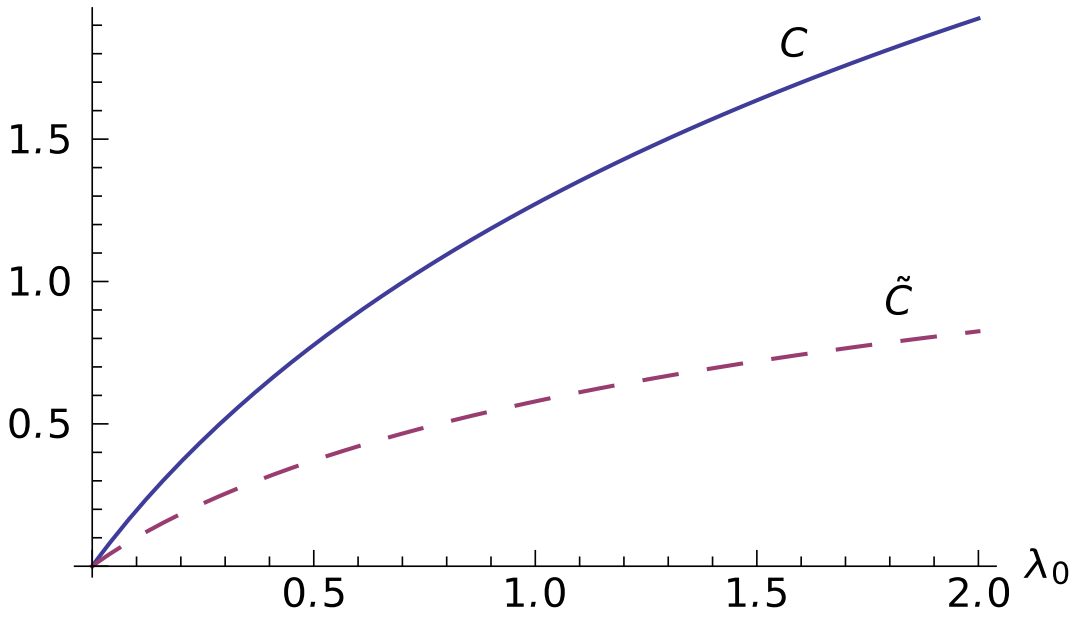


Abbildung B.5: Die Cutoff-Funktionen $C(\lambda_0)$ und $\tilde{C}(\lambda_0)$.

B.2 Nicht-analytische Korrekturen in Fermi-Flüssigkeitstheorie

Im zweiten Teil dieser Arbeit beschäftigen wir uns mit Fermi-Flüssigkeitstheorie und betrachten ein System von wechselwirkenden Fermionen in einem schwachen externen Magnetfeld. Von dem fundamentalen Ansatz der Fermi-Flüssigkeitstheorie könnte man erwarten, dass verschiedene thermodynamische Größen durch die Sommerfeld Entwicklung beschrieben werden. Beispielsweise dass die Suszeptibilität χ und der Wärmekapazitäts-parameter $\gamma = C/T$ bei endlichem Magnetfeld oder Temperatur durch

$$\gamma(T, H = 0) = \gamma(0, 0) + \mathcal{O}(T^2), \quad (\text{B.16a})$$

$$\chi(T, H = 0) = \chi(0, 0) + \mathcal{O}(T^2), \quad (\text{B.16b})$$

$$\chi(T = 0, H) = \chi(0, 0) + \mathcal{O}(H^2), \quad (\text{B.16c})$$

gegeben sind. In den letzten Jahren hat sich aber gezeigt, dass dies nur bis zur führenden Ordnung korrekt ist[101, 102, 104, 103, 105, 106, 107, 108, 109, 110, 111, 112, 113, 114, 115, 116]. Insbesondere hat man in zweidimensionalen Systemen lineare Korrekturen gefunden (in drei Dimensionen sind die führenden Korrekturen logarithmisch). Diese Korrekturen für sich alleine stehen nicht im Gegensatz zu der Fermi-Flüssigkeitstheorie, weil diese im Allgemeinen nur führende Ordnung enthält. Diese ist durch die Sommerfeld Entwicklung gegeben. Um die nächste Ordnung zu beschreiben müssen die Systeme mikroskopisch betrachtet werden. Man findet unter anderem, dass

die nicht-analytischen linearen Terme von weit-reichender Wechselwirkung kommen, die zur Folge haben, dass die Polarisierung nicht-analytisch ist[114], zum Beispiel in Form der Landau'schen Dämpfung oder der Kohn Anomalie. Diese führt dann wieder zu nicht-analytischen Termen in den thermodynamischen Parametern. Die Vorfaktoren der linearen nicht-analytischen Terme haben große Aufmerksamkeit erhalten.

Es gibt auch andere Parameter die nicht-analytisch im Kontrollparameter (Magnetfeld, Temperatur, etc.) zum Quadrat sein können. Insbesondere haben wir uns in diesem Teil mit den Quasiteilcheneigenschaften, wie dem Quasiteilchenresiduum, dem Impulsrenormierungsfaktor, und dem Landé g-Faktor, in einem kleinen externen Magnetfeld beschäftigt. Dafür betrachten wir ein zweidimensionales System wechselwirkender Fermionen in einem schwachen externen Magnetfeld. Der freie Propagator ist dann durch

$$G_0^\sigma(i\omega, \mathbf{k}) = \frac{1}{i\omega - \xi_{\mathbf{k}}^\sigma}, \quad (\text{B.17})$$

gegeben, wobei σ die Spinprojektion der Fermionen und

$$\xi_{\mathbf{k}}^\sigma = \frac{k^2 - (k_F^\sigma)^2}{2m} = \xi_{\mathbf{k}} - \sigma h, \quad (\text{B.18})$$

ihre Dispersion in einem Magnetfeld sind. Bei $\xi_{\mathbf{k}} = k^2/(2m) - \mu$, mit dem chemischen Potential μ (das für $T = 0$ die Fermi Energie entspricht) handelt es sich um die Dispersion ohne Magnetfeld. Das Magnetfeld H tritt durch die Zeeman Energie $h = g\mu_B H$, wobei μ_B die Bohr Magneton und g der Landé g-factor sind, ein. Die Dispersion hängt vom Magnetfeld ab, da die Fermi Fläche durch die spin-abhängigkeit des Fermi-impulses k_F^σ gesplittet wird. Die Quasiteilchenparameter erhalten wir durch eine Entwicklung der Selbstenergie um die Fermi Fläche

$$\Sigma^\sigma(i\omega, \mathbf{k}) = \Sigma^\sigma(0, k_F^\sigma) + (1 - Z^{-1})i\omega - (1 - Y^{-1})\xi_{\mathbf{k}}^\sigma + \dots \quad (\text{B.19})$$

Bei Z handelt es sich um das Quasiteilchenresiduum und bei Y um den Impulsrenormierungsfaktor. Über diese Größen erhalten wir auch die renormierte Masse

$$\frac{m_*}{m} = \frac{Y}{Z}, \quad (\text{B.20})$$

mit der unrenormierten Masse m . Letztendlich definieren wir noch einen dritten Renormierungsfaktor X durch

$$X = 1 - \frac{\Sigma^\uparrow(0, k_F^\uparrow) - \Sigma^\downarrow(0, k_F^\downarrow)}{2h}. \quad (\text{B.21})$$

Der renormierte Landé g-factor kann dann mit

$$g_* = \frac{Z}{Y} X \quad (\text{B.22})$$

berechnet werden.

Für die Berechnung der drei Renormierungsfaktoren X , Y , und Z lassen wir die Fermionen durch eine konstante Wechselwirkung U , die nur Streuung zwischen Fermionen mit verschiedenen Spins erlaubt, interagieren. Nun berechnen wir die Selbstenergie bis zur zweiten Ordnung in dieser Wechselwirkungskonstante. Der Beitrag zweiter Ordnung zur Selbstenergie lässt sich in drei äquivalenten Formen schreiben, die in Abbildung B.6 gezeigt sind. Für den Anfang wählen wir das zweite Diagramm und führen eine Integration und die entsprechenden Ableitungen analytisch durch. Die zwei verbleibenden Integrationen müssen numerisch durchgeführt werden. So extrahieren wir die Renormierungsfaktoren. Wir finden

$$X(h) = X(0) + X_1|h| + \mathcal{O}(h^2), \quad (\text{B.23a})$$

$$Y(h) = Y(0) + Y_1|h| + \mathcal{O}(h^2), \quad (\text{B.23b})$$

$$Z(h) = Z(0) + Z_1|h| + \mathcal{O}(h^2), \quad (\text{B.23c})$$

mit

$$X_1 \approx Y_1 \approx Z_1 \approx 0.50 \frac{u^2}{E_F} + \mathcal{O}(u^3). \quad (\text{B.24})$$

Hier ist $u = \nu U$ wobei $\nu = m/(2\pi)$ die Zustandsdichte pro zweidimensionaler Spinprojektion auf die Fermi Fläche ist, eine dimensionslose Wechselwirkungskonstante. Aufgrund $X_1 = Y_1$ gibt es bis zu dieser Ordnung keine linearen nicht-analytischen Terme in der renormierten Masse. Außerdem finden wir, dass im Gegensatz zu Y und Z , aber in Übereinstimmung mit der Suszeptibilität, nur der Austauschkanal zu den nicht-analytischen Korrekturen zu X beiträgt.

Um die numerischen Ergebnisse zu überprüfen und die Form der Streuung zu klassifizieren haben wir eine sogenannte Phasenraumdekomposition durchgeführt[38, 103]. In zwei Dimensionen sind die drei Prozesse in Abbildung B.6 die einzigen Streuprozesse mit niedrigen Energien in der Nähe der Fermi Fläche. Die Prozesse sind in Abbildung B.7 gezeigt.

Nach der Phasenraumdekomposition können wir die Polarisierungen für niedrige Impulse und Frequenzen approximieren, und alle Berechnungen analytisch durchführen. Wir finden schließlich

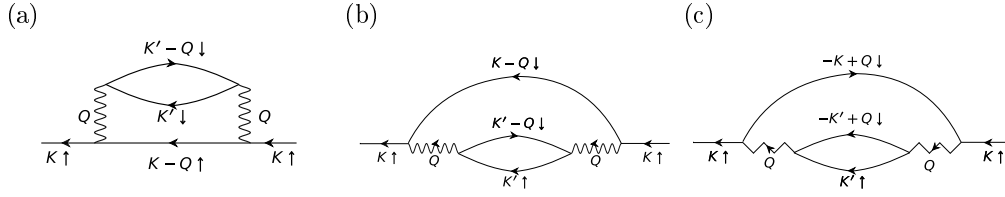


Abbildung B.6: In dieser Abbildung sehen wir den Beitrag zweiter Ordnung in der Wechselwirkung zur Selbstenergie in drei äquivalenten Schreibweisen. Bei den Diagrammen (a) und (b) handelt es sich um die Teilchen-Loch Diagramme und bei (c) um das Teilchen-Teilchen Diagramm. Ohne ultraviolett Cutoff in der Impulsintegration beschreiben die drei Diagramme die gleichen Streuprozesse. Wenn man aber einen Cutoff $\Lambda \ll k_F$ einführt, beschreiben die Diagramme drei verschiedene Streuprozesse. Es handelt sich dabei um (a) “Vorwärtsstreuung”, (b) “Austauschstreuung” und (c) “Cooper Streuung”. Eine durchgezogene Linie entspricht einem fermionischen Propagator. Die Wellenlinie ohne Pfeil beschreibt die Wechselwirkung im Vorwärtskanal, die Wellenlinie mit Pfeil beschreibt die Wechselwirkung im Austauschkanal, und die Zickzacklinie mit Pfeil die Wechselwirkung im Cooper Kanal.

$$X_1 = \frac{u^2}{2E_F} + \mathcal{O}(u^3), \quad (\text{B.25a})$$

$$Y_1 = \frac{u^2}{2E_F} + \mathcal{O}(u^3), \quad (\text{B.25b})$$

$$Z_1 = \frac{u^2}{2E_F} + \mathcal{O}(u^3). \quad (\text{B.25c})$$

Die analytischen Resultate stimmen mit den numerischen Werten überein. Wie man sieht sind unsere Ergebnisse cutoffunabhängig und wir schließen daraus, dass die führenden nicht-analytischen Terme von universellen niederenergetischen Streuprozessen in der Nähe der Fermi Fläche kommen.

Die nicht-analytischen Terme können in verschiedenen Experimenten gemessen werden. Beispielsweise kann das Quasiteilchenresiduum in Fotoemissionsexperimenten bestimmt werden. Außerdem hat der Renormierungsfaktor Y Einfluss auf die Zustandsdichte in Tunnelexperimenten und die Leitfähigkeit. Wir erwarten also, dass diese Größen bei kleinen Magnetfeldern linear im Magnetfeld sind. Für die Leitfähigkeit ist dies schon bekannt [132, 133, 134, 135], allerdings vermuten wir, dass die bisherige gekannte lineare Abhängigkeit anderen Ursprungs ist.

Die selben Rechnungen lassen sich auch bei endlichen Temperaturen oder Frequenzen durchführen. Für Y finden wir bei endlichen Temperaturen auch eine lineare nicht-analytische Korrektur. Diese sollte auch experimentell

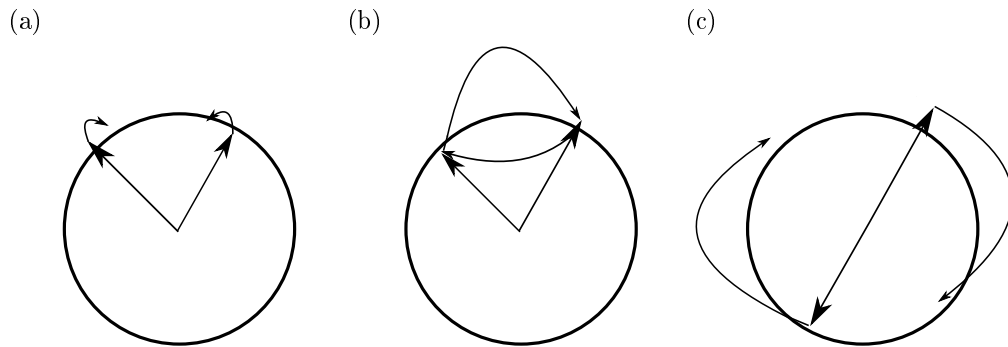


Abbildung B.7: Hier sind die drei möglichen Streuprozesse. (a) entspricht Vorwärtsstreuung (Streuung mit kleinem Impulsübertrag), (b) repräsentiert Austauschstreuung (Streuung über einen großen Winkel), und (c) entspricht Cooper Streuung (Streuung zwischen Zustände die $2k_F$ voneinander entfernt sind).

messbar sein. Außerdem haben wir auch die Selbstenergie bei endlichen Frequenzen bestimmt. In diesem Fall finden wir nicht-analytische Terme der Form $\omega|\omega|$. In den Arbeiten [105, 107, 129, 130] wurde gezeigt, dass hier die nicht-analytischen Terme nur von Impulsen um $q = 0$ und $q = 2k_F$ kommen. Zu unseren Vorfaktoren gibt es Beiträge aus dem ganzen Bereich $q \in [0, 2k_F]$. Daher muss die Selbstenergie bei endlicher Frequenz und endlichem Magnetfeld eine Skalierungsform annehmen. Für endliche Temperaturen und Frequenzen ist diese Skalierungsform bekannt[105] aber für endliches Magnetfeld wurden noch keine Berechnung durchgeführt.

Die Arbeit in diesem Teil wurde mit Philipp Lange, Peter Kopietz, und Dmitrii Maslov durchgeführt und ist in [123] publiziert.

Bibliography

- [1] P. Kopietz, L. Bartosch, and Florian Schütz, *Introduction to the Functional Renormalization Group*, Springer, Berlin (2010).
- [2] J. W. Negele and H. Orland, *Quantum many particle systems*, Frontiers in physics; 68, Addison-Wesley, Redwood City, CA (1988).
- [3] A. Altland and B. Simons, *Condensed Matter Field Theory*, Cambridge University Press, Cambridge (2006).
- [4] H. Bruus and K. Flensberg, *Many-Body Quantum Theory in Condensed Matter Physics*, Oxford University Press, Oxford (2004).
- [5] E. M. Lifshitz and L. P. Pitaevskii, *Statistical Physics II*, Pergamon Press, London (1980).
- [6] J. Cardy, *Scaling and Renormalization in Statistical Physics*, Cambridge lecture notes in physics, Cambridge University Press, Cambridge (1996).
- [7] M. Stone and P. Goldbart, *Mathematics for Physics*, Cambridge University Press, Cambridge (2009).
- [8] K. Efetov, *Supersymmetry in Disorder and Chaos*, Cambridge University Press, Cambridge (1997).
- [9] M. E. Peskin and D. V. Schroeder, *An Introduction to Quantum Field Theory*, Westview Press, Boulder, CO (1995).
- [10] H. Goldstein, C. Poole, and J. Safko, *Classical Mechanics*, Addison-Wesley, Redwood City, CA (2002).
- [11] W. Metzner, M. Salmhofer, C. Honerkamp, V. Meden, and K. Schönhammer, *Functional renormalization group approach to correlated fermion systems*, Rev. Mod. Phys. **84**, 299 (2012).
- [12] K. G. Wilson, *Non-Lagrangian Models of Current Algebra*, Phys. Rev. **179**, 1499 (1969).
- [13] K. G. Wilson, *Renormalization Group and Critical Phenomena. I. Renormalization Group and the Kadanoff Scaling Picture*, Phys. Rev. B **4**, 3174 (1971).

-
- [14] K. G. Wilson, *Renormalization Group and Critical Phenomena. II. Phase-Space Cell Analysis of Critical Behavior*, Phys. Rev. B **4**, 3184 (1971).
- [15] K. G. Wilson, *Feynman-Graph Expansion for Critical Exponents*, Phys. Rev. Lett. **28**, 548 (1972).
- [16] K. G. Wilson and M. E. Fisher, *Critical Exponents in 3.99 Dimensions*, Phys. Rev. Lett. **28**, 240 (1972).
- [17] K. G. Wilson and J. Kogut, *The renormalization group and the ϵ expansion*, Physics Reports **12** (2), 75 (1974).
- [18] K. G. Wilson, *The renormalization group: Critical phenomena and the Kondo problem*, Rev. Mod. Phys. **47**, 773 (1975).
- [19] S. Streib, A. Isidori, and P. Kopietz, *Solution of the Anderson impurity model via the functional renormalization group*, Phys. Rev. B **87**, 201107(R) (2013).
- [20] T. Kloss and P. Kopietz, *Nonequilibrium time evolution of bosons from the functional renormalization group*, Phys. Rev. B **83**, 205118 (2011).
- [21] D. F. Litim, *Optimized renormalization group flows*, Phys. Rev. D **64**, 105007 (2001).
- [22] J. Berges, N. Tetradis, and C. Wetterich, *Non-perturbative renormalization flow in quantum field theory and statistical physics*, Phys. Rep. **363**, 223 (2002).
- [23] C. Husemann and M. Salmhofer, *Efficient parametrization of the vertex function, Ω scheme, and the t, t' Hubbard model at van Hove filling*, Phys. Rev. B **79**, 195125 (2009).
- [24] K.-U. Giering and M. Salmhofer, *Self-energy flows in the two-dimensional repulsive Hubbard model*, Phys. Rev. B **86**, 245122 (2012)
- [25] C. Wetterich, *Exact evolution equation for the effective potential*, Phys. Lett. B **301**, 90 (1993).
- [26] M. Bonini, M. D'Attanasio, and G. Marchesini, *Perturbative renormalization and infrared finiteness in the Wilsonian renormalization group: The massless scalar case*, Nucl. Phys. B **409**, 441 (1993).
- [27] C. Bagnuls and C. Bervillier, *Classical-to-critical crossovers from field theory*, Phys. Rev. E **65**, 066132 (2002).
- [28] J. M. Pawłowski, *Aspects of the functional renormalisation group*, Ann. Phys. **322**, 2831 (2007).

- [29] T. R. Morris, *The exact renormalisation group and approximate solutions*, Int. J. Mod. Phys. A **9**, 2411 (1994).
- [30] L. D. Landau, *Theory of Fermi liquids*, Zh. Eksp. Teor. Fiz. **30**, 1058 (1956) [Sov. Phys. JETP **3** 920 (1957)].
- [31] L. D. Landau, *On the theory of the Fermi-liquid*, Zh. Eksp. Teor. Fiz. **35**, 97 (1958) [Sov. Phys. JETP **8** 70 (1959)].
- [32] L. D. Landau, *Oscillations in a Fermi-liquid*, Zh. Eksp. Teor. Fiz. **32**, 59 (1957) [Sov. Phys. JETP **5** 101 (1957)].
- [33] D. S. Greywall, *Specific heat of normal liquid ^3He* , Phys. Rev. B **27**, 2747 (1983).
- [34] D. S. Greywall, *^3He specific heat and thermometry at millikelvin temperatures*, Phys. Rev. B **33**, 7520 (1986).
- [35] A. Paramekanti, L. Balents, and M. P. A. Fisher, *Ring exchange, the exciton Bose liquid, and bosonization in two dimensions*, Phys. Rev. B **66**, 054526 (2002).
- [36] S. Sachdev, *Scratching the Bose surface*, Nature **418**, 739 (2002).
- [37] K. Riedl, C. Drukier, P. Zalom, and P. Kopietz, *Spontaneous ferromagnetism in the spinor Bose gas with Rashba spin-orbit coupling*, Phys. Rev. A **87**, 063626 (2013).
- [38] R. Shankar, *Renormalization-group approach to interacting fermions*, Rev. Mod. Phys. **66**, 129 (1994).
- [39] A. V. Chubukov and D. L. Maslov, *First-Matsubara-frequency rule in a Fermi liquid. I. Fermionic self-energy*, Phys. Rev. B **86**, 155136 (2012).
- [40] T. Timusk and B. Statt, *The pseudogap in high-temperature superconductors: an experimental survey*, Rep. Prog. Phys. **62**, 61 (1999).
- [41] A. Abanov, A. V. Chubukov, and J. Schmalian, *Quantum-critical theory of the spin-fermion model and its application to cuprates: Normal state analysis*, Adv. Phys. **52**, 119 (2003).
- [42] Y. Ando, K. Segawa, S. Komiya, and A. N. Lavrov, *Electrical Resistivity Anisotropy from Self-Organized One Dimensionality in High-Temperature Superconductors*, Phys. Rev. Lett. **88**, 137005 (2002).
- [43] R. A. Borzi, S. A. Grigera, J. Farrell, R. S. Perry, S. J. S. Lister, S. L. Lee, D. A. Tennant, Y. Maneno, and A. P. Mackenzie, *Formation of a Nematic Fluid at High Fields in $\text{Sr}_3\text{Ru}_2\text{O}_7$* , Science **315**, 214 (2007).

- [44] Y. Kohsaka, C. Taylor, K. Fujita, A. Schmidt, C. Lupien, T. Hanaguri, M. Azuma, M. Takano, H. Eisaki, H. Takagi, S. Uchida, and J. C. Davis, *An Intrinsic Bond-Centered Electronic Glass with Unidirectional Domains in Underdoped Cuprates*, Science **315**, 1380 (2007).
- [45] V. Hinkov, D. Haug, B. Fauqué, P. Bourges, Y. Sidis, A. Ivanov, C. Bernhard, C. T. Lin, and B. Keimer, *Electronic Liquid Crystal State in the High-Temperature Superconductor $YBa_2Cu_3O_{6.45}$* , Science **319**, 597 (2008).
- [46] R. Daou, J. Chang, D. LeBoeuf, O. Cyr-Choinière, F. Laliberté, N. Doiron-Leyraud, B. Ramshaw, R. Liang, D. Bonn, W. Hardy, and L. Taillefer, *Broken rotational symmetry in the pseudogap phase of a high- T_c superconductor*, Nature (London) **463**, 519 (2010).
- [47] S. Nandi, M. G. Kim, A. Kreyssig, R. M. Fernandes, D. K. Pratt, A. Thaler, N. Ni, S. L. Bud'ko, P. C. Canfield, J. Schmalian, R. J. McQueeney, and A. I. Goldman, *Anomalous Suppression of the Orthorhombic Lattice Distortion in Superconducting $Ba(Fe_{1-x}Co_x)_2As_2$ Single Crystals*, Phys. Rev. Lett. **104**, 057006 (2010).
- [48] E. Fradkin, S. A. Kivelson, M. J. Lawler, J. P. Eisenstein, and A. P. Mackenzie, *Nematic Fermi Fluids in Condensed Matter Physics*, Annu. Rev. Cond. Mat. Phys. **1**, 153 (2010).
- [49] M. J. Lawler, D. G. Barci, V. Fernández, E. Fradkin, and L. Oxman, *Nonperturbative behavior of the quantum phase transition to a nematic Fermi fluid*, Phys. Rev. B **73**, 085101 (2006).
- [50] Y. Huh and S. Sachdev, *Renormalization group theory of nematic ordering in d-wave superconductors*, Phys. Rev. B **78**, 064512 (2008).
- [51] W. Metzner, L. Dell'Anna and H. Yamase, *Nematic order and non-Fermi liquid behavior from a Pomeranchuk instability in a two-dimensional electron system*, J. Phys.: Conf. Ser. **150** 032058 (2009).
- [52] P. Jakubczyk, W. Metzner, and H. Yamase, *Turning a First Order Quantum Phase Transition Continuous by Fluctuations: General Flow Equations and Application to d-Wave Pomeranchuk Instability*, Phys. Rev. Lett. **103**, 220602 (2009).
- [53] M. Garst and A. V. Chubukov, *Electron self-energy near a nematic quantum critical point*, Phys. Rev. B **81**, 235105 (2010).
- [54] M. A. Metlitski and S. Sachdev, *Quantum phase transitions of metals in two spatial dimensions. I. Ising-nematic order*, Phys. Rev. B **82**, 075127 (2010).

- [55] D. F. Mross, J. McGreevy, H. Liu, and T. Senthil, *Controlled expansion for certain non-Fermi-liquid metals*, Phys. Rev. B **82**, 045121 (2010).
- [56] H. Yamase, P. Jakubczyk, and W. Metzner, *Nematic quantum criticality without order*, Phys. Rev. B **83**, 125121 (2011).
- [57] S. Thier and W. Metzner, *Singular order parameter interaction at nematic quantum critical point in two dimensional electron systems*, Phys. Rev. B **84**, 155133 (2011).
- [58] T. Holder and W. Metzner, *Incommensurate nematic fluctuations in two-dimensional metals*, Phys. Rev. B **85**, 165130 (2012).
- [59] D. G. Barci and D. Reyes, *Pomeranchuk-nematic instability in the presence of a weak magnetic field*, Phys. Rev. B **87**, 075147 (2013).
- [60] K. Reidy, K. Quader, and Kevin Bedell, *Approaching Pomeranchuk instabilities from ordered phase: A crossing-symmetric equation method*, Nucl. Phys. A **928**, 168 (2014).
- [61] S. A. Hartnoll, R. Mahajan, M. Punk, and S. Sachdev, *Transport near the Ising-nematic quantum critical point of metals in two dimensions*, Phys. Rev. B **89**, 155130 (2014).
- [62] T. Senthil, *On non-Fermi liquid quantum critical points in heavy fermion metals*, Ann. Phys. **321**, 1669 (2006).
- [63] H. v. Löhneysen, A. Rosch, M. Vojta, and Peter Wölfle, *Fermi-liquid instabilities at magnetic quantum phase transitions*, Rev. Mod. Phys. **79**, 1015 (2007).
- [64] T. Senthil, *Critical Fermi surfaces and non-Fermi liquid metals*, Phys. Rev. B **78**, 035103 (2008).
- [65] M. A. Metlitski and S. Sachdev, *Quantum phase transitions of metals in two spatial dimensions. II. Spin density wave order*, Phys. Rev. B **82**, 075128 (2010).
- [66] T. R. Kirkpatrick and D. Belitz, *Theory of a Fermi-Liquid to Non-Fermi-Liquid Quantum Phase Transition in Dimensions $d > 1$* , Phys. Rev. Lett. **108**, 086404 (2012).
- [67] R. Mahajan, M. Barkeshli, and S. A. Hartnoll, *Non-Fermi liquids and the Wiedemann-Franz law*, Phys. Rev. B **88**, 125107 (2013).
- [68] A. L. Fitzpatrick, S. Kachru, J. Kaplan, and S. Raghu, *Non-Fermi-liquid fixed point in a Wilsonian theory of quantum critical metals*, Phys. Rev. B **88**, 125116 (2013).

- [69] M. A. Metlitski, D. F. Mross, S. Sachdev, and T. Senthil, *Are non-Fermi liquids stable to Cooper pairing?*, arXiv:1403.3694 [cond-mat.str-el] (2014).
- [70] I. Mandal, S.-S. Lee, *UV/IR mixing in Non-Fermi Liquids*, arXiv:1407.0033 [cond-mat.str-el] (2014).
- [71] C. Nayak and F. Wilczek, *Non-Fermi liquid fixed point in 2+1 dimensions*, Nucl. Phys. B **417**, 359 (1994).
- [72] J. Polchinski, *Low-energy dynamics of the spinon-gauge system*, Nucl. Phys. B **422**, 617 (1994).
- [73] B. L. Altshuler, L. B. Ioffe, and A. J. Millis, *Low-energy properties of fermions with singular interactions*, Phys. Rev. B **50**, 14048 (1994).
- [74] P. Kopietz, *Vertex corrections in gauge theories for two-dimensional condensed matter systems*, Int. J. Mod. Phys. B **12**, 1673 (1998).
- [75] J. Rech, C. Pépin, and A. V. Chubukov, *Quantum critical behavior in itinerant electron systems: Eliashberg theory and instability of a ferromagnetic quantum critical point*, Phys. Rev. B **74**, 195126 (2006).
- [76] T. A. Sedrakyan and A. V. Chubukov, *Fermionic propagators for two-dimensional systems with singular interactions*, Phys. Rev. B **79**, 115129 (2009).
- [77] S.-S. Lee, *Low-energy effective theory of Fermi surface coupled with $U(1)$ gauge field in $2 + 1$ dimensions*, Phys. Rev. B **80**, 165102 (2009).
- [78] P. A. Lee, *Gauge field, Aharonov-Bohm flux, and high- T_c superconductivity*, Phys. Rev. Lett. **63**, 680 (1989).
- [79] Y. B. Kim, A. Furusaki, X.-G. Wen, and P. A. Lee, *Gauge-invariant response functions of fermions coupled to a gauge field*, Phys. Rev. B **50**, 17917 (1994).
- [80] I. Pomeranchuk, *On the stability of a Fermi liquid*, Soviet. Phys. JETP **8**, 361 (1958).
- [81] C. J. Halboth and W. Metzner, Phys. Rev. Lett. **85**, 5162 (2000)
- [82] J. A. Hertz, *Quantum critical phenomena*, Phys. Rev. B **14**, 1165 (1976).
- [83] A. J. Millis, *Effect of a nonzero temperature on quantum critical points in itinerant fermion systems*, Phys. Rev. B **48**, 7183 (1993).
- [84] C. Drukier, L. Bartosch, A. Isidori, and P. Kopietz, *Functional renormalization group approach to the Ising-nematic quantum critical point of two-dimensional metals*, Phys. Rev. B **85**, 245120 (2012).

- [85] T. Moriya, *Spin Fluctuations in Itinerant Electron Magnetism*, Springer, Berlin (1985).
- [86] T. Holstein, R. E. Norton, and P. Pincus, *de Haas-van Alphen Effect and the Specific Heat of an Electron Gas*, Phys. Rev. B **8**, 2649 (1973).
- [87] M. Y. Reizer, *Relativistic effects in the electron density of states, specific heat, and the electron spectrum of normal metals*, Phys. Rev. B **40**, 11571 (1989).
- [88] P. A. Lee and N. Nagaosa, *Gauge theory of the normal state of high- T_c superconductors*, Phys. Rev. B **46**, 5621 (1992).
- [89] O. Motrunich, *Variational study of triangular lattice spin-1/2 model with ring exchanges and spin liquid state in $\kappa - (ET)_2Cu_2(CN)_3$* , Phys. Rev. B **72**, 045105 (2005).
- [90] S.-S. Lee and P. A. Lee, *$U(1)$ Gauge Theory of the Hubbard Model: Spin Liquid States and Possible Application to $\kappa - (BEDT-TTF)_2Cu_2(CN)_3$* , Phys. Rev. Lett. **95**, 036403 (2005).
- [91] B. I. Halperin, P. A. Lee, and N. Read, *Theory of the half-filled Landau level*, Phys. Rev. B **47**, 7312 (1993).
- [92] S. Sachdev, *Quantum Phase Transitions*, 2nd ed., Cambridge University Press, Cambridge (2011).
- [93] S. J. Yamamoto and Q. Si, *Renormalization group for mixed fermion-boson systems*, Phys. Rev. B **81**, 205106 (2010).
- [94] L.G. Aslamazov and A.I. Larkin, *The influence of fluctuation pairing of electrons on the conductivity of normal metal*, Phys. Lett. A **26** (6), 238 (1968).
- [95] A. V. Chubukov, *Viewpoint: Hidden one-dimensional physics in 2D critical metals*, Physics **3**, 70 (2010).
- [96] F. Schütz, L. Bartosch, and P. Kopietz, *Collective fields in the functional renormalization group for fermions, Ward identities, and the exact solution of the Tomonaga-Luttinger model*, Phys. Rev. B **72**, 035107 (2005).
- [97] L. Bartosch, H. Freire, J. J. Ramos Cardenas, and P. Kopietz, *A functional renormalization group approach to the Anderson impurity model*, J. Phys.: Condens. Matter **21**, 305602 (2009).
- [98] A. Neumayr and W. Metzner, *Fermion loops, loop cancellation, and density correlations in two-dimensional Fermi systems*, Phys. Rev. B **58**, 15449 (1998).

- [99] P. Pirooznia, F. Schütz, and P. Kopietz, *Dynamic structure factor of Luttinger liquids with quadratic energy dispersion and long-range interactions*, Phys. Rev. B **78**, 075111 (2008).
- [100] N. W. Ashcroft and N. D. Mermin, *Solid State Physics*, Saunders College, Philadelphia (1976).
- [101] D. Coffey and K. S. Bedell, *Nonanalytic contributions to the self-energy and the thermodynamics of two-dimensional Fermi liquids*, Phys. Rev. Lett. **71**, 1043 (1993).
- [102] M. A. Baranov, M. Y. Kagan and M.S. Mar'enko, *Singularity in the quasiparticle interaction function in 2D Fermi gas*, Pis'ma Zh. Eksp. Teor. Fiz. **58**, 734 (1993) [JETP Lett. **58**, 709 (1993)].
- [103] D. Belitz, T. R. Kirkpatrick, and T. Vojta, *Nonanalytic behavior of the spin susceptibility in clean Fermi systems*, Phys. Rev. B **55**, 9452 (1997).
- [104] G. Y. Chitov and A. J. Millis, *Leading Temperature Corrections to Fermi-Liquid Theory in Two Dimensions*, Phys. Rev. Lett. **86**, 5337 (2001).
- [105] A. V. Chubukov and D. L. Maslov, *Nonanalytic corrections to the Fermi-liquid behavior*, Phys. Rev. B **68**, 155113 (2003).
- [106] V. M. Galitski, A. V. Chubukov, and S. Das Sarma, *Temperature-dependent spin susceptibility in a two-dimensional metal*, Phys. Rev. B **71**, 201302(R) (2005).
- [107] A. V. Chubukov, D. L. Maslov, S. Gangadharaiah, and L. I. Glazman, *Singular perturbation theory for interacting fermions in two dimensions*, Phys. Rev. B **71**, 205112 (2005).
- [108] J. Betouras, D. Efremov, and A. Chubukov, *Thermodynamics of a Fermi liquid in a magnetic field*, Phys. Rev. B **72**, 115112 (2005).
- [109] A. V. Chubukov, D. L. Maslov, and A. J. Millis, *Nonanalytic corrections to the specific heat of a three-dimensional Fermi liquid*, Phys. Rev. B **73**, 045128 (2006).
- [110] I. L. Aleiner and K. B. Efetov, *Supersymmetric low-energy theory and renormalization group for a clean Fermi gas with a repulsion in arbitrary dimensions*, Phys. Rev. B **74**, 075102 (2006).
- [111] G. Schwiete and K. B. Efetov, *Temperature dependence of the spin susceptibility of a clean Fermi gas with repulsion*, Phys. Rev. B **74**, 165108 (2006).

- [112] A. Shekhter and A. M. Finkelstein, *Temperature dependence of spin susceptibility in two-dimensional Fermi liquid systems*, Phys. Rev. B **74**, 205122 (2006).
- [113] A. V. Chubukov and I. Eremin, *Strong-coupling theory of the universal linear temperature dependence of the nodal Fermi velocity in layered cuprates*, Phys. Rev. B **78**, 060509(R) (2008).
- [114] D. L. Maslov and A. V. Chubukov, *Nonanalytic paramagnetic response of itinerant fermions away and near a ferromagnetic quantum phase transition*, Phys. Rev. B **79**, 075112 (2009).
- [115] S. Chesi, R. A. Zak, P. Simon, and D. Loss, *Momentum dependence of the spin susceptibility in two dimensions: Nonanalytic corrections in the Cooper channel*, Phys. Rev. B **79**, 115445 (2009).
- [116] D. Belitz and T. R. Kirkpatrick, *Nonanalyticities in a strongly correlated Fermi liquid: Corrections to scaling at the Fermi-liquid fixed point*, Phys. Rev. B **89**, 035130 (2014).
- [117] A. Casey, H. Patel, J. Nyeki, B. P. Cowan, and J. Saunders, *Evidence for a Mott-Hubbard Transition in a Two-Dimensional ^3He Fluid Monolayer*, Phys. Rev. Lett. **90**, 115301 (2003).
- [118] G-M, Zhang, Y-H, Su, Z-Y. Lu, Z-Y. Weng, D-H. Lee, T. Xiang, *Universal linear-temperature dependence of static magnetic susceptibility in iron-pnictides*, Eur. Phys. Lett. **86**, 37006 (2009).
- [119] O. Prus, Y. Yaish, M. Reznikov, U. Sivan, and V. Pudalov, *Thermodynamic spin magnetization of strongly correlated two-dimensional electrons in a silicon inversion layer*, Phys. Rev. B **67**, 205407 (2003).
- [120] V. M. Pudalov, M. E. Gershenson, and H. Kojima, pp. 309-327 in: *Fundamental Problems of Mesoscopic Physics. Interaction and Decoherence*, Eds. I.V.Lerner, B.L.Altshuler, and Y.Gefen, Nato sci. series, Kluwer (2004).
- [121] J. Zhu, H. L. Stormer, L. N. Pfeiffer, K. W. Baldwin, and K. W. West, *Spin Susceptibility of an Ultra-Low-Density Two-Dimensional Electron System*, Phys. Rev. Lett. **90**, 056805 (2003).
- [122] T. Gokmen, M. Padmanabhan, E. Tutuc, M. Shayegan, S. De Palo, S. Moroni, and G. Senatore, *Spin susceptibility of interacting two-dimensional electrons with anisotropic effective mass*, Phys. Rev. B **76**, 233301 (2007).
- [123] C. Drukier, P. Lange, and P. Kopietz, *Non-analytic magnetic field dependence of quasi-particle properties of two-dimensional metals*, arXiv:1407.4131 [cond-mat.str-el] (2014).

- [124] A. V. Chubukov, D. L. Maslov, S. Gangadharaiah, and L. I. Glazman, *Thermodynamics of a Fermi Liquid beyond the Low-Energy Limit*, Phys. Rev. Lett. **95**, 026402 (2005).
- [125] A. Kreisel, F. Sauli, N. Hasselmann, and P. Kopietz, *Quantum Heisenberg antiferromagnets in a uniform magnetic field: Nonanalytic magnetic field dependence of the magnon spectrum*, Phys. Rev. B **78**, 035127 (2008).
- [126] J. Sólyom, *The Fermi gas model of one-dimensional conductors*, Adv. Phys. **28**, 201 (1979).
- [127] J. Lindhard, *On the Properties of a Gas of Charged Particles*, K. Dan. Vidensk. Selsk. Mat. Fys. Medd. **28**, 8 (1954).
- [128] B. Mihaila, *Lindhard function of a d-dimensional Fermi gas*, arXiv:1111.5337 [cond-mat.quant-gas] (2011).
- [129] S. Fujimoto, *Anomalous Damping of Quasiparticles in Two-Dimensional Fermi Systems*, J. Phys. Soc. Jpn. **59**, 2316 (1990).
- [130] C. Halboth and W. Metzner, *Spectral function of two-dimensional Fermi liquids*, Phys. Rev. B **57**, 8873 (1998).
- [131] P. Kopietz, *Bosonization of Interacting Fermions in Arbitrary Dimensions*, Springer, Berlin (1997).
- [132] G. Zala, B. N. Narozhny, and I. L. Aleiner, *Interaction corrections at intermediate temperatures: Magnetoresistance in a parallel field*, Phys. Rev. B **65**, 020201(R) (2001).
- [133] G. Zala, B. N. Narozhny, and I. L. Aleiner, *Interaction corrections at intermediate temperatures: Longitudinal conductivity and kinetic equation*, Phys. Rev. B **64**, 214204 (2001).
- [134] I. V. Gornyi and A. D. Mirlin, *Interaction-Induced Magnetoresistance: From the Diffusive to the Ballistic Regime*, Phys. Rev. Lett. **90**, 076801 (2003)
- [135] I. V. Gornyi and A. D. Mirlin, *Interaction-induced magnetoresistance in a two-dimensional electron gas*, Phys. Rev. B **69**, 045313 (2004).
- [136] J. S. Langer, *Theory of Impurity Resistance in Metals. II*, Phys. Rev. **124**, 1003 (1961).
- [137] J. S. Langer, *Thermal Conductivity of a System of Interacting Electrons*, Phys. Rev. **128**, 110 (1962).
- [138] G. M. Eliashberg, *Transport equation for a degenerate system of fermi particles*, Zh. Eksp. Teor. Fiz. **41**, 1241 (1961) [Sov. Phys. JETP **14**, 886 (1962)].

- [139] G. M. Eliashberg, *A microscopic theory of the damping of zero sound in a fermi liquid*, Zh. Eksp. Teor. Fiz. **42**, 1658 (1962) [Sov. Phys. JETP **15**, 1151 (1962)].
- [140] K. Michaeli and A. M. Finkel'stein, *Quantum kinetic approach for studying thermal transport in the presence of electron-electron interactions and disorder*, Phys. Rev. B **80**, 115111 (2009).
- [141] D. L. Maslov and A. V. Chubukov, *First-Matsubara-frequency rule in a Fermi liquid. II. Optical conductivity and comparison to experiment*, Phys. Rev. B **86**, 155137 (2012).
- [142] K. Yamada, *Electron Correlation in Metals*, Cambridge University Press, Cambridge (2004).
- [143] J. A. N. Bruin, H. Sakai, R. S. Perry, and A. P. Mackenzie, *Similarity of Scattering Rates in Metals Showing T-Linear Resistivity*, Science **339**, 804 (2013).
- [144] T. A. Sedrakyan, E. G. Mishchenko, and M. E. Raikh, *Smearing of the Two-Dimensional Kohn Anomaly in a Nonquantizing Magnetic Field: Implications for Interaction Effects*, Phys. Rev. Lett. **99**, 036401 (2007).
- [145] T. A. Sedrakyan, E. G. Mishchenko, and M. E. Raikh, *Zero-Bias Tunneling Anomaly in a Clean 2D Electron Gas Caused by Smooth Density Variations*, Phys. Rev. Lett. **99**, 206405 (2007).
- [146] T. A. Sedrakyan and M. E. Raikh, *Magneto-Oscillations due to Electron-Electron Interactions in the ac Conductivity of a Two-Dimensional Electron Gas*, Phys. Rev. Lett. **100**, 086808 (2008).
- [147] S. F. Edwards, *A new method for the evaluation of electric conductivity in metals*, Phil. Mag. **3**, 1020 (1958).
- [148] A. A. Abrikosov, L. P. Gorkov, and I. E. Dzyaloshinski, *Methods of Quantum Field Theory in Statistical Physics*, Prentice Hall, New York (1963).
- [149] B. L. Altshuler, A. G. Aronov, D. E. Khmel'nitskii, and A. I. Larkin in: *Quantum Theory of Solids*, ed. I. M. Lifshitz, MIR Publishers, Moscow (1983).
- [150] P. A. Lee and T. V. Ramakrishnan, *Disordered electronic systems*, Rev. Mod. Phys. **57**, 287 (1985).
- [151] A. Kamenev and A. Levchenko, *Keldysh technique and non-linear σ -model: basic principles and applications*, Adv. Phys. **58**, 3 (2009).

- [152] L. P. Gorkov, A. I. Larkin, and D. E. Khmel'nitskii, *Particle conductivity in a two-dimensional random potential*, Pis'ma Zh. Eksp. Teor. Fiz. **30**, 248 [JETP Lett. **30**, 228] (1979).
- [153] E. Abrahams, P. W. Anderson, and T. V. Ramakrishnan, *Non-ohmic effects of anderson localization*, Phil. Mag. **42**, 827 (1980).

Acknowledgements

Many people have, in one way or another, contributed to this thesis. Here I would like to thank all those people.

First and foremost I would like to thank my supervisor Professor Peter Kopietz for allowing me to work on very interesting problems and for always being available to help and explain when needed. I have learnt a great deal from his intuition and knowledge, and his approach to physical problems. I am also very grateful for the opportunity to do part of my work with him in Florida during his sabbatical there, and for the relaxed atmosphere he promoted in his group.

I am grateful to all my office mates Johannes Hick, Kira Riedl, and Philipp Lange, for creating a very nice environment to work in and for always making it a pleasure to come to the office. In particular I have benefited a lot from discussions with Johannes Hick and Philipp Lange, both about physics and other things and would like to thank Kira Riedl for our collaboration during a common project. I would also like to thank Philipp Lange for his friendship and the nice time we spent sharing a house in Florida.

The first part of this work was based on work done also together with Lorenz Bartosch and Aldo Isidori. I would like to thank them for their help and input in this project. Aldo Isidori I also thank for his friendship and for always being ready to help and for the many discussions about physics that we had. From these I learnt a lot.

The last part of this thesis was done in close collaboration with Philipp Lange. For this I am very grateful. I would also like to thank Professor Dmitrii Maslov for his input in the project, and Andreas Rückriegel and Tim Herfurth for checking some of the numeric calculations.

I would like to thank all members, past and present, of the group of Professor Peter Kopietz for creating an atmosphere in which it is enjoyable to work. To all my friends and colleagues in the Institute of Theoretical Physics in Frankfurt I am also grateful for making the last couple of years interesting

and enjoyable.

Part of the work done for this thesis was done while visiting the University of Florida in Gainesville. I would like to thank everyone in the UF Physics Department for making me feel welcome and for providing me with a very productive work environment. I am also grateful to the many other people who made my stay an enjoyable experience.

I am also indebted to Philipp Lange and Jan Krieg for proofreading my thesis. Professor Walter Hofstetter I would like to thank for agreeing to referee the thesis. I am also grateful to Andreas Kreisel for help with the layout of this thesis and to Rodrigo Echeveste, Bulcsú Sándor, and Kira Riedl for help with L^AT_EX and figures.

Finally I am very thankful for all the love and support I have always received from my parents which has always enabled me to pursue the things I am interested in.

Thank you!

Lebenslauf

Geburtsdatum 13. November 1985
Geburtsort Hvidovre, Dänemark
Staatsangehörigkeit Dänisch

Ausbildung

- **Institut für Theoretische Physik, Goethe Universität Frankfurt** 2011 - Heute
 - Doktorand in der Gruppe von Professor Peter Kopietz
- **Sidney Sussex College, University of Cambridge** 2005 - 2009
 - B.A. (Hons) & M.Sci.:
 - “Final year research project” Titel:
Band Tail from Supersymmetry
Betreuer: Professor David Khmelnitskii
Note: 2.i
 - 2012: M.A. verliehen.
- **Ingrid Jespersens Gymnasieskole, Kopenhagen** 1991 - 2004
 - 2004: Dänisches Abitur.